The Copper Centers of Particulate Methane Monooxygenase: Differentiation of C- and E-Clusters

Thesis by

Sean J. Elliott

In Partial Fulfillment of the Requirements

For the Degree of

Doctor of Philosophy

California Institute of Technology

Pasadena, CA

2000

(Submitted January 10, 2000)

Acknowledgements

To try to sum up everything, to acknowledge all of the countless people who I am indebeted to, seems to be a fool's errand at best. But I will throw what I can at it, and my hope is to inadvertantly exclude as few people as possible.

The Chan Group, headed by my mentor **Sunney I. Chan**, must lead this charge of acknowledged gratitude. Sunney is always leading Our charge, and he has provided a truly unique staging ground for my intellectual development as well as my personal growth, and I cannot thank him appropriately in words alone. Those from the Chan group that have preceded me intellectually also deserve special mention: **Hoa Nguyen**, **Mei Zhu**, **John Yip** have all worked on the pMMO problem before me. They set the tone and the pace for much of my own work. **Reggie Waldeck**, **Hung-Kay "Bruce" Lee**, **Sigfried Musser**, **Ron Rock**, **Michael Stowell**, **Ted DiMagno**, **Silvia Cavagnero**, **Ruth Ann Bertsch** and **Dennis Anderson** are all former group members that I have had the pleasure of working with and seeing day to day. Reggie and Bruce and Mike have shared many cups of coffee in the middle years of my career, and their suggestions and encouragement pushed my work ethic to new heights.

The current group members **Tim Cheng, Kirk Hanson**, **Shao-Ching Hung**, **Brian Schultz**, and **David Zheng** have all proven to be excellent colleagues, adept scientists, and good friends. **Steven Yu** at the Academia Sinica in Taipei has been a great help in all matters regarding travel to Taipei and work with pMMO.

I owe a sincere debt of gratitude to the many co-workers that I've labored with over the years. **David Britt** and **David Randall** of UC-Davis; **Jennifer DuBois** and

her mentors **Keith Hodgson** and **Britt Hedman** of Stanford; and the group of **Mary E. Lidstrom** have all be instrumental. I would particularly like to thank **Sergei Stolyar** for teaching me about molecular biology, **Heather Rothfuss** for extreme hospitality during my stay in Seattle.

Outside of "Work" there have been many that have touched my life in such strong ways that I would be the greatest of knaves if I did not mention them here.

Joy Beardsley, and **Claire Underwood** who re-entered my life at precisely the right moment, waving magic wands and daring me to Dream a powerful dream…

Charles Ofria, who has been alongside, fighting the good fight from day one, whether with boffer weapons, games, or his fiercely friendly intelligence…

Elana Rubenstein, who gave my own army and the courage to use it…

Danielle Allen, who proved more to me in a few weeks than I thought possible…

Andy Ashcraft, **Lesley Mathieson**, **Cheryl Vuong**, **Brian McInnis**, **Kristen Lovelady**, **Ian Fagan**, **Alex** and **Angel Epstein**, **Bill** and **Nikki Maxwell**, and **Marc** and **Kim Unger**, who have shared my highs and lows, who have fought many fictitious battles for me and with me and against me, and who have taken each instance of my lunacy for better or worse, and returned, asking for more ...

Lady Jane Taylor, who never doubted for an instant …

Jeff DeConcini and **Reed Krider**, who simply are the best of the best…

And my entire family, **Butch** and **Barbara**, **Michael** and **Jennoir** and **Peter**, who have been an endless well of concern, support and love…

… You all have my gratitude, my admiration, my confidence and my love.

Abstract

This dissertation investigates the approximately 15 copper ions of pMMO from *M. capsulatus* by a variety of spectroscopic, biochemical and molecular biological techniques. The first chapters describe spectroscopy studies of the C- and E-clusters of the protein. The pMMO protein is prepared in a number of chemical states which access the differentially oxidized of the C- and E-clusters. Investigation of these states by X-ray Absorption Spectroscopy (XAS) reveals unique oxidation states of pMMO copper ions upon anaerobic preparation, and oxidation with air, pure dioxygen, or hydrocarbon suicide substrate. Structural implications for the copper ions of the protein are discussed, and a model for the ability of acetylene to highly oxidize pMMO is explored. The differentiation of the copper ions of pMMO is explored by the use of proteolytic enzymes and chemical treatment with *N,N,N',N'*-Ethylenediamine-tetraacetic acid (EDTA), monitoring the ability of pMMO to form a Cu(II)-ferrocyanide adduct upon treatment with ferricyanide and subsequent electron transfer. Soluble, copper-binding domains are found, as well as specific centers that are buried in the transmembrane domain. The inability of an EDTA-treated preparation to regenerate a fully oxidized form of the protein indicates that the copper ions bound by pMMO do interact with one via electron transfer. The ability to assess the potential ligands of the copper ions of pMMO is determined by Electron Spin Echo Envelop Modulation (ESEEM) spectroscopy, revealing potential interactions between histidine residues and the enzyme active site.

Subsequent chapters probe reported characteristic of the pMMO active site, thought to be located within the PmoA sub-unit. First, the identity of potential ligands for copper ions bound by the PmoA protein is assessed by a homology of *pmoA*. Next, the role of ion in pMMO is explored by treatement with NO(g), and it is concluded that the resulting signals in the $g \approx 4.0$ region of the Electron Paramagnetic Resonance (EPR) spectrum were due to an iron-nitrosyl adduct. The identity of the iron is assigned to adventitious iron bound to pMMO. A final chapter probes the overall structure and geometry of the active site by examining the regio- and stereoselectivity of pMMO-mediated hydroxylation and epoxidation chemistry.

Table of Contents

Abbreviations and Nomenclature

amo	Ammonia Monooxygenase (gene)
AMO	Ammonia Monooxygenase
cyt *c*	Cytochrome *c*
DβM	Dopamine-β-Monooxygenase
EDTA	N,N,N',N'-Ethylenediamine-tetraacetic acid
ENDOR	Electron-Nuclear Double Resonance
EPR	Electron Paramagnetic Resonance
ESEEM	Electron Spin Echo Envelop Modulation
EXAFS	Extended X-Ray Absorption Fine Structure
FT	Fourier Transform
ICP-MS	Induced Coupled Plasma Mass Spectrometry
NADH	Reduced Nicotinamide Adenine Dinucleotide Disodium Salt
NO	Nitric Oxide
PHM	Peptidyl Hydroxylating Monooxygenase
Pipes	Piperazine-N,N'-bis[2-ethanesulfonic acid]
pMMO	Particulate Methane Monooxygenase
pmo	Particulate Methane Monooxygnease (gene)
SDS-PAGE	Sodium Dodecyl Sulfate – Polyacrylamide Gel Electrophoresis
sMMO	Soluble Methane Monooxygenase
TCA	Trichloro Acetic Acid
TCE	Trichloro Ethylene
μM	micromolar
mM	milimolar
W	Watts
XAS	X-ray Absorption Spectrscopy

Chapter 1: Particulate Methane Monooxygenase Biology and Chemistry: The State of the Art

Introduction to Methane Activation

Methane gas represents an untapped reservoir for both liquid fuels as well as chemical feedstocks. Huge methane reserves are located principally in the former Soviet Union and the Middle East, but occur throughout the globe, and reserves of methane trapped as methane hydrates in marine subsurface sediments are thought to be substantial as well. Methane is the largest constituent in natural gas, and is often a substantive constituent of petroleum reserves, and in these forms it is heretofore under-utilized. As methane is often found in remote locations, the hazardous nature of transporting a flammable gas limits the attractiveness of using methane as either chemical feedstock or fuel. Refrigerated methane (LNG, liquid natural gas) does represent a safe way to transport methane over a long distance, but the costs associated with refrigeration and transport are prohibitively high. An ideal solution to this dilemma would involve the conversion of methane into a safer liquid chemical that does not have the same requisite costs of transportation. Such a conversion process is by no means facile, however.

Methane is considered to have the most inert C-H bonds of hydrocarbons, and while the overall conversion of methane to methanol or formaldehyde is thermodynamically favorable (ΔG°=-25.4 kcal/mol for methanol, -69.0 kcal/mol for formaldehyde, at 400K), the instability of the possible reaction intermediates, and the increased reactivity of the products, typically renders selective methane oxidation very difficult proposition. Considerable efforts, past and present, have pursued convenient and inexpensive methane conversion, including industrial processes (such

as methane oxidation *via* Syngas) which require high temperatures and pressures. Similar problems plague attempts to catalytically convert hydrocarbons higher in order than methane, particularly if selective oxidation is desired. Generally the order of reactivity of C-H bonds decreases from $3^{o} > 2^{o} > 1^{o}$ bonds. Often this is the reverse of what is desired.

Stepping over to the natural world reveals a remarkably different picture of methane conversion, however. In terms of emission, consumption and net production, methane is an incredibly important biological molecule[1]. Methane is considered both in terms of its role as a potential greenhouse gas[2] as well as an end product of methanogenesis by methanotrophic archaea, and the sole carbon and energy source of methanotrophic bacteria. Methane oxidation and emission processes are considered to be significant in marine, soil, freshwater and atmospheric environments.

Methanogenesis appears as a characteristic of methanogenic archaea which generate methane as a byproduct of metabolisms that typically feature using hydrogen gas and carbon dioxide (the former as an electron donor, and the latter as electron acceptor). Methanogens span many genera, are either Gram positive or negative, and all are obligate anaerobes.

Methanotrophy harnesses methane as both a carbon and an energy source, making this biological process the epitome of success for synthetic chemists with an interest in methane as a chemical feedstock or liquid fuel source. Thus, the investigation of methanotrophy and the mechanisms that give methanotrophs the ability to selectively oxidize methane, will inform our understanding of methane

activation in our man-made world. Selectivity is a central issue in the biological milieu as well as the synthetic. The first reaction of methanotrophic metabolism is the selective conversion of methane to methanol, and incredibly, methanotrophic organisms carry out this process under the additional burden of the inherent toxicity of the product, methanol. As chemists we can appreciate the difficulty in generating a product that is more reactive than its predecessor, and methanotrophs achieve this goal while concomitantly monitoring the concentrations of reactants and products, and regulating their own metabolic pathways appropriately.

The molecular machine that carries out the unique chemistry of methane oxidation in all methanotrophic organisms is methane monooxygenase (MMO). The reaction catalyzed by this remarkable enzyme is shown below:

$$CH_4 + O_2 + H^+ + NADH \rightarrow CH_3OH + H_2O + NAD^+ \qquad (\mathbf{1})$$

	I	X	II
Cell Shape	Short rods	Cocci	Rod or Pear
Growth at 45°C	No	Yes	No
GC content	50-64	62.5	62.5
Membrane arrangement:			
Bundles of disks	Yes	Yes	No
Paired membranes parallel to cell periphery	No	No	Yes
Resting Stages			
Azotobacter cysts	Present	Present	Absent
Exospores	Absent	Absent	Present
HMP Pathway – 3-hexulose phosphate synthase	Present	Present	Absent
Serine Pathway -- hydroxypyruvate reductase	Absent	Present	Present
Ketoglutarate dehydrogenase and a complete TCA cycle	Absent	Absent	Present
Fixes elemental nitrogen, and has a Nitrogenase	Absent	Present	Present
Predominant phosholipid fatty acid	C-16	C-16	C-18
Autotrophic CO_2 fixation and ribulose bisphosphate carboxylase	Absent	Present	Absent

Table 1

Methanotrophs

While all methanotrophs express an MMO protein, whether or not all methanotrophs are indeed obligate methanotrophs is a point of some controversy in the literature. A very few species have been identified with more complicated metabolisms than that depicted in Scheme 1[3]. *Methylomonas* sp. Strain 761 is appears to contain a complete tricarboxylic acid cycle and variants of this strain have been grown on glucose[4]. However, this is a unique example, and the vast majority of methanotrophs utilize the central metabolism shown in Scheme 1 exclusively. Separations from the central metabolism help differentiate methanotrophs, as Type I

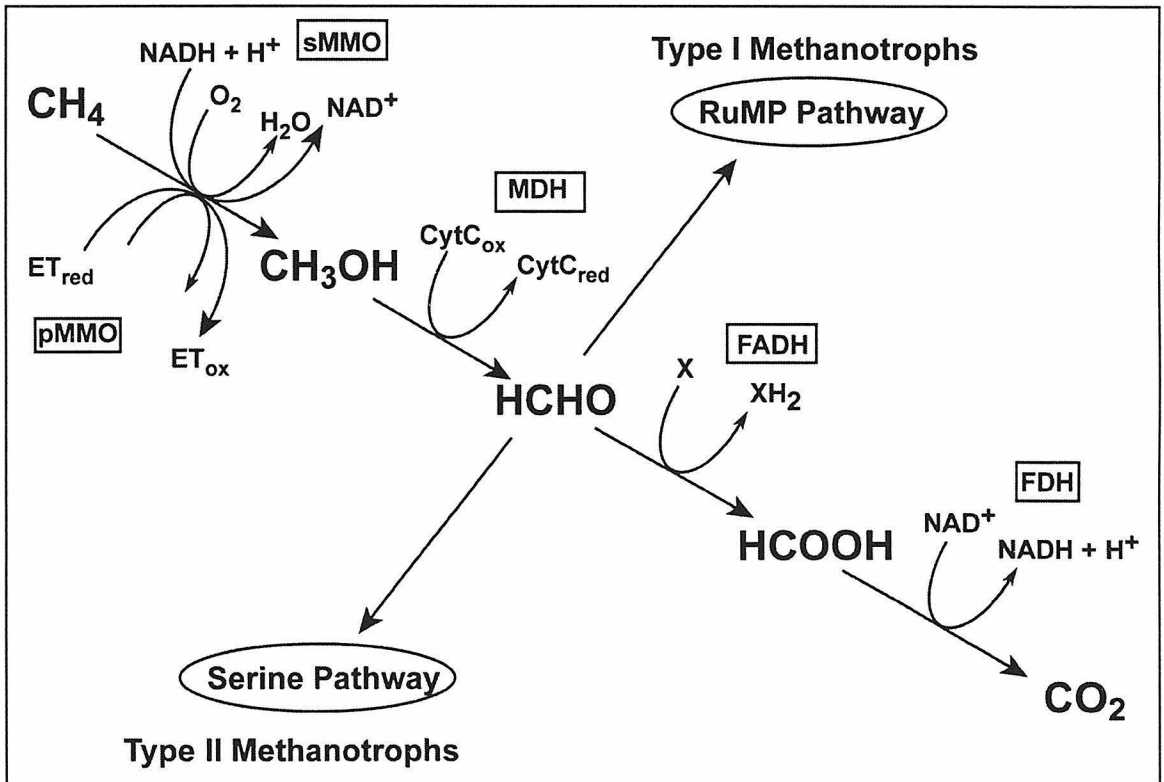

Scheme 1. Pathwways for the oxidation of methane and assimilation of formaldehyde. Abbreviations: CytC, cytochrome *c*; FADH, formaldehyde dehydrogenase; FDH, formate dehydrogenase; MDH, methanol dehydrogenase. Figure modified from Hanson and Hanson, *Mircobiol. Rev.* (1996) *60*(2), 439-471.

methanotrophs utilize the "RuMP Pathway" for carbon assimilation, and Type II methanotrophs use the "Serine Pathway[5]." Methanotrophs have several other characteristics which differentiate them into groups: intracytosolic membrane morphology, G+C content, 16s rRNA, and predominant phospholipid fatty acid are a few of these distinguishing characteristics. These and others are markers of methanotroph type and are listed in Table 1[6], and are used to differentiate Type I and II methanotrophs, as well as a smaller third group (Type X). Type X methanotrophs have some Type I characteristics and some Type II characteristics, and are exemplified by the organism studied in this dissertation, *Methylococcus capsulatus* (Bath).

The conversion of methane to methanol is the first step in the pathway of carbon assimilation for methanotrophic organisms. Subsequent transformation of methanol to formaldehyde by the periplasmic protein methanol dehydrogenase (MDH) allows for the branching of the energy and carbon pathways, as carbon is assimilated at the aldehyde level. Type I and II methanotrophs differ explicitly in the pathway they utilize for assimilation of formaldehyde. This branching, and the overall pathway(s) of carbon assimilation in methanotrophs is shown in Scheme 1.

As the development of new molecular tools allow for the identification of methanotrophs in environmental isolates, methanotrophs have recently been identified from frozen tundra[7], from thermal hotsprings, marine[8] and freshwater[9] systems, and soil sources. A new sense of diversity of methanotrophs cell biology and ecology is emerging from the increasing number of new species. Yet, while the number of new methanotrophs grows and their characteristics are elucidated, all

methanotrophs appear to produce particulate MMO, the membrane bound methane monooxygenase.

The search for methanotrophs, and the study of their unique metabolism, has been driven by a desire to utilize methanotrophy as a tool in environmental biodegradation as well as industrially significant hydroxylation reactions[10]. Many groups have pursued using whole cell cultures of methanotrophs as an active catalyst for the biodegradation of a variety of inert compounds[11-16]. Methanotrophs expressing sMMO have been found to be capable of co-metabolizing a large number of substrates, including the significant environmental pollutant trichloroethylene (TCE) [17-20]. The fastest reported rates for TCE degradation have been found for *Methylosinus trichosporium* OB3b, expressing sMMO. (As will be discussed in Chapter 7, pMMO does not display the same kind of proficiency at co-metabolism that is observed with sMMO, although *Methylosinus trichosporium* OB3b expressing pMMO has been found to successfully degrade TCE[20]). The potential for biodegrading otherwise inert, harmful compounds using either a native organism, a genetically modified strain, or individual proteins from methanotrophs is an exciting motivation for the study of MMO proteins.

Methane Monooxygenases- Lessons from History

The growth of the modern field of biological methane activation begins with initial experiments to identify the enzyme that catalyzed the methane oxidation chemistry of methanotrophs. Cellular sub-fractionation of *M. capsulatus* (Bath) revealed methane monooxygenase activity localized to either the soluble or the

membrane fraction. Ribbons and Michalover identified activity within the particulate (membrane) fraction of *Methylococcus capsulatus* (Texas), and subsequent work by others on *Methylomonas methanica* and *Methylosinus trichosporium* OB3b confirmed this[21-23]. Tonge and co-workers were able to liberate activity from the membranes fraction and described a methane monooxygenase system comprised of a CO-binding *c*-type cytochrome, a copper-binding protein, and a third, small protein[24]. However, these initial findings were promising only in that they spurred groups on to more insightful results. The preparation from Tonge and co-workers has been since found to be an artifact, and the next insight that pushed the field forward came from Colby and Dalton, that found growth conditions of *M. capsulatus* (Bath) which allowed methane monooxygenase activity to be detected in the soluble fraction of cell lysates[25]. Specifically, a soluble, or sMMO, protein was found to be expressed by *M. capsulatus* (Bath), and though it was not appreciated until significantly later, the expression of this enzyme was unique to *M. capsulatus* (Bath), as compared to other strains under study due to the growth conditions of the methanotrophs. The Dalton group went on to demonstrate that sMMO could be resolved into three components[26], and that individual components could be independently purified[27].

This is appreciated now in greater detail for the sMMO was discovered through a matter of fortune. On one hand, the sMMO protein is only expressed in a handful of species, whereas pMMO has been found in every methanotroph examined. Further, the expression of sMMO is linked intimately to the relative and absolute concentrations of copper and iron present in the growth conditions. In greater detail, sMMO can be expressed by *Methylococcus capsulatus* (Bath), *Methylosinus*

trichosporium OB3b, *Methylosinus sporium*, *Methylocystis* sp. M, and *Methylomonas methanica* 68-1[28]. And the presence of iron at sufficient levels, and copper at limiting levels are requisites for the expression of sMMO. The bioavailability of copper has been tied to the expression of pMMO[29], and it was found that copper also stimulated the growth of intracytosolic membranes by looking at micrographs of methanotroph thin-sections prepared over a time course of exposure to increased copper concentrations[30]. Simultaneously, a switch-over from the expression of sMMO polypeptides to pMMO polypeptides has been observed in correspondence to the alteration of the growth conditions from low to 5μM copper[31]. Since the time of these reports, it is has been quite clear that the successful expression of pMMO, the constituitively expressed methane monooxygenase, is tied to the presence of copper.

The impressive developments in the early 1980's demonstrated the separation of pMMO and sMMO, and some of the factors that govern their expression and comparative chemistries. While pMMO proved to be difficult to handle, and impossible to fully and reproducibly purify, the sMMO field has mushroomed since the detailed report of conditions for purification of the enzyme[32,33]. A slew of spectroscopic studies and biochemical studies has investigated the soluble protein from many different experimental techniques. Now thoroughly characterized, the three cytosol-soluble components of sMMO are a 250 kDa hydroxylase ($\alpha^2\beta^2\gamma^2$ subunits), a 39 kDa reductase, and a 16 kDa regulatory component (B) (*Methylococcus capsulatus* (Bath))[28]. The hydroxylase catalyzes reaction (**1**) at a binuclear Fe(II) site in either of its α subcomponents. X-ray crystal structures of the hydroxylase component from *M. capsulatus* (Bath) and from *Methylosinus*

trichosporium OB3b have been obtained, as well as NMR structures of component B from both species[34-36]. In terms of resting states of the enzyme, as well as intermediates formed during catalysis, sMMO has been well characterized chemically, biochemically and spectroscopically[37-45]. Mechanistic studies have used both steady-state and fast-time scale methods for spectroscopy[46-51], and have included a study of the product chemistry with chiral alkane[52,53]and radical clock substrates[54] and spectroscopic characterization of the various intermediates formed in its reaction with O_2[44,55]. The role of protein interactions between the sub-units of sMMO have always been appreciated, and recent studies have begun to examine the interactions between the three components of the sMMO enzyme system, and their motions are the subject of recent investigations[56,57].

In comparison to the barrage of papers on sMMO (and related dinuclear non-heme enzymes), pMMO has not benefited from the same level of attention, largely due to the difficulties associated with working with the protein. The sMMO problem has moved all the way from crude experiments on cell-lysates to state of the art spectroscopy looking at highly reactive reaction intermediates. The pMMO problem has not moved forward with such blistering pace, however. The next section will describe some of the analogous developments in the story of pMMO.

State of the pMMO Problem

The ongoing study of particulate methane monooxygenase has benefited from several different research efforts. Again, the pioneering work of Dalton and co-workers has led the way, establishing the connection between pMMO activity and copper concentration[29,31,58]. Since these early findings, and initial attempts to

solubilize the enzyme[59], the field suffered from a dearth of publications until the recent work began to appear from the Chan group at Caltech. Initial studies from Chan and co-workers have analyzed pMMO from *Methylococcus capsulatus* (Bath), and in particular, the copper centers associated with pMMO as well as the protein components themselves[60]. Initial studies of membrane fractions that contain the protein revealed the protein exists as the primary constituent of the membranes, and elemental analysis suggested that there is ~15 copper ions bound per protein unit[61]. Magnetic susceptibility and electron paramagnetic resonance (EPR) experiments suggested that the copper ions of the protein were best described as a series of trinuclear copper clusters[61]. Further developments from Chan and co-workers have utilized a combination of EPR and X-ray Absorption Spectroscopy (XAS) to probe the oxidation state of the copper ions of pMMO, and this has led to the proposed model of the protein in which the copper ions are separated into catalytically active clusters (C-clusters) and those that serve another function, possibly electron transfer[62]. Indeed, subsequent studies have demonstrated the key catalytic role for copper in the protein[63,64]. A further study utilizing pulsed EPR and electron spin echo envelop modulation (ESEEM) experiments that there must be at least two histidine residues present at the active site of pMMO[65] (a finding that will be discussed below as Chapter 5 of this dissertation).

Developments from the Chan group have also approached the reactivity of pMMO, both focusing on the regio- and stereoselectivity of the product chemistry that is available to pMMO[66] as well as mechanistic studies using chiral ethanes[67]. Together these experiments have drawn a picture of the reactivity of pMMO, which

suggests that the enzyme proceeds by a concerted mechanism for the small substrates (such as methane) which are exclusively selected for hydroxylation.

A final effort from the Chan group has produced a reproducible preparation for the purified pMMO protein, and this has confirmed many of the suggestions made previously regarding metal content, sub-unit composition, and reactivity with oxidants[68].

Because of the above findings in pMMO protein chemistry, further developments in pMMO genetics have been possible. N-terminal sequences generated from pMMO polypeptides were proven to be key components in the successful cloning and complete sequencing of the first two *pmo* genes, *pmoA* and *pmoB*[69]. Other reports from the molecular biology community have demonstrated conclusively that copper acts as a reciprocal transcriptional activation agent, simultaneously down-regulating the expression of sMMO, and activating pMMO[70]. And evidence has developed for an evolutionary relationship between pMMO and an analogous system found in ammonia-oxidizing bacteria, AMO[71].

For the considerable progress that has been made on understanding various aspects of pMMO, other investigators have proposed some alternative findings. The work of DiSpirito and co-workers has also generated a purified pMMO preparation from *M. capsulatus* (Bath)[72]. The DiSpirito preparation does contain a large number of copper ions associated with it, but DiSpirito has suggested these are mostly bound by small copper-binding cofactors, small peptide-derived organic molecules a few hundred daltons in size that bind several copper ions each[73]. Further, DiSpirito utilizes observations of pMMO-mediated NO chemistry as evidence for a constituent

iron atom associated with the pMMO active site[72]. Neither of these findings is consistent with the Chan group model, and regarding the copper-binding cofactors, no other group has reported a similar finding to date.

Okura and co-workers have focused their attention on the pMMO from *Methylosinus trichosporium* OB3b[74-79]. It shares most of the properties of the pMMO preparation described by the Chan group, including the same compliment of copper ions, their suggested involvement in catalysis, and the ESEEM findings which point to histidine ligation at the active site. The Okura preparations do appear to contain some iron as well, and have observable EPR signals in the g=6 and g=4.3 regions, which are interpreted as indications of a high-spin iron atom associated with the protein[78]. As the iron signal is reported to decrease somewhat after the enzyme reacts with the suicide substrate acetylene, it was suggested that the iron play a role in the enzyme active site.

As the above summary suggests, there are few experiments currently discussed in the literature that bring true insight to the pMMO problem. The general pieces are there: copper plays a significant role, iron may be involved in some fashion, investigations of product chemistry reveal what the enzyme is capable of, but the equivalent spectroscopic studies as have been witnessed for sMMO are not forthcoming. This is due to the difficulty in measuring bulk properties for such a large number of metal centers, and the difficulty in handling pMMO itself, which is marked by a lability of activity. However, the disparity between the reported preparations, and the need to unravel the complexity of pMMO, are strong motivators for the

development of new methodologies for understanding multi-copper metalloproteins, and pMMO in particular.

The generation of such novel, insightful experiments are the principal aims of this Thesis, and are discussed in an overview below.

Overview and Aims of this Thesis

This dissertation represents a body of work that has attempted to address some of the confusion regarding pMMO. Perhaps the biggest issue regarding the protein is the matter of attempting to understand the difference between the copper ions of the protein. All findings point to a large number of pMMO-specific copper ions, but very rare are the experiments that cleanly produce novel insights specific to any copper site. This dissertation represents the state of the problem, and represents work with which addresses that very issue.

Chapter 2 builds upon the previously explored model of the C- and E-clusters and their differential ability to react with chemical oxidants. In it, an attempt to specifically probe the C-clusters due to potential interactions with dioxygen and suicide-substrate inhibitors is explored. As a result of this study, novel properties regarding the reaction of pMMO with acetylene were discovered, and several new insights into the nature of the pMMO copper ions were elucidated.

Chapter 3 deals with the chemical modification of pMMO, returning to the role of ferricyanide as a chemical oxidant for the copper ions associated with the protein. It is found that ferricyanide specifically interacts with a number of sites on pMMO's solvent-accessible surface, and undergoes a facile electron transfer reaction

with the reduced copper ions of the protein, forming a ferrocyanide adduct with accessible copper-ions. The precise nature and location of the copper ions are not known, but can be mapped to the physical structure of pMMO as determined by lability after treatment with proteolytic enzymes. A further experiment utilizes a pre-treatment of pMMO with EDTA, a chelator that has been shown to specifically remove a sub-set of copper ions. It is shown that ~40% of the copper ions are specifically retained by the protein, and those that are retained are protected from treatment with ferricyanide – indicating that they are effectively buried in the transmembrane domains of pMMO.

Due to the obvious complexity of the pMMO system, and what may be viewed as the inability for spectroscopy alone to answer questions about the many copper ions of pMMO, Chapter 4 represents a new study that attempts to harness the power of molecular biological techniques to answer some of the pressing questions regarding pMMO. In it, PmoA is examined explicitly, as it is thought to contain the acetylene binding site, and therefore, at least a considerable portion of the pMMO active site. In a collaboration with Mary Lidstrom of the University of Washington, previously sequenced fragments of *pmoA* genes were assembled, and double-stranded DNA sequences of *pmoA* which represent the N-terminal and C-terminal domains (previously unsequenced) were achieved. These sequences allow for a study of the homology within PmoA and AmoA sequences, and reveal several candidates for copper binding residues within the protein.

Chapter 5 returns to spectroscopy, and refocuses on what can be learned about the pMMO active site on the basis of knowledge gained in the first two sections.

Specifically, pulsed EPR-Electron Spin Echo Envelop Modulation (ESEEM) and Electron Nuclear Double Resonance (ENDOR) spectroscopies are used to reveal features of the pMMO C-clusters, those copper ions that specifically oxidize in the presence of dioxygen. The study positively identifies well-resolved histidine residues at the active site. Also, the identity of this site is partially confirmed by the existence of an exchangeable water molecule, a characteristic one would consider a necessary feature from a site that carries out dioxygenase chemistry. From the findings of Chapters 3, 4 and 5, it is quite clear that pMMO's active site is indeed located at the crux of the membrane-periplasm interface, in a buried pocket that is inaccessible to ferricyanide ion.

Whereas the initial chapters of this dissertation mainly consider the question "What are the nature of the copper ions of pMMO?", the final two chapters more intimately attempt to assess "How does pMMO work?" Chapter 6 considers the role pMMO plays as an enzyme that binds and activated dioxygen, by specifically considering the chemistry of the enzyme initiated by the dioxygen mimic, nitric oxide. This work initially began as a means to demonstrate that a dioxygen analog does indeed bind to a copper-based active site, but instead led to the presented below. As described in Chapter 6, nitric oxide appears to bind to an adventitious iron atom associated with pMMO, and that the iron atom in question does not appear to have relevance to pMMO catalysis.

The final chapter continues the examination of reactivity by considering not dioxygen, but hydrocarbon substrates. Chapter 7 examines the regio- and stereospecificity of pMMO epoxidation and hydroxylation chemistry. The efficacy of

suicide substrate inhibitors, all alkynes, is also considered in this chapter. The results of this study of the product (and inhibition) chemistry of pMMO builds a spatial model for the active site of the enzyme, based on the steric constraints that were observed for reactants and products.

References Cited

1)Cicerone, R. J.; Oremland, R. S. *Global Biogeochem. Cycles* **1988**, *2*, 299-327.

2)Reeburgh, W. S.; Whalen, S. C.; Alperin, M. J. *The Role of Methylotrophy in the Global Methane Budget*; Murrell, J. C. and Kelly, D. P., Ed.; Intercept: Andover, Hampshire, U.K., 1992, pp 1-14.

3)Hanson, R. S.; Hanson, T. E. *Microbiol. Rev.* **1996**, *60*, 439-471.

4)Zhao, S.; Hanson, R. S. *Appl. Environ. Microbiol.* **1984**, *48*, 807-812.

5)Anthony, C. *The Biochemistry of Methylotrophs*; Academic Press: London, 1982.

6)Hanson, R. S.; Netrusov, A. I.; Tsuji, K. *The Obligate Methanotrophic Bacteria Methylococcus, Methylomonas, and Methylosinus*; Balows, A., Truper, H. G., Dworkin, M., Harder, W. and Schleifer, K.-H., Ed.; Springer-Verlag: New York, 1992; Vol. III, pp 2350-2364.

7)Omel'chenko, M. V.; Vasil'eva, L. V.; Zavarzin, G. A.; Savel'eva, N. D.; Lysenko, A. M.; Miyushina, L. L.; Khmelenina, V. A.; Trotsenko, Y. A. *Microbiology (Russ.)* **1996**, *65*, 339-343.

8)Murrell, J. C.; McDonald, I. R.; Bourne, D. G. *Fems Microbiology Ecology* **1998**, *27*, 103-114.

9)Costello, A. M.; Lidstrom, M. E. *Applied and Environmental Microbiology* **1999**, *65*, 5066-5074.

10)Higgins, I. J.; Best, D. J.; Hammond, R. C. *Nature* **1980**, *286*, 561-564.

11)Aziz, C. E.; Georgiou, G.; Speitel, G. E. *Biotechnology and Bioengineering* **1999**, *65*, 100-107.

12)Sullivan, J. P.; Dickinson, D.; Chase, H. A. *Critical Reviews in Microbiology* **1998**, *24*, 335-373.

13)Sutfin, J. A.; Ramey, D. *Environmental Progress* **1997**, *16*, 287-296.

14)Uchiyama, H.; Kato, C.; Kokufuta, E.; Yagi, O. *Environmental Technology* **1997**, *18*, 1123-1131.

15)Chang, W. K.; Criddle, C. S. *Biotechnology and Bioengineering* **1997**, *56*, 492-501.

16)Moran, B. N.; Hickey, W. J. *Applied and Environmental Microbiology* **1997**, *63*, 3866-3871.

17)Oldenhuis, R.; Vink, R. L. J. M.; Janssen, D. B.; Witholt, B. *Appl. Environ. Microbiol.* **1989**, *55*, 2819-2826.

18)Oldenhuis, R.; Janssen, D. B. *Degradation of Tricholorethylene by Methanotrophic Bacteria*; Murrell, J. C. and Kelly, D. P., Ed.; Intercept: Andover, Hampshire, U.K., 1993, pp 121-133.

19)Brusseau, G. A.; Tsien, H.-C.; Hanson, R. S.; Wackett, L. P. *Biodegradation* **1990**, *1*, 19-29.

20)Lontoh, S.; Semrau, J. D. *Applied and Environmental Microbiology* **1998**, *64*, 1106-1114.

21)Ferenci, T. *FEBS Lett.* **1974**, *11*, 94-97.

22)Ribbons, D. W.; Michalover, J. L. *FEBS Lett.* **1970**, *11*, 41-44.

23)Tonge, G. M.; Harrison, D. E. F.; Knowles, C. J. *FEBS Lett.* **1975**, *58*, 293-299.

24)Tonge, G. N.; Harrison, D. E. F.; Higgins, I. J. *Biochem. J.* **1977**, *161*, 333-344.

25)Colby, J.; Dalton, H. *Biochem. J.* **1976**, *157*, 495-497.

26)Colby, J.; Dalton, H. *Biochem. J.* **1978**, *171*, 461-468.

27)Woodland, M. P.; Dalton, H. *J. Biol. Chem.* **1984**, *259*, 53-59.

28)Lipscomb, J. D. *Annual Review of Microbiology* **1994**, *48*, 371-399.

29)Stanley, S. H.; Prior, S. D.; Leak, D. J.; Dalton, H. *Biotechnology Letters* **1983**, *5*, 487-492.

30)Prior, S. D.; Dalton, H. *J. Gen. Microbiol.* **1985**, *131*, 155-163.

31)Burrows, K. J.; Cornish, A.; Scott, D.; Higgins, I. J. *J. Gen. Microbiol.* **1984**, *130*, 3327-3333.

32)Fox, B. G.; Lipscomb, J. D. *Biochemical and Biophysical Research Communications* **1988**, *154*, 165-170.

33)Fox, B. G.; Froland, W. A.; Dege, J. E.; Lipscomb, J. D. *Journal of Biological Chemistry* **1989**, *264*, 10023-10033.

34)Rosenzweig, A. C.; Brandstetter, H.; Whittington, D. A.; Nordlund, P.; Lippard, S. J.; Frederick, C. A. *Proteins-Structure Function and Genetics* **1997**, *29*, 141-152.

35)Elango, N.; Radhakrishnan, R.; Froland, W. A.; Wallar, B. J.; Earhart, C. A.; Lipscomb, J. D.; Ohlendorf, D. H. *Protein Science* **1997**, *6*, 556-568.

36)Walters, K. J.; Gassner, G. T.; Lippard, S. J.; Wagner, G. *Proceedings of the National Academy of Sciences of the United States of America* **1999**, *96*, 7877-7882.

37)Dalton, H.; Wilkins, P. C.; Deighton, N.; Podmore, I. D.; Symons, M. C. R. *Faraday Discussions* **1992**, 163-171.

38)DeRose, V. J.; Liu, K. E.; Lippard, S. J.; Hoffman, B. M. *Journal of the American Chemical Society* **1996**, *118*, 121-134.

39)Dewitt, J. G.; Rosenzweig, A. C.; Salifoglou, A.; Hedman, B.; Lippard, S. J.; Hodgson, K. O. *Inorganic Chemistry* **1995**, *34*, 2505-2515.

40)Fox, B. G.; Hendrich, M. P.; Surerus, K. K.; Andersson, K. K.; Froland, W. A.; Lipscomb, J. D.; Munck, E. *Journal of the American Chemical Society* **1993**, *115*, 3688-3701.

41)Kauffmann, K. E.; Popescu, C. V.; Dong, Y. H.; Lipscomb, J. D.; Que, L.; Munck, E. *Journal of the American Chemical Society* **1998**, *120*, 8739-8746.

42)Paulsen, K. E.; Liu, Y.; Fox, B. G.; Lipscomb, J. D.; Munck, E.; Stankovich, M. T. *Biochemistry* **1994**, *33*, 713-722.

43)Pulver, S. C.; Froland, W. A.; Lipscomb, J. D.; Solomon, E. I. *Journal of the American Chemical Society* **1997**, *119*, 387-395.

44)Shu, L. J.; Nesheim, J. C.; Kauffmann, K.; Munck, E.; Lipscomb, J. D.; Que, L. *Science* **1997**, *275*, 515-518.

45)Willems, J. P.; Valentine, A. M.; Gurbiel, R.; Lippard, S. J.; Hoffman, B. M. *Journal of the American Chemical Society* **1998**, *120*, 9410-9416.

46)Deeth, R. J.; Dalton, H. *Journal of Biological Inorganic Chemistry* **1998**, *3*, 302-306.

47)Froland, W. A.; Andersson, K. K.; Lee, S. K.; Liu, Y.; Lipscomb, J. D. *Journal of Biological Chemistry* **1992**, *267*, 17588-17597.

48)Jiang, Y.; Wilkins, P. C.; Dalton, H. *Biochimica Et Biophysica Acta* **1993**, *1163*, 105-112.

49)Lee, S. Y.; Lipscomb, J. D. *Biochemistry* **1999**, *38*, 4423-4432.

50)Liu, Y.; Nesheim, J. C.; Paulsen, K. E.; Stankovich, M. T.; Lipscomb, J. D. *Biochemistry* **1997**, *36*, 5223-5233.

51)Valentine, A. M.; Stahl, S. S.; Lippard, S. J. *Journal of the American Chemical Society* **1999**, *121*, 3876-3887.

52)Priestley, N. D.; Floss, H. G.; Froland, W. A.; Lipscomb, J. D.; Williams, P. G.; Morimoto, H. *Journal of the American Chemical Society* **1992**, *114*, 7561-7562.

53)Valentine, A. M.; Wilkinson, B.; Liu, K. E.; KomarPanicucci, S.; Priestley, N. D.; Williams, P. G.; Morimoto, H.; Floss, H. G.; Lippard, S. J. *Journal of the American Chemical Society* **1997**, *119*, 1818-1827.

54)Valentine, A. M.; LeTadic-Biadatti, M. H.; Toy, P. H.; Newcomb, M.; Lippard, S. J. *Journal of Biological Chemistry* **1999**, *274*, 10771-10776.

55)Liu, K. E.; Valentine, A. M.; Qiu, D.; Edmondson, D. E.; Appelman, E. H.; Spiro, T. G.; Lippard, S. J. *Journal of the American Chemical Society* **1995**, *117*, 4997-4998.

56)Gallagher, S. C.; Callaghan, A.; Zhao, J.; Dalton, H.; Trewhella, J. *Biophysical Journal* **1999**, *76*, A117-A117.

57)Gassner, G. T.; Lippard, S. J. *Biochemistry* **1999**, *38*, 12768-12785.

58)Prior, S. D.; Dalton, H. *Journal of General Microbiology* **1985**, *131*, 155-163.

59)Drummond, D.; Smith, S.; Dalton, H. *European Journal of Biochemistry* **1989**, *182*, 667-671.

60)Chan, S. I.; Nguyen, H.-H. T.; Shiemke, A. K.; Lidstrom, M. E. *Studies Toward Characterization of Methane Monooxygenase*; Murrell, J. C. and Kelly, D. P., Ed.; Intercept: Andover, Hampshire, U.K., 1993, pp 93-107.

61)Nguyen, H. H. T.; Shiemke, A. K.; Jacobs, S. J.; Hales, B. J.; Lidstrom, M. E.; Chan, S. I. *Journal of Biological Chemistry* **1994**, *269*, 14995-15005.

62)Nguyen, H. H. T.; Nakagawa, K. H.; Hedman, B.; Elliott, S. J.; Lidstrom, M. E.; Hodgson, K. O.; Chan, S. I. *Journal of the American Chemical Society* **1996**, *118*, 12766-12776.

63)Semrau, J. D.; Zolandz, D.; Lidstrom, M.; Chan, S. I. *J. Inorg. Biochem.* **1995**, *58*, 235-244.

64)Cook, S. A.; Shiemke, A. K. *J. Inorg. Biochem.* **1996**, *64*, 273-284.

65)Elliott, S. J.; Randall, D. W.; Britt, R. D.; Chan, S. I. *Journal of the American Chemical Society* **1998**, *120*, 3247-3248.

66)Elliott, S. J.; Zhu, M.; Tso, L.; Nguyen, H. H. T.; Yip, J. H. K.; Chan, S. I. *Journal of the American Chemical Society* **1997**, *119*, 9949-9955.

67)Wilkinson, B.; Zhu, M.; Priestley, N. D.; Nguyen, H. H. T.; Morimoto, H.; Williams, P. G.; Chan, S. I.; Floss, H. G. *Journal of the American Chemical Society* **1996**, *118*, 921-922.

68)Nguyen, H. H. T.; Elliott, S. J.; Yip, J. H. K.; Chan, S. I. *Journal of Biological Chemistry* **1998**, *273*, 7957-7966.

69)Semrau, J. D.; Chistoserdov, A.; Lebron, J.; Costello, A.; Davagnino, J.; Kenna, E.; Holmes, A. J.; Finch, R.; Murrell, J. C.; Lidstrom, M. E. *J. Bacteriol.* **1995**, *177*, 3071-3079.

70)Nielsen, A. K.; Gerdes, K.; Murrell, J. C. *Mol. Microbiol.* **1997**, *25*, 399-409.

71)Holmes, A. J.; Costello, A.; Lidstrom, M. E.; Murrell, J. C. *Fems Microbiology Letters* **1995**, *132*, 203-208.

72)Zahn, J. A.; DiSpirito, A. A. *Journal of Bacteriology* **1996**, *178*, 1018-1029.

73)DiSpirito, A. A.; Zahn, J. A.; Graham, D. W.; Kim, H. J.; Larive, C. K.; Derrick, T. S.; Cox, C. D.; Taylor, A. *Journal of Bacteriology* **1998**, *180*, 3606-3613.

74)Takeguchi, M.; Miyakawa, K.; Okura, I. *BIOMETALS* **1998**, *11*, 229-234.

75)Takeguchi, M.; Miyakawa, K.; Okura, I. *JOURNAL OF MOLECULAR CATALYSIS A-CHEMICAL* **1998**, *132*, 145-153.

76)Takeguchi, M.; Ohashi, M.; Okura, I. *BIOMETALS* **1999**, *12*, 123-129.

77)Takeguchi, M.; Yamada, T.; Kamachi, T.; Okura, I. *BIOMETALS* **1999**, *12*, 27-33.

78)Takeguchi, M.; Miyakawa, K.; Okura, I. *JOURNAL OF MOLECULAR CATALYSIS A-CHEMICAL* **1999**, *137*, 161-168.

79)Takeguchi, M.; Fukui, K.; Ohya, H.; Okura, I. *Chemistry Letters* **1999**, 617-618.

Chapter 2: X-ray Absorption Spectroscopy of Redox-poised Particulate Methane Monooxygenase

Abstract

EXAFS spectroscopy was used to probe specific redox-poised preparation of particulate methane monooxygenase (pMMO). The fully reduced enzyme is best modeled by an average 3-4 coordinate Cu(I) with one heavy (Cl/S) ligand at ~2.3 Å, as well as a distant atom(s) at 2.7 Å. The identity of this distant atom is unclear. Membranes on isolation in air have only ~30% Cu(II), according to both K-edge and EPR spin quantitation. Extended exposure of membranes to O_2 results in up to ~60% oxidation of the coppers, significant attenuation in the amplitudes of the ~2.3 Å and ~2.7 Å Cu···ligand scattering interactions, and inactivation of the enzyme. By contrast, turnover with O_2 and acetylene results in the near complete oxidation of the copper ions and their conversion to a Cu(II)-like geometry with no evidence of Cu···S/Cl or Cu···Cu interactions. Together, these findings demonstrate the reactivity of the copper-based active site, and imply that suicide substrate inactivation disrupts the normal chain of events in pMMO catalysis.

Introduction

Particulate methane monooxygenase (pMMO) is the membrane-bound biochemical machinery that all methanotrophic bacteria can produce and utilize for the initial oxidation of methane to methanol by the following reaction.

$$CH_4 + O_2 + H^+ + NADH \rightarrow CH_3OH + H_2O + NAD^+ \qquad (1)$$

Bacterial methane oxidation plays a significant role in the global carbon cycle and while synthetic methane oxidation has proven to be a difficult task for chemists, the biological equivalent occurs at ambient temperatures and pressures readily. The pMMO system is constitutive expressed by obligate methanotrophs. In the few species that are capable of expressing a soluble methane monooxygenase (sMMO), pMMO expression is activated by the presence of micromolar copper concentrations[1-4]. The link between copper-content and pMMO expression and activity has been studied heavily to date. Murrell and co-workers have elucidated a reciprocal transcriptional regulation system for *pmo* and

mmo genes (which code for pMMO and sMMO, respectively) which show the activation of *pmo* genes and the inhibition of *mmo* genes upon incubation with copper[5]. More generally, copper content has also been correlated to the formation of the intracytosolic membranes which house pMMO[6], and to the MMO activity of the intracytosolic membranes[3]. Finally, copper has been directly linked to pMMO protein content and activity in membrane fractions from *Methylococcus capsulatus* (Bath)[7,8]. In terms of the ability of pMMO to binding copper ions, pMMO has uniformly been found to bind a large number of copper ions: the *M. capsulatus* (Bath) is found to possess 12-15[9], and *Methylosinus trichosporium* OB3b was found to bind 12.8 copper ions[10]. In all cases, there is significant variation from preparation to preparation.

The vast bulk of the copper ions associated with pMMO, as isolated in highly enriched membrane fragments, exist in an EPR-silent state. Recently we have discerned that this phenomena can be quantitatively accounted for by the reduced copper (Cu(I)) ions bound by the protein. Therefore, there seems to be little contribution from other arrangements of copper ions, such as the antiferromagnetically coupled Type III bi-nuclear Cu(II) centers. Previously, we have successfully differentiated the many reduced copper ions of pMMO based upon their reactivity with the oxidants dioxygen and ferricyanide ion. Through the correlation between features in the X-ray Absorption edge (a particularly useful tool for quantifying the existence of Cu(I) and Cu(II) simultaneously) and liquid helium temperature X-band EPR spectroscopy, it was conclusively determined that of the ~15 copper ions of pMMO, a sub-set of ~6 copper ions are readily oxidized by dioxygen, and that all 15 are oxidized upon treatment with millimolar concentrations of ferricyanide. Together, these findings led to the proposal of

dividing the copper ions of pMMO into clusters that are either synonymous with catalysis and dioxygen chemistry ("C-clusters") and those that are involved in other processes, potentially electron-transfer chemistry ("E-clusters"). This chemical distinction has been utilized in a pulsed-EPR study of the C-cluster copper ions of pMMO, which is the subject of Chapter 5. Both the previous study as well as Chapter E of this work illustrate the essential difficulty in any spectroscopic study of the copper ions of pMMO: as spectroscopic data represents a sampling of all potentially detectable species, the large number of copper ions bound by pMMO severely complicates the interpretation of data, due to variability within the sampled population. Without outstanding, unique spectroscopic features that can be easily detected from the background of other copper-related signals, it is very difficult to assess, specifically and accurately, the meaning and identity of spectroscopic features.

As a way of attempting to differentiate the properties of the copper ions of pMMO further still, the current study expands on prior work with the x-ray absorption K-edge to include analysis of the Extended X-ray Absorption Fine Structure (EXAFS). From the EXAFS, information on the average Cu site structure, including possible ligand types, coordination number, and average Cu-ligand distances, is obtained. In some cases, evidence for the arrangement of metals into clusters can also be obtained. As all of the copper ions associated with pMMO contribute to the x-ray absorption spectrum, structural information derived from EXAFS will reflect the average ligand environment of the total Cu population. Therefore, while the information is expected to be general in nature, we present experiments that are designed to represent discreet steps in the reaction cycle of pMMO. Thereby, comparison of the data from one preparation with another can

be considered in terms of discreet changes in the copper ions of pMMO, and it is presumed that proceeding in this manner will yield conclusions specific to particular sub-sets of copper ions of pMMO, such as the C-clusters.

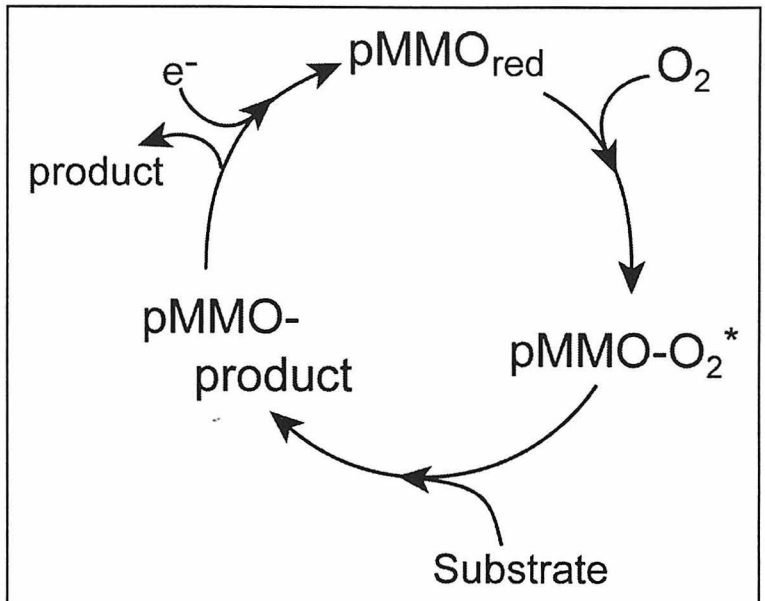

Figure 1. A schematized view of the pMMO catalytic cycle.

K-edges and EXAFS were analyzed for pMMO membranes prepared under a variety of conditions, in order to probe for condition-dependent changes in the structural environment of the pMMO copper ions. Considering a very simple version of pMMO catalysis, depicted in Figure 1, one can think of starting with fully reduced enzyme ($pMMO_{red}$) and proceeding to add dioxygen, which can form one product, or adding dioxygen and substrate, which go on to generate products. In accord with this general scheme, spectra were measured for membranes prepared with the copper ions redox poised in the fully reduced state. This then serves as a beginning point to represent the "resting" enzyme in the catalytic cycle. In order to attempt to probe the C-clusters specifically, spectra were also measured for membranes exposed independently to each of the two types of co-substrates of pMMO: O_2 and a hydrocarbon substrate, and to both co-substrates together. Currently it is not known whether *in vivo* dioxygen binding and activation precedes

hydrocarbon binding and activation, though it is presumed that independent dioxygen activation is possible in pMMO.

To probe the affect of hydrocarbon at the active site of pMMO, we have opted to use a suicide substrate in order to attempt to trap the C-cluster in a redox-poised state. Acetylene is a well-known suicide substrate for pMMO and it has been suggested that in the presence of O_2, the suicide substrate is activated, forming unstable species (such as a ketene) which is then covalently attacked by nucleophilic amino-acid side-chains within the enzyme active site[1,11]. The protein is then rendered irreversibly inactivated, and the active site copper ions are presumed to be trapped in an oxidized state. If binding of suicide substrates does indeed occur near Cu centers, they may be detectable in the EXAFS. The suicide substrates acetylene and 3-bromopropyne were used, with the latter used to see if the heavy halogen label could be detected and therefore positioned by the spectrum.

Results obtained from this series of experiments are far from unraveling the complex environment of the many coppers in pMMO. However, they do provide evidence for Cu···S/Cl and unique long-range (~2.7 Å) Cu···ligand interactions in the reduced state, features that are lost upon oxidation. Reaction with O_2 and suicide substrate results in near complete conversion of the membrane-associated coppers to Cu(II), suggesting that the majority of these coppers are indeed involved in O_2/hydrocarbon reactivity. Structural consequences of this reaction are presented in detail.

Materials and Methods

Growth of Methanotrophs.

The organisms used in the studies were maintained on Petri plates containing Nitrate Mineral Salts (NMS) medium with added $CuSO_4$ (20 μM) and solidified with 1.7% agar. Cultures were maintained under an atmosphere of 20% methane in air, and streaked onto fresh plates every 4-6 weeks. Large-scale cultures were grown in 300 mL batches in 2 L Erlenmeyer flasks using the above medium, a 20% methane-in-air atmosphere, and continual shaking; or, they were grown in a fermentor containing 8 L of the above described medium with added 30 μM $CuSO_4$ and 20 μM CuEDTA. Each batch was inoculated with a culture grown to late-log phase. *M. capsulatus* (Bath) was grown at 42°C. Cells were harvested in late-log phase (typically 48-52 hours after inoculation) by centrifugation at 15,000 rpm in a SS-34 Beckman rotor for 15 minutes, washed once with 20 mM Pipes (pH 7.2), and re-suspended in the Pipes buffer.

Membrane Isolation.

Cytosolic and membrane fractions were separated by passing a cell suspension (~0.5 g wet weight of cells per mL) three times through a French pressure cell at 20,000 psi. Un-lysed cells and cell debris were removed by centrifugation at 15,000 rpm for 40 minutes. The supernatant was then ultracentrifuged at 60,000 rpm for 90 minutes to pellet the membrane fraction. The clear supernatant obtained after ultracentrifugation was used as the cytosolic fraction. The membrane pellet was washed by suspending it in 0.25 N NaCl in 20 mM Pipes (pH 7.2) using a Dounce homogenizer. The membrane fraction was repelleted by ultracentrifugation and resuspended in a volume of 20 mM Pipes buffer (pH 7.2) equivalent to the volume of the original cell suspension. This process was repeated

one or two more times until the supernatant was virtually free of heme-containing soluble proteins and/or soluble protein as determined by absorption at 280 nm and 412 nm.

MMO Activity Assay.

The MMO activity of samples was measured by the propene epoxidation assay. For whole cell assays, sodium formate was used as a reductant; for membrane fractions the reductant was NADH. In both cases, the reductant was added to the cell or membrane suspensions to give a final concentration of 5 mM in a total volume of 1.0 mL. The assay was performed at 42°C, and at ~5-7 minute intervals a 1 μL aliquot of the solution was removed and injected directly onto a gas chromatograph (Carbograph 60/80 mesh, AllTech) at 165°C for chemical analysis. The propene oxide produced from the propene epoxidation reaction catalyzed by the pMMO was detected by flame ionization. The activity of the pMMO was determined from the limiting initial slope of a propene oxide concentration versus time plot. Specific activity was then obtained by dividing the activity by the total amount of protein in the sample determined by the Lowry method. A small volume of 100 mM $CuSO_4$ was added to a number of samples in order to assay the activity of the pMMO in the presence of excess copper.

Sample Preparations and Redox Poising.

Fully-reduced samples were prepared by treating the membrane suspensions with dithionite or a dye (thionein) under anaerobic conditions as described previously. Additionally, an anaerobic isolation procedure using non-sulfur-containing NADH as a reductant was used. The "as-isolated" pMMO membranes were prepared by either rapidly preparing membrane fragments from *M. capsulatus* (Bath) using de-oxygenated buffers and no external reductants. Alternatively, a "fully reduced" preparation was

prepared by purging repeatedly with dioxygen-free argon, mixing anaerobically with de-oxygenated dithionite solution (20 mM dithionite in 20 mM Pipes, pH = 7.2) and repelleting.

Re-oxidized samples were prepared by treating de-oxygenated membranes with dithionite (5 mM) anaerobically, followed by re-exposing the suspension to air with vigorous shaking for 10 minutes or less (in the absence of hydrocarbon co-substrate). The reduction and re-oxidation processes were monitored by EPR spectroscopy.

Inhibited samples were prepared as follows: a large scale (10 mL) assay mixture as described above was prepared without the addition of propylene. In replacement of propylene, either 1 mL acetylene gas was injected into the serum vial headspace, or 5 μL of liquid alkyne (3-bromo-propyne, Aldrich) was injected into the assay mixture as a 50% dimethylsulfoxide (DMSO) solution. The DMSO was found to be required for solubility of the alkyne, and did not affect the inhibition of pMMO. These preparations were then incubated at 42°C until the inhibition was complete (more than 2h). For those samples that were treated with hydrocarbon suicide substrate anaerobically, membrane preparations and buffers were first degassed thoroughly by several pump and purge cycles and were then taken into an anaerobic chamber, where they were diluted into a serum vial with an appropriate amount of NADH. The vial was then sealed, and subsequently incubated at 42°C.

The reduced, "as-isolated," re-oxidized, and inhibited membranes were pelleted immediately upon their preparations and resuspended in de-oxygenated glycerol (50%) and/or buffer for EPR and x-ray absorption measurements. Multiple samples for each

experimental condition were prepared and their data measured, to check for reproducibility.

Elemental Analysis.

Copper concentrations were determined chemically by induced-coupled plasma mass spectrometry (ICP-MS). An aliquot (~250 µl) of the sample was digested in neat, Redistilled Nitric Acid (GFS Chemicals) and digested at room temperature for 1 hr. This was then diluted to 0.1% nitric acid with ultra-pure water, and the resulting diluted sample was assessed for copper content. Copper concentrations were determined with comparison to a reference curve constructed using standards of 2.5 mM to 150 mM in copper concentration (0.1% nitric acid), which were prepared by dilution of a commercially available standard (GFS Chemicals). Measurements were repeated in order to ensure reproducibility.

EPR Spectroscopy.

EPR spectra were recorded on a Varian E-line Century X-band spectrometer. In the EPR experiments, sample temperature was maintained at 77 K with a liquid nitrogen dewar, and at 4.2 K with an ESR-900 Oxford Instruments (Oxford, England) liquid helium cryostat. The EPR samples were prepared by sealing 200 µL of membrane suspensions under an atmosphere of Ar in quartz EPR tubes at a total protein concentration of ~50 mg/mL (~0.53 mM in 94 kDa protein) in 20 mM Pipes (pH 7.2). Following preparation of the samples, the membrane fractions were rapidly frozen in liquid nitrogen. Quartz EPR tubes equipped with a septum port were used in anaerobic reductive experiments. Solutions of freshly prepared sodium dithionite were purged with argon and added anaerobically to the sample with a gas-tight Hamilton syringe. The

concentration of the dithionite solution was determined by spectrophotometric titration with ferricyanide (ε_{420nm} = 1,010 $M^{-1}cm^{-1}$). Spin quantitation of the samples was carried out precisely as described previously[12].

XAS Data Collection.

Samples of pMMO-enriched membranes were prepared as frozen glasses (50% degassed glycerol added) in 1 or 2 mm thick lexan cells with x-ray transparent Mylar windows. X-ray absorption spectra were measured on unfocused wiggler beamline 7-3 at the Stanford Synchrotron Radiation Laboratory (SSRL), with the ring operating at 3 GeV and 50-100 mA. Samples were maintained at 10 K inside an Oxford Instruments CF-1208 liquid helium continuous flow cryostat. A Si(220) double-crystal monochromator was used, detuned 50% at 9684 eV in order to minimize contamination of the radiation by higher harmonics. Vertical 1 mm pre-monochromator slits defined the beam size, minimizing divergence and allowing for an energy resolution of ≤1-1.7 eV at the Cu K-edge. K-edge and EXAFS data were measured, for all samples, over the energy range 8660-9684 eV. Protein spectra were collected in fluorescence mode, using either a Lytle detector (an ion chamber equipped with a nickel filter and Soller slits) or a 13 element Ge detector (Canberra). The spectrum of Cu foil was collected concomitantly, allowing for internal energy calibration of the spectra (first inflection point energy of the Cu foil spectrum was set to 8980.3 eV). Multiple (15-30) scans over the complete energy range were averaged for each sample. Data were truncated at k =13 $Å^{-1}$ due to interference from absorption at the Zn edge (9659 eV), as is commonly seen in biological samples. Fourier transforms (FT) of EXAFS data were made over the range k = 3-13 $Å^{-1}$. This range was also used in all fits to EXAFS data. In addition a sample of solid

$[Cu(II)(imidazole)_4](NO_3)_2$ was prepared according to published methods, ground with BN, and pressed into a 1 mm aluminum sample plate for measurement. Data were measured under the same conditions specified but in the transmission mode, over the energy range k = 3-16 $Å^{-1}$ (6 scans averaged).

XAS Data Analysis.

For each spectrum, a smooth second-order polynomial was fit to the pre-edge region, then extrapolated and subtracted from the data. A three-segment spline (polynomial curves of orders 2, 3, and 3) was fit and subtracted from the EXAFS region, and the data normalized at 9000 eV, using the SPLINE program. EXAFS data were then k^3-weighted, where the photoelectron wave vector $k = [2m_e/(E - E_0)/\hbar^2]^{1/2}$, E = energy, E_0 = the energy of onset of the EXAFS, and m_e = the mass of an electron. The general expression used to model the EXAFS $\chi(k)$ in the single-scattering approximation is:

$$x(k) = \sum_s \frac{N_s A_s(k) S_0^2}{k R_{as}^2} \exp(-2R_{as}/\lambda(k)) \exp(-2k^2\sigma_{as}^2) \cdot \sin(2k R_{as} + \varphi_{as}(k)) \qquad (2)$$

Each sinusoidal contribution to the total EXAFS describes the scattering interaction between the absorbing atom (a) and a set of equivalent backscatterers (s) and the sum is carried out over all of these sets. N_s is the number of equivalent backscatters at a distance R_{as} from the photoabsorbing atom, $A_s(k)$ is the backscattering amplitude function for a given atom type, S_0^2 is the many-body amplitude reduction factor, $\lambda(k)$ is the photoelectron mean free path, σ^2_{as} is the Debye-Waller factor (modeling both thermal and static disorder) for a given a···s interaction, and $\phi_{as}(k)$ is a function describing variations in the phase of each sinusoidal component contributing to the total EXAFS. Phase and amplitude functions ($\varphi_{as}(k)$ and $A_s(k)$) calculated by *feff* version 7.0 were used in creating

a simulated EXAFS spectrum, which was adjusted by a least-squares fitting process to match the data (using the EXAFSPAK programs by Dr. G. N. George, SSRL, which utilize the public domain MINPAK fitting library). Several different structural models were used as input for calculating $\varphi_{as}(k)$ and $A_s(k)$, depending on the types of backscatterers postulated by a given fit. In a given fit, R_{as} and σ^2_{as} were varied for each equivalent set of backscattering atoms. Since σ^2_{as} and N_s are correlated variables (*i.e.*, both modulate the EXAFS amplitude, though in functionally different ways), it is not possible to determine the value of either one independently. However, fitting data for crystallographically defined Cu(I) and Cu(II) complexes provides a means for broadly estimating reasonable values for σ^2_{as}, for a given type of scatterer. Coordination numbers (*i.e.*, N_s) were therefore in general varied at intervals of 0.5, and were chosen based on the combined reasonability of the associated σ^2_{as} and the overall goodness of the fit. Coordination numbers here therefore have an error bar of at least ± 0.5, as is typical for EXAFS measurements.

Other parameters included in the fits were E_0 and S_0^2. E_0 was allowed to vary within ranges defined by fits to crystallographically characterized Cu(I) and Cu(II) complexes. S_0^2 was allowed to vary between 0.9 and 1. Fits were constructed in a building-up process, where components to the fit were included on the basis of visual improvement to the EXAFS fit, chemical reasonability of non-structural parameters (*e.g.*, the various σ^2_{as} factors), and reduction in a goodness-of-fit parameter, $R = [\Sigma k^6(\chi_{obs} - \chi_{calc})^2/Nk^6]^{1/2}$, where N = the number of points in the EXAFS spectrum, χ_{obs} is the observed spectrum, and χ_{calc} is the fitted simulated spectrum.

Detailed analyses of outer-shell scattering were made for selected data sets (see Results and Analysis). These included analyses of Fourier-filtered data, which are presented in Supplementary Information. Investigations of multiple scattering (MS) contributions to data were also made for several samples. Criteria used in selecting MS pathways for fits are described below.

Results

Fully Reduced pMMO.

In order to investigate what is presumed to be the active, "resting-state" of pMMO, we have attempted to generate a variety of "fully reduced" preparations, presuming that they will mimic a naturally occurring state of pMMO. Fully reduced samples were prepared in three ways. The first two treatments involved the use of excess chemical reductant: one case utilized 25 mM dithionite ($E^{o\prime}$ = -0.527 V vs SCE), and in another case the large, non-coordinating reductant thionein ($E^{o\prime}$ = 0.064 V vs SCE). To minimize any potential artefacts due to the addition of an exogenous reductant, we also isolated a third sample, pMMO-enriched membranes isolated and prepared anaerobically in the presence of 0.5 mM NADH ($E^{o\prime}$ = -0.320 V vs SCE). K-edge and EXAFS spectra from all three preparations are highly similar (Figure 2), suggesting that their Cu site-structures are similar. EXAFS data for all three preparations were fit, producing indistinguishable results. The analysis that follows is for data collected on the anaerobically isolated membranes, as these data were the least noisy and as the samples were prepared in the absence of exogenous sources of sulfur.

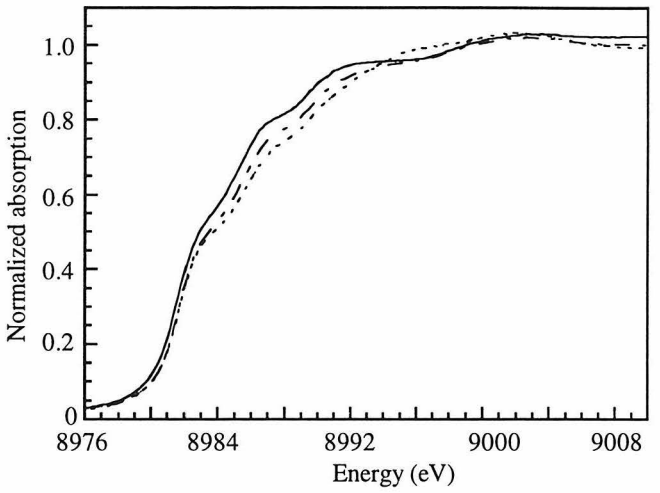

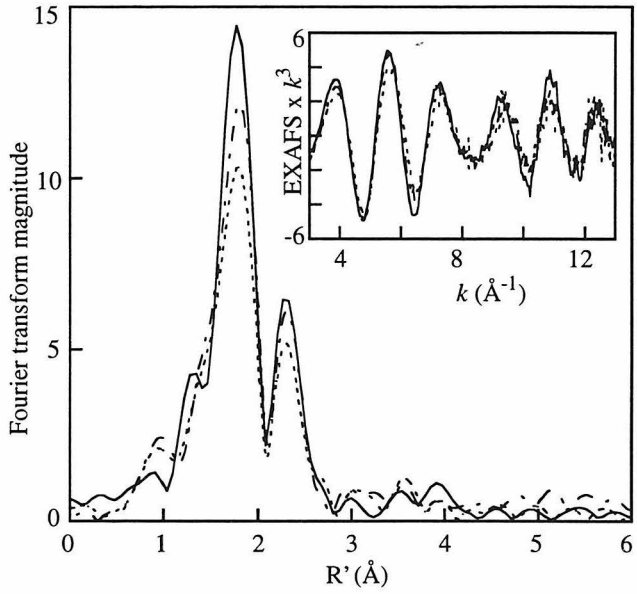

Figure 2. Comparison of Cu K-edge (top), Fourier transform (bottom), and EXAFS (bottom, inset) data for three fully reduced samples: membranes prepared by anaerobic isolation with NADH (solid line), treated with excess dithionite (dot-dash line), and treated with excess thionein (dashed line). Data from all three preparations are nearly identical.

K-edges for all three samples indicate that the Cu in each is largely or entirely Cu(I) (Table 1). Consistent with these results, the samples lack any appreciable EPR signal (Table 1). The edge shape is quite telling, and indicates a large presence of Cu(I)

by the 1s→4p transition observed at 8984 eV, a characteristic energy observed for Cu(I). The 1s→4p transition is additionally an indicator of the average Cu(I) site geometry. The 1s→4p transition for reduced pMMO appears as a very weak shoulder on the rising edge, consistent with transitions observed for non-planar trigonal, trigonal pyramidal, or tetrahedral Cu(I) complexes.

EXAFS data for reduced pMMO consist of an intense oscillatory pattern (Figure 2), indicative of homogeneity within the sample. Inhomogeneity would likely cause dampening of the EXAFS signal due to deconstructive interference. The Fourier transform (FT) of the EXAFS consists of two peaks – a broad peak centered at 1.9 Å and a smaller peak at 2.4 Å. There are no further prominent peaks at longer distances in the FT, such as the prominent double peaked structure typically observed at ~2.8-3.5 Å due to Cu-imidazole (histidine-derived) scattering. Although ESEEM spectroscopy on oxidized membranes has indicated the presence of histidine ligands, as will be discussed

Table 1. Summary and description of XAS samples used

condition	sample	description	%Cu(II) (EPR / XAS)[a]
redox poised	fully reduced	membranes treated with excess (25 mM) dithionite	0 / 0
		membranes treated with excess (25 mM) thionein	0 / 0
		anaerobically isolated membranes in 5 mM NADH	0 / 0
O_2 exposed	as isolated in air	membranes as isolated in air, in 5 mM NADH	30 / 30
	poised turnover with O_2	membranes fully reduced (50 mM dithionite) then air exposed, 10 minutes	30 / 30
	O_2 saturated/inactivated	membranes exposed to pure O_2, 2 hours	60 / 60
suicide substrate exposed	excess acetylene (anaerobic)	anaerobically isolated membranes in 5 mM NADH and treated with excess acetylene	0 / 0
O_2 and suicide substrate exposed	excess acetylene (in air)	aerobically isolated membranes in 5 mM NADH and treated with excess acetylene	70 / 70
	excess 3-Br-propyne (in air)	aerobically isolated membranes in 5 mM NADH and treated with excess 3-bromo-propyne	70 / 80

[a] Approximate error bars for either measurement are ± 10%

in Chapter 5 of this dissertation, evidence of imidazole scattering does not appear in the fully reduced spectra. A small pair of peaks at ~3.6 Å and ~3.9 Å are observed in all three FTs, distances likely too long to be ascribed to imidazole scattering.

The first FT peak corresponds to scattering from nearest-neighbor ligands. Several different structural models to account for near-neighbor contributions to the data were considered (Table 2A, Figure 3). The raw (unfiltered) data are poorly fit by a single set of equivalent oxygen/nitrogen ligands (fit 1-1, Figure 3, Table 2A). Including two sets of O/N ligands greatly improves the fit, but an unreasonably large number of near-neighbors (*i.e.*, $\geq$ 5) is then required (fit 2, Fig. 3, Table 2). This result suggests that a heavy atom may contribute to the exceptionally strong scattering from the first coordination sphere. Fits including a sulfur/chloride ligand fit the data well, with the remaining 2-3 ligands modeled as O/N (fit 3, Fig. 4, Table 2). Because of strong inverse correlations between the Debye-Waller factor and coordination number, coordination numbers typically cannot be deduced to better than ± 20% from EXAFS data. A coordination number of 1 S/Cl ligand per Cu produced better fits than coordination numbers of 0.5 or 1.5, and so was used. The Cu···S/Cl distance refines to ~2.3 Å. Several different configurations were proposed for the remaining 2-3 O/N ligands, either grouping them as equivalent or splitting them into two inequivalent groups. Splitting this contribution into two groups gave somewhat better fits to the data, and also yielded Debye-Waller factors more consistent with those typically determined for coordinated ligands in model complexes. The best fit of the nearest-neighbor ligands of the fully-reduced samples included 0.5 O/N at 1.90 Å, 2.0 O/N at 2.11 Å, and 1.0 S/Cl at 2.32 Å (fit 4, Fig. 3, Table 2).

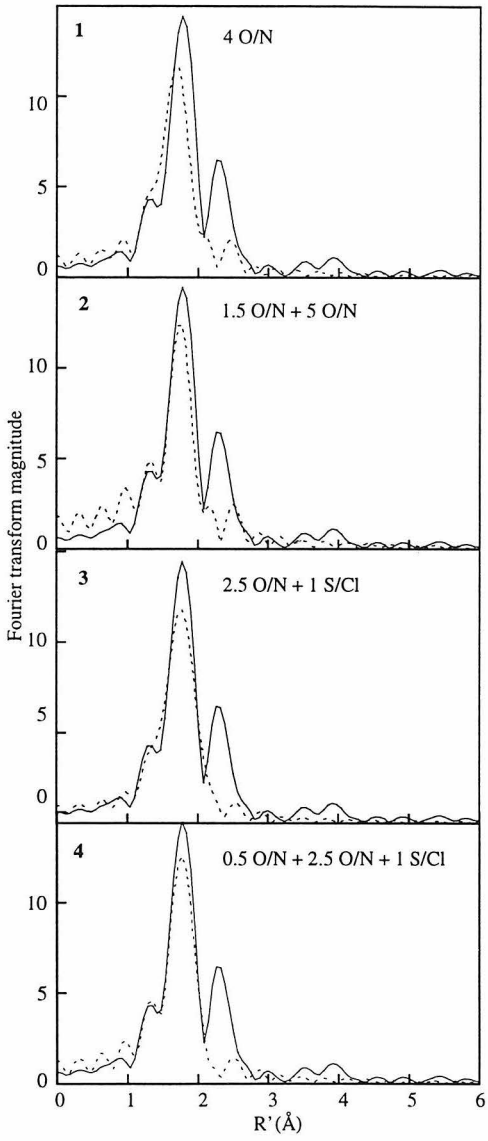

Figure 3. Fourier transform (solid line) and fits 1-4 to data (dashed lines) for fully reduced pMMO membranes (anaerobically isolated in 5 mM NADH). Successive fits show the effect of varying the coordinated ligands in the structural model, and the substantial improvement afforded by inclusion of a heavy sulfur ligand. Structural parameters refined in these fits are summarized in Table 2A.

The second FT peak corresponds to scattering from more distant (outer-shell) ligands. This peak is fairly intense and occurs at an unusually short distance in the non-

phase-corrected FT. Its origin is not obvious. Several structural models that might account for it were considered. Fit 4 to the near-neighbor ligand set (Fig. 3, Table 2A) was used as a starting point in each case where fits were extended to include the more distant scatterers (fits 5-10, Fig. 4, Table 2B). When near-neighbor absorber-scatterer distances and Debye-Waller factors were allowed to vary in fits 5-10, they did not deviate significantly from values determined in fit 4. E_0 and S_0^2 were allowed to vary within prescribed ranges, as described previously. Metalloproteins frequently have metal···carbon scattering contributions to their EXAFS; the outer-shell scattering was therefore first modeled by a single Cu···C scattering component (fit 5, Fig. 4, Table 2B). This fit reproduces the data well, but requires a large number of carbons (5 per Cu) at a very short distance (2.70 Å). Outer-shell scattering might also be due to a heavier atom. Fits employing either Cu···S or Cu···Cu scattering components were tried. These fits likewise predicted short metal···backscatterer distances of 2.84 Å and 2.70 Å for 1 S and 0.5 Cu, respectively (fits 6 and 7, Fig. 3, Table 2). Whether C, S, or Cu is used as the backscatterer, the goodness-of-fit parameter (*R*) is not substantially different. However, visual inspection suggests that fits employing 1 S or 0.5 Cu as backscatterers are somewhat poorer. The FT data illustrate this point most clearly (Fig. 3, fits 5-7).

Table 2A. Results of Fits to EXAFS data for Fully Reduced pMMO-Enriched Membranes : Near-Neighbors

sample	fit	Cu···O/N CN[a]	Cu···O/N R^b (σ^2)[c]	Cu···O/N CN	Cu···O/N R (σ^2)	Cu···S/Cl CN	Cu···S/Cl R (σ^2)	E_0 (eV)	R (%)[d]
Fully-reduced (**1**) :	**1-1**	4.0	2.13 (0.004)					8990.0	64.0
anaerobically	**1-2**	1.5	1.92 (0.006)	5.0	2.13 (0.004)			8991.9	52.6
isolated	**1-3**	2.5	2.12 (0.005)			1.0	2.29 (0.004)	8990.9	51.3
	1-4	0.5	1.90 (0.001)	2.5	2.11 (0.002)	1.0	2.32 (0.004)	8990.1	48.1
Fully-reduced (**2**) :	**2-4**	0.5	1.90 (0.001)	2.5	2.11 (0.002)	1.0	2.32 (0.004)	8990.1	48.1
excess dithionite									
Fully-reduced (**3**) :	**3-4**	0.5	1.90 (0.001)	2.5	2.11 (0.002)	1.0	2.32 (0.004)	8990.1	48.1
excess thionein									

Table 2B. Results of Fits to EXAFS data for Fully Reduced pMMO-Enriched Membranes : Outer-Shell Included [†]

sample	fit	Cu···C CN[a]	Cu···C R^b (σ^2)[c]	Cu···S/Cl CN	Cu···S/Cl R (σ^2)	Cu···Cu CN	Cu···Cu R (σ^2)	Cu···C CN	Cu···C R (σ^2)	E_0 (eV)	R (%)[d]
Fully-reduced (**1**)	**1-5**	5.0	2.70 (0.003)							8990.8	21.2
anaerobically	**1-6**			1.0	2.84 (0.002)					8989.5	24.3
isolated	**1-7**					0.5	2.70 (0.002)			8991.4	25.1
	1-8[e]	5.0	2.70 (0.003)					3.0	3.10 (0.005)	8990.7	16.7
								2.0	3.29 (0.004)		
	1-9[e]			1.0	2.84 (0.002)			4.0	3.20 (0.004)	8990.8	16.9
								2.0	3.39 (0.004)		
	1-10[e]					0.5	2.70 (0.002)	3.0	3.15 (0.003)	8990.7	18.6
								3.0	3.32 (0.004)		
Fully-reduced (**2**)	**2-10**					0.5	2.70 (0.002)	3.0	3.15 (0.004)	8990.7	18.6
excess dithionite								3.0	3.32 (0.004)		
Fully-reduced (**3**)	**3-10**					0.5	2.70 (0.002)	3.0	3.15 (0.004)	8990.7	18.6
excess thionein								3.0	3.32 (0.004)		

[a] Number of equivalent ligands of the given type. [b] Absorber-scatterer distance in Å. [c] Debye-Waller factor: approximately equal to bond variance, if bond distance distribution is assumed to be Gaussian. [d] Goodness-of-fit parameter, where $R = [\Sigma k^6(\chi_{obs} - \chi_{calc})^2/Nk^6]^{1/2}$ (N = number of points in EXAFS spectrum). [e] These fits are roughly equivalent in quality.
[†] First shell fit **4** from Table 2A is used to model the coordinated ligands in each of these fits.

Deficiencies in the Cu···S or Cu···Cu fits, as well as the near-featurelessness of the FT above R' ≈ 2.8 Å (not phase corrected) suggested the possible involvement of additional, and potentially destructively interfering, outer-shell scattering components. Metal···C scattering at ≥3 Å commonly contributes to the EXAFS of metals in proteins,

resulting in small peaks at R' ≈ 2.5-3.5 Å in the non-phase-corrected FT. Consequently, additional Cu···C scattering components were added to the fits to determine their effects (Table 2, Fig. 4, fits 8-10). Adding a single Cu···C scattering component to each fit did not afford significant improvement (data not shown). Adding a pair of Cu···C scattering components, by contrast, allowed for marked improvement, particularly in the fits employing heavier scatterers (S or Cu) in the outer shell. Fits using C, S, or Cu as the primary (most strongly contributing) backscatterer in the outer shell produced indistinguishably good fits when these additional Cu···C components were included. The Cu···C distances refined to ~3.1-3.2 Å and 3.3-3.4 Å. Both are biologically reasonable Cu···C separations. A representative best-fit is presented in Figure 5.

pMMO after Reaction with O_2.

The ability of pMMO to interact with dioxygen was probed next, as a precursor to investigating the interaction with substrate. In order to investigate the dioxygen-oxidized regime, two different samples were used: those which had been exposed to air in the isolation process, and those that had been further treated under pure O_2 for two hours. The latter treatment results in the loss of activity of pMMO, but does allow for the further oxidation of copper ions associated with the protein.

Figure 6A depicts Cu K-edges for fully-reduced membranes (anaerobically isolated, 5 mM NADH), for membranes as-isolated in air, and for membranes kept under pure O_2 pressure for two hours (with consequent irreversible loss of enzyme activity). Figure 6B shows the Fourier Transforms (FTs) of the EXAFS for these three samples. The three data sets illustrate the effects of successively increasing exposure to O_2. Data were also measured for membranes after full reduction followed by brief exposure (~10 min.) to air in the absence of substrate. K-edge and EXAFS data for these reoxidized

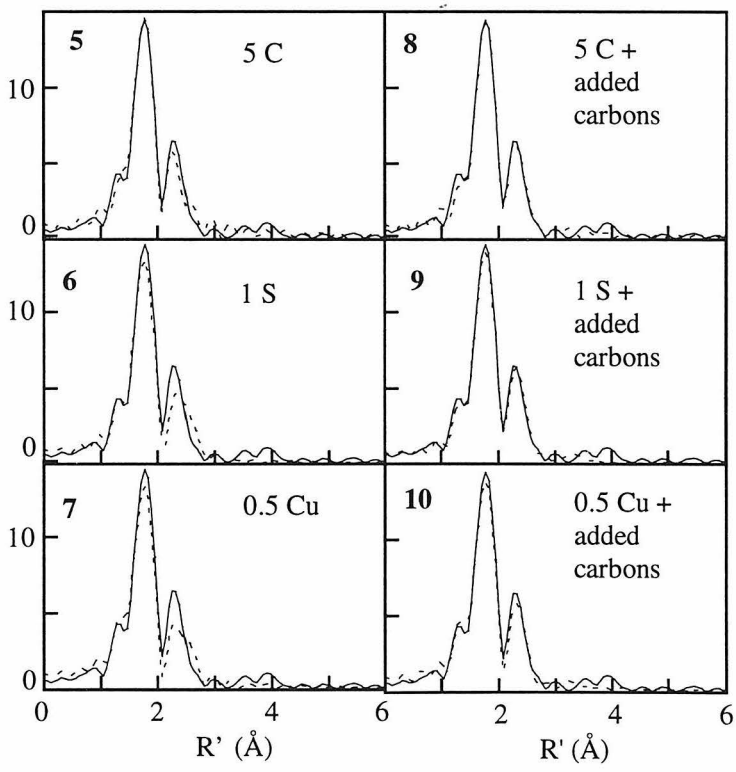

Figure 4. Fourier transform (solid line) and fits 5-10 to data (dotted lines) for fully reduced pMMO membranes (anaerobically isolated). Fits 5-7 employ one primary absorber-backscatterer interaction in simulating the second FT peak. Fits 8-10 demonstrate the improvement in the second peak simulations when scattering from carbon atoms at >3 Å is included. Structural parameters refined in these fits are summarized in Table 2B.

samples and for aerobic as-isolated samples are effectively identical (data not shown). Data for the as-isolated samples are discussed.

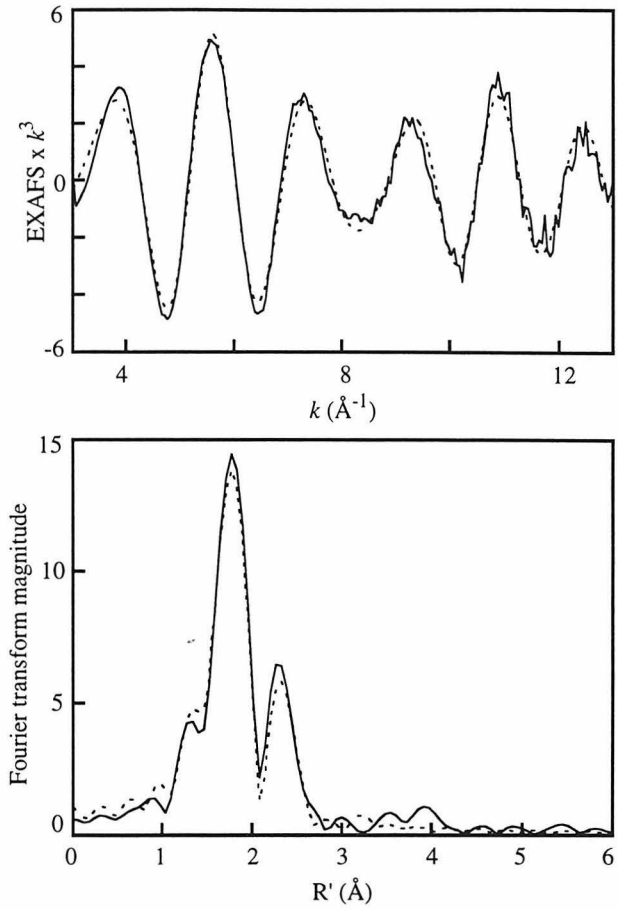

Figure 5. Representative best-fit to data for fully-reduced pMMO membranes (anaerobically isolated, 5 mM NADH). Top: EXAFS data. Bottom: Fourier transform. Data are presented as solid lines and fits as dotted lines. Structural parameters refined in this fit are included in Table 2A, fit 1-4 **(coordinated ligands) and Table 2B, fit** 1-10 **(outer-shell ligands). Modeling the outer shell according to fits** 1-8 **or** 1-9 **resulted in data simulations indistinguishable from the one presented here.**

Based on the K-edge data, it is quite clear that the treatments sucessfully oxidize pMMO copper ions. The characteristic Cu(I) ~8984 eV 1s→4p transition in the K-edge decreases in intensity, as indicated by the arrow to the left in Figure 6A. A shoulder at ~8987 eV also decreases in intensity, and the edge absorbance maximum moves from ~8992 eV to ~8996 eV, narrowing to form a sharper peak with a secondary peak at 9001 eV (see arrow, Figure 6A). The three edge spectra share an isosbestic point at ~8993 eV, indicating the conversion of one species into another species. The edge maximum has been ascribed to multiple scattering (MS) between the metal and its nearest neighbors (separated by a

distance R). Its energy position is approximately proportional to 1/R. Hence the higher energy edge maximum in the more oxidized samples reflects their shift toward shorter average metal-ligand distances, i.e., the edge reveals more Cu(II) character. Finally, prior K-edge and EPR-spin-quantitation estimates of the %-Cu(II) in these samples correlated well, suggesting that the Cu(II) formed is all EPR active, and does not exists as an antiferromagnetically coupled (and hence EPR-silent) Cu(II) center.

Effects of increasing O_2 exposure are also evident in the FTs for these three samples. Whereas the first FT peak for the fully-reduced sample is intense and centered at ~1.9 Å, this peak is broadened, flattened, and split, in the analogous FT for the air-oxidized sample. This reflects distinct groups of long and short Cu-ligand distances in the first coordination sphere of the pMMO copper ions in this mixed valence sample. In particular, the region of the FT peak corresponding to contributions from the ~2.3 Å Cu···S/Cl interaction appears to diminish (Figure 6B, left-most arrow). The first FT peak for the O_2–inactivated sample, by contrast, is a narrow peak centered at $R' \approx 1.4$ Å, suggesting greater conversion to an average copper geometry characterized by Cu(II)-like, short Cu-ligand distances. At the same time, the outer-shell peak at 2.4 Å is diminished in the air-isolated sample, and is nearly absent in data for the O_2–inactivated sample (Figure 6B, center arrow). Small peaks at ~2.7 Å, ~3.1 Å, and ~3.5 Å also appear above the noise level (indicated by the FT intensity at $R' \geq 4$ Å) in spectra for as-isolated and O_2–inactivated samples (Figure 6B, right-most arrow). Peaks at ~2.8 Å and ~3.5 Å are characteristically seen in FTs for Cu(II)-imidazole complexes (see below).

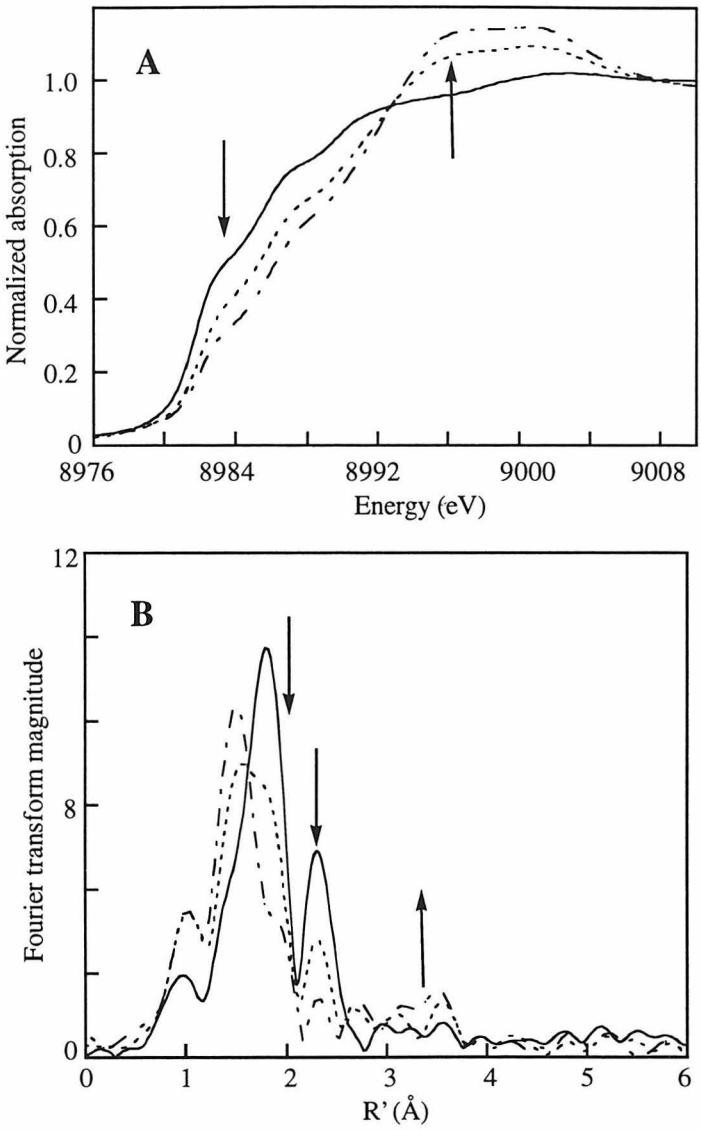

Figure 6. Comparison of Cu K-edge (A) **and Fourier transform** (B) **data for fully reduced pMMO membranes (solid lines), membranes as-isolated in air (dotted lines), and membranes after 2h O_2 exposure (O_2-inactivated) (dot-dash lines). Arrows indicate the direction of changes in the spectra on increasing O_2 exposure of the coppers.**

Table 3A. Results of Fits to EXAFS data for O_2-Exposed pMMO-Enriched Membranes : Near-Neighbors

sample	fit	Cu···O/N CN[a]	Cu···O/N R^b (σ^2)[c]	Cu···O/N CN	Cu···O/N R (σ^2)	Cu···S/Cl CN	Cu···S/Cl R (σ^2)	E_0 (eV)	R (%)[d]
As-isolated in air	**1**	4.0	2.07 (0.009)					8993.0	55.3
	2	2.0	1.98 (0.003)	2.0	2.13 (0.003)			8992.9	49.3
	3	1.3	1.97 (0.003)	2.0	2.10 (0.003)	0.7	2.31 (0.005)	8991.9	44.1
Reduced/reoxidized	**1**	4.0	2.07 (0.011)					8995.9	57.8
(in air)	**2**	2.0	1.98 (0.002)	2.0	2.14 (0.003)			8993.0	48.5
	3	1.3	1.97 (0.003)	2.0	2.10 (0.003)	0.7	2.31 (0.005)	8992.0	44.2
O_2-inactivated	**1**	4.0	2.03 (0.009)					8992.2	49.6
	2	2.0	1.98 (0.001)	2.0	2.13 (0.002)			8993.2	39.0
	3	1.6	1.96 (0.001)	2.0	2.09 (0.002)	0.4	2.33 (0.004)	8993.1	40.7

Table 3B. Results of Fits to EXAFS data for O_2-Exposed pMMO-Enriched Membranes : Outer-Shell Included †

sample	fit	Cu···C CN[a]	Cu···C R^b (σ^2)[c]	Cu···S/Cl CN	Cu···S/Cl R (σ^2)	Cu···Cu CN	Cu···Cu R (σ^2)	Cu···C (long) CN	Cu···C (long) R (σ^2)	E_0 (eV)	R (%)[d]
As-isolated in air	**4**	2	2.69 (0.004)							8993.0	35.1
	5			0.7	2.83 (0.004)					8991.8	34.4
	6					0.35	2.68 (.004)			8991.8	35.6
	7	2	2.69 (0.004)					2.0	3.91 (0.005)	8993.2	32.8
	8			0.7	2.83 (0.004)			2.0	3.91 (0.005)	8991.9	32.1
	9					0.35	2.68 (.004)	2.0	3.91 (0.005)	8991.9	33.7
	10					0.35	2.68 (.004)	2.0	3.14 (0.006)	8992.8	32.9
								2.0	3.91 (0.005)		
Reduced/	**4**	2	2.69 (0.003)							8992.9	32.5
reoxidized	**5**			0.7	2.83 (0.004)					8991.9	32.3
(in air)	**6**					0.35	2.67 (.004)			8991.8	36.7
	7	2	2.69 (0.003)					2.0	3.90 (0.004)	8992.8	31.9
	8			0.7	2.82 (0.004)			2.0	3.89 (0.004)	8991.9	29.8
	9					0.35	2.68 (.004)	2.0	3.90 (0.004)	8991.8	33.0
O_2-inactivated	**4**							2.0	3.92 (0.004)	8993.5	34.8
	5							1.0	3.07 (0.006)	8993.5	32.8
								2.0	3.92 (0.004)		

[a] Number of equivalent ligands of the given type. [b] Absorber-scatterer distance in Å. [c] Debye-Waller factor: approximately equal to bond variance, if bond distance distribution is assumed to be Gaussian. [d] Goodness-of-fit parameter, where $R = [\Sigma k^6(\chi_{obs} - \chi_{calc})^2/Nk^6]^{1/2}$ (N = number of points in EXAFS spectrum). [e] These fits are roughly equivalent in quality.
† For each sample, first shell fit **3** from Table 3A is used to model the coordinated ligands in each of these fits.

Results of fits to EXAFS data for the as-isolated and O_2-inactivated samples are given in Tables 2 and 3, respectively. Prior K-edge and EPR-spin-quantitation analyses

concurred that the as-isolated sample contains ~30% Cu(II). The EXAFS data were well fit by assuming a ~70% weighted contribution from the ~2.3 Å Cu···S/Cl and outer-shell ~2.7 Å Cu···Cu/C/S scattering components measured for the fully reduced pMMO (*e.g.*, 0.7 S/Cl and 0.35 Cu). The 30% Cu(II) fraction of the sample has the added effect of reducing the average Cu···O/N bond lengths slightly, from 2.08 Å to 2.06 Å. The O_2-inactivated sample was previously determined to have ~60% Cu(II). EXAFS data were fit well by assuming a ~40% weighted contribution of the ~2.3 Å Cu···S/Cl interaction (0.4 S/Cl per Cu). The inclusion of a Cu···Cu scattering interaction did not improve the fit to the data. Because of the heterogeneity (mixed Cu(I)/Cu(II)) of the as-isolated and O_2-inactivated samples, their EXAFS data are somewhat amplitude damped relative to EXAFS of the homogeneous, fully-reduced sample (Figures 2, 7, and 6). Fits to the EXAFS for these mixed-species are consequently somewhat approximate. Fractional coordination numbers in particular are difficult to determine with accuracy. The coordination numbers used produce good fits with Debye-Waller factors comparable to those obtained in fits to homogeneous fully-reduced samples, but are subject to at least the typically observed error bar of ± 20% for EXAFS-derived coordination numbers.

Outer-shell scattering was most prominent in the FT for the O_2-inactivated samples (peaks at ~2.8 Å and ~3.5 Å). Two Cu···C scattering components could be added to the fits for these data: 1 C at 3.07 Å and 4 C at 3.92 Å. These distances are comparable to those determined from fits to $[Cu(II)(imidazole)_4](NO_3)_2$ (see below).

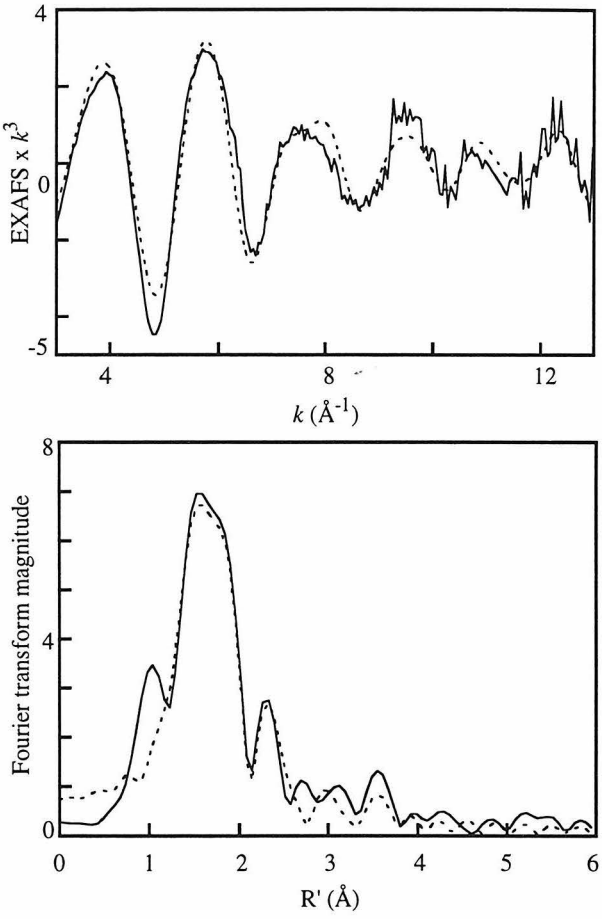

Figure 7. Representative best-fit to data for pMMO membranes as-isolated in air. Top: EXAFS data. Bottom: Fourier transform. Data are presented as solid lines and fits as dotted lines. Structural parameters refined in this fit are included in Table 3A, fit 3 (coordinated ligands) and Table 3B, fit 10 (outer-shell ligands). Modeling the outer shell according to fits 8 or 9 resulted in data simulations indistinguishable from the one presented here.

Anaerobic Treatment with Suicide Hydrocarbon.

Reduced pMMO was prepared by anaerobic isolation of the pMMO membranes in 5 mM NADH, and were found to have the characteristics described above in the *Fully Reduced pMMO* section. Suicide substrates acetylene and degassed 3-bromopropyne were added anaerobically to the reconstituted pMMO, in the presence of NADH. Addition of suicide substrates had no apparent effect on the K-edge or EXAFS data (Figure 9). Data for pMMO with either substrate added are nearly identical to data measured on the control sample, anaerobically prepared pMMO *without* substrates added. Cu K-edges and EPR spin quantitation agree that all of the anaerobically prepared samples are indeed fully reduced (Table 1).

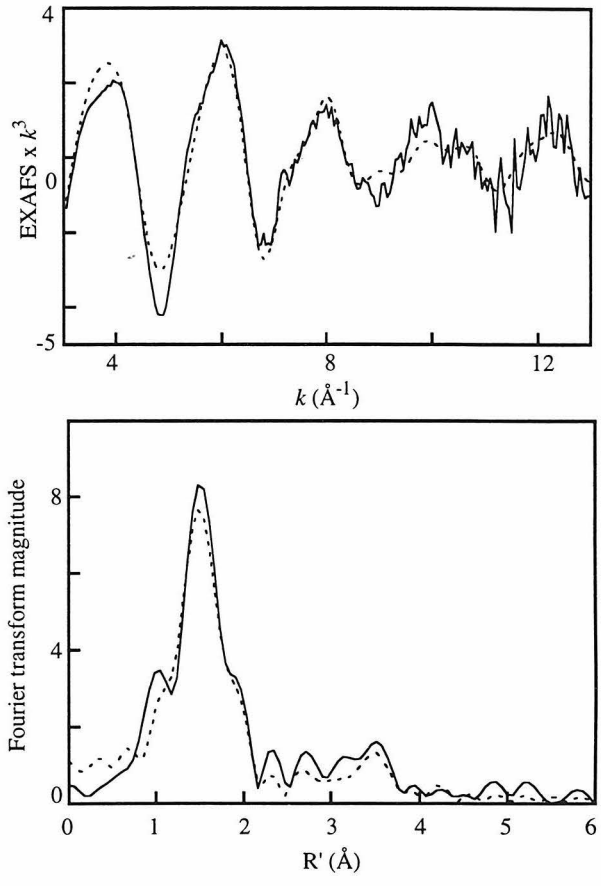

Figure 8. Representative best-fit to data for pMMO membranes after 2h O_2 exposure (O_2-inactivated). Top: EXAFS data. Bottom: Fourier transform. Data are presented as solid lines and fits as dotted lines. Structural parameters refined in this fit are included in Table 3A, fit 3 (coordinated ligands) and Table 3B, fit 5 (outer-shell ligands).

pMMO after Reaction with Both Cosubstrates.

Samples of pMMO-enriched membranes were prepared anaerobically (5 mM NADH), again, as above. Control samples were exposed to air alone while other samples were exposed for the same time period (~10 min.) to both air and suicide substrate (acetylene or 3-bromopropyne). Samples were then immediately frozen in liquid N_2.

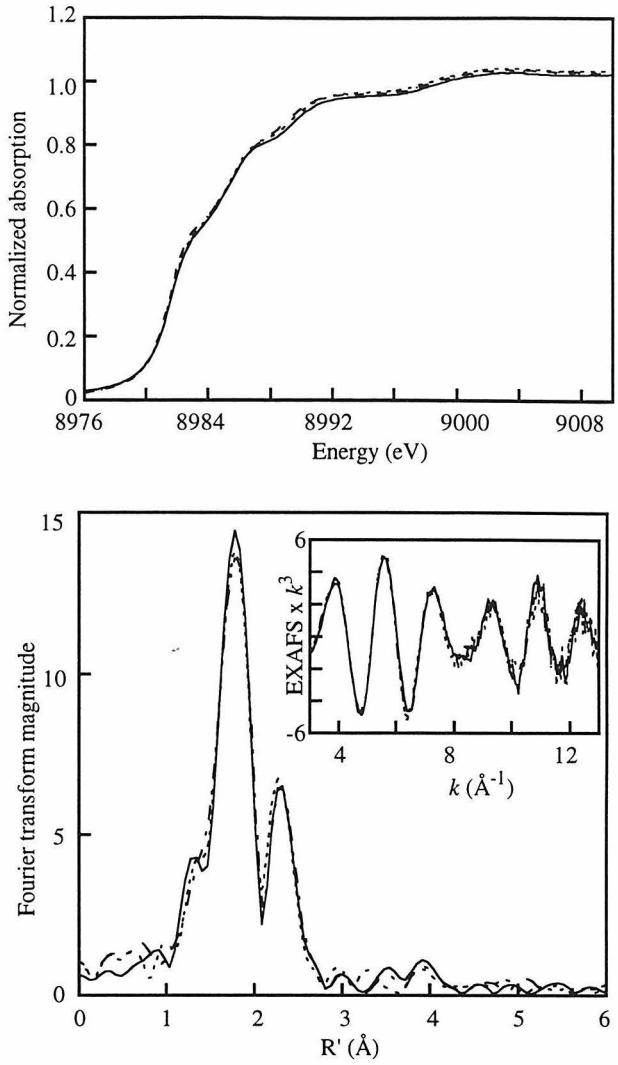

Figure 9. Comparison of Cu K-edge (top), Fourier tranform (bottom), and EXAFS (bottom, inset) data for three fully reduced membranes, isolated and maintained under anaerobic conditions (5 mM NADH): no substrate added (solid line), acetylene added (dot-dash line), and 3-bromopropyne added (dotted line). Spectra do not appear to change on anaerobic addition of either suicide substrate.

Several dramatic differences are found between the control experiment (no substrate added) and the experiment. EPR spin quantitation and the Cu K-edge concur that the air-only control sample is mainly reduced, ~80% Cu(I), analogous to samples isolated in air (Table 1). By contrast, identically prepared pMMO samples given an identical exposure to air and a suicide

substrate for ~10 minutes were far more oxidized: ≥70% Cu(II) (Table 1, Figure 10), regardless of which substrate was used. Again, EPR spin quantitation and the Cu K-edge predict similarly high levels of Cu(II) in the samples, suggesting that an EPR silent species is not formed upon co-addition of O_2 and suicide substrate.

EXAFS data and fits for the air-exposure-only sample (Figure 10; fit not shown) indicate an average Cu coordination environment only slightly perturbed from that of the fully-reduced samples. This again is similar to what is observed for membrane samples isolated in air (Table 3A, Figure 7). EXAFS data for air-and-substrate exposed pMMO, by contrast, are clearly changed (Figure 10). The first peak in the FT shifts to a much shorter distance (R' ~ 1.5 Å), indicating a reduction in average Cu-ligand bond lengths consistent with oxidation of the coppers. In addition, data are nearly indistinguishable whether acetylene or 3-bromopropyne is used as substrate, and analyses of their data yielded identical results.

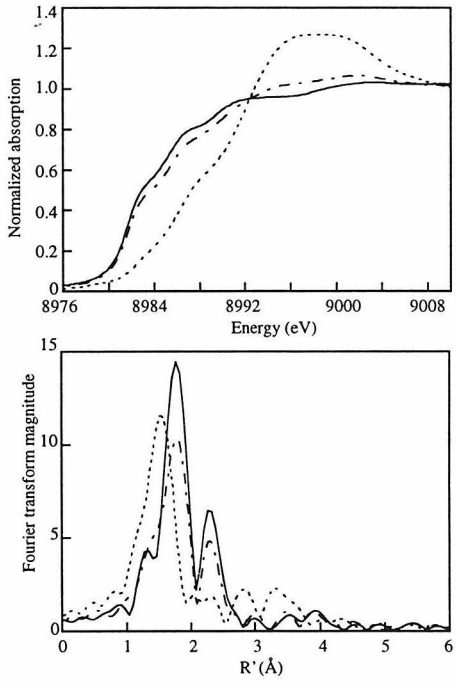

Figure 10. Comparison of Cu K-edges (top) and Fourier transforms (bottom) for fully reduced pMMO membranes (solid line), fully reduced membranes after brief exposure to air (dot-dash line), and isolated and fully reduced membranes after brief exposure to air and 3-bromopropyne (dotted line). All samples were made in 5 mM NADH.

Near-neighbor ligands for either the acetylene or 3-bromopropyne samples are well modeled by four O/N atoms at 1.99

Table 4. Results of Single-Scattering Fits to EXAFS data for Suicide-Substrate Exposed (Aerobically) pMMO-Enriched Membranes and Comparison to [Cu(II)(imidazole)$_4$](NO$_3$)$_2$

		Cu···O/N		Cu···O/N		Cu···C		Cu···C			
sample	fit	CN[a]	R[b] (σ^2)[c]	CN	R (σ^2)	CN	R (σ^2)	CN	R (σ^2)	E_0 (eV)	R (%)[d]
Excess acetylene	1	4.0	1.99 (0.005)							8992.6	40.1
(in air)	2	2.0	1.95 (0.002)	2.0	2.06 (0.002)					8992.1	43.0
	3	2.0	1.95 (0.002)	2.0	2.06 (0.002)					8992.5	38.3
				1.0	2.25 (0.005)						
	4	2.0	1.95 (0.002)	2.0	2.05 (0.002)	2.0	3.01 (0.004)			8992.1	37.3
	5	2.0	1.94 (0.002)	2.0	2.05 (0.002)	2.0	3.00 (0.004)	3.0	3.93 (0.004)	8992.4	32.8
Excess 3-bromo-	1	4.0	1.99 (0.005)							8991.5	33.4
propyne (in air)	2	2.0	1.95 (0.002)	2.0	2.05 (0.003)					8992.6	33.5
	3	2.0	1.96 (0.002)	2.0	2.04 (0.003)	2.0	3.03 (0.004)			8992.8	31.0
	4	2.0	1.95 (0.002)	2.0	2.05 (0.002)	2.0	3.01 (0.004)			8992.1	37.3
	5	2.0	1.95 (0.002)	2.0	2.04 (0.002)	2.0	3.02 (0.004)	3.0	3.92 (0.005)	8993.0	27.9
[Cu(II)(imidazole)$_4$](NO$_3$)$_2$	1	4.0	2.00 (0.003)	1.0	2.49 (0.002)	2.0	3.02 (0.004)	2.0	4.00 (0.005)	8993.0	27.9

[a] Number of equivalent ligands of the given type. [b] Absorber-scatterer distance in Å. [c] Debye-Waller factor: approximately equal to bond variance, if bond distance distribution is assumed to be Gaussian. [d] Goodness-of-fit parameter, where $R = [\Sigma k^6(\chi_{obs} - \chi_{calc})^2/Nk^6]^{1/2}$ (N = number of points in EXAFS spectrum). [e] These fits are roughly equivalent in quality.

~3.5 Å. The prominence of these peaks may be due to the relative homogeneity of the samples (*i.e.*, the copper is at least ~70% oxidized). Therefore, a quantitative assessment of potential MS from imidazole rings was carried out for this pair of data sets. The rigidity and relative structural invariance of the ring allow for enhancement of both single scattering (SS) and multiple scattering (MS). To quantify the effects of SS and MS from imidazole rings in general, fits to EXAFS data for crystallographically characterized [Cu(II)(imidazole)$_4$](NO$_3$)$_2$ were used as a guide. Four-atom models consisting of Cu-N-C^{α}-C^{γ} or equivalently Cu-N-C^{α}-N were constructed, based on the crystal structure for [Cu(II)(imidazole)$_4$](NO$_3$)$_2$. MS pathways from constituent three- and four-atom configurations (*e.g.*, Cu-N-C^{α}, Cu-N-C^{γ}, and Cu-N-C^{α}-C^{γ}), were delineated by *feff*. Pathways identified by *feff* as most strongly contributing to the EXAFS were retained.

These were used in initial fits to data previously collected for $[Cu(II)(imidazole)_4](NO_3)_2$. Two sets of SS waves contribute to outer-shell scattering: one Cu···C interaction at ~3 Å from the two proximal C^{α} carbons, and one Cu···C/N interaction at ~4 Å from the more distant C^{γ}/N pair (where C and N are indistinguishable by EXAFS). Calculated signals from the Cu-N-C^{γ} or equivalent Cu-N-N atom configurations (average Cu-N-C^{γ}/N angles ~160°) were of highest amplitude, while signals from the Cu-N-C^{α} configuration (average Cu-N-C angle ~130°) were secondary. This result is consistent with observed trends in EXAFS, where more linear (≥150°) disposition of the atoms in a scattering pathway results in greater MS. To minimize the number of independent variables in the fit, distances and Debye-Waller factors for MS pathways were coupled to the distances/Debye-Waller factors of their parent SS pathways and constrained to vary in proportion to them. This is an approximation, as the vibrational motions of different pairs of atoms in a given Cu-N-C pathway may be correlated, with resulting correlations in their radial separations in distance and their Debye-Waller factors. The inability to rigorously simulate correlations in distances and Debye-Waller factors is a limitation in MS modeling. However, even given the approximation used, the fits to the data are quite adequate. Additionally, identical approximations have been successfully applied to 3- and 4-atom MS simulations using *feff*/EXAFSPAK in prior work by others. Similar approaches to simulating scattering from imidazole rings have long been known. Inclusion of MS components to the fit yields a visible improvement to the fit and reduction of the *R* factor from X for the SS-only fit **5** to Y (Table 4).

The crystal structure of $[Cu(II)(imidazole)_4](NO_3)_2$ was used as a starting model for calculation of phase and amplitude functions by *feff* for the O_2+acetylene/O_2+3-

bromopropyne sample data. Variations on this structure were also used to test for possible structural elements in the O_2+acetylene/O_2+3-bromopropyne (for example, the presence of Cu···Cu scattering interactions). Fits using SS components only were made first (Table 4). Cu···Cu scattering interactions did not improve the fit and therefore were not retained. Cu···C interactions at ~3.0 Å and ~3.9 Å were included, similar to the ~3 and 4 Å interactions fit in data for [Cu(II)(imidazole)$_4$](NO$_3$)$_2$ (Table 4). When added, the same MS components refined from fits to [Cu(II)(imidazole)$_4$](NO$_3$)$_2$ contributed significantly and were retained. A per-Cu coordination number of 3 for each outer-shell scattering component reproduced the data well and yielded Debye-Waller factors comparable to those obtained in fits to [Cu(II)(imidazole)$_4$](NO$_3$)$_2$. Since each imidazole ring has two C^{α}, and a more distant C^{γ}/N pair (resulting in Cu-C^{α}-C^{γ} and Cu-C^{α}-N scattering pathways per each imidazole ring), a per-Cu coordination number of two would be consistent with one imidazole ring per Cu. Therefore the measured coordination number of three is consistent with 1.5 imidazole rings per Cu. As there are potentially other, non-imidazole carbons in the 3-4 Å range that might contribute to the EXAFS, this approximate number may be an upper limit. Moreover, consultation with the available sequences for pMMO and the analogous AMO reveal there are but 14 conserved histidine residues in the proteins. Therefore ~1.5 imidazole rings per Cu should be viewed as an upper bound.

Discussion

The experiments reported above have described specific states of pMMO in terms of changes observed in the K-edge absorption, which reflects information regarding the extent of copper oxidation, and the EXAFS, which reveals insights regarding the

coordination of said copper ions. It is quite clear that copper plays a critical role in the activity of pMMO, and the changes observed in the K-edge and EXAFS for the preparations examined in this study simultaneous clarify some issues regarding pMMO catalysis, as well as point to further questions.

Copper Coordination in the Reduced Enzyme.

Our experimental study began with the fully reduced state of the enzyme. Initially, it was not known if such a preparation had specific relevance to pMMO *in vivo*, as it was impossible to determine whether a 100% reduced enzyme might be found in pMMO in a living cell. The existence of the large number of pMMO-bound copper ions has always indicated that copper ions might act as a buffer of reducing equivalents for the active site of pMMO, such that at any given time in the life of a pMMO complex, the copper ions may not be a uniform, Cu(I), population. However, we have indeed determined that anaerobically prepared pMMO, as isolated in intracytosolic membrane fragments and in the presence of a reasonably low concentration (sub-millimolar) of NADH gives nearly identical copper K-edge absorption and EXAFS as a preparation forcibly reduced with exogenous (multi-millimolar) reductants, such as dithionite.

The identical data (Figure 2) and data fits (Table 1) reveal that the best model for copper coordination is 3-4 coordination with an average non-planar trigonal or tetrahedral geometry. This fit includes 0.5 close (1.90 Å) and 2.0 more distant (2.15 Å) oxygen/nitrogen ligands. These distances are typical of those found for Type 2 and/or Type 3 coppers found in other metalloenzymes. An additional, heavier ligand which could be equivalently modeled as a sulfur or chloride was also required to fit the data. Fits that attempted to exclude this heavier ligand required an average coordination

number for Cu(I) (>5) that is too large to be chemically feasible. The heavier ligand cannot be due to exogenous reductant (i.e., dithionite) as identical results are achieved for all of the reduced preparations studied.

This finding appears to be a promising beginning for determining the coordination environment for pMMO copper ions. However, the identity of the proposed ligand is quite unclear based on what is known of the primary sequence of the *pmo* genes. Typically, thiolate ligation from a cysteine residue is a hallmark of Cu(I) coordination chemistry in biological systems. Consultation of amino acid sequences for the PmoA, B, and C proteins (available from analysis of the corresponding *pmo* nucleotide sequences) show that thiolate linkage is not a likely possibility in pMMO. Specifically, PmoA, B and C contain 0, 1 and 3 cysteines respectively. Futher, there has been no alternative spectroscopic evidence for the existence of a copper-thiolate complex in pMMO, such as the intense charge-transfer (CT) optical absorption bands that are synonymous with blue-copper proteins in the oxidized state.

Alternatively we can consider methionine residues for the identity of the heavier ligand. The proposed distance of the interaction (2.3 Å) does correspond to other crystallographically determined Cu---S_{met} bond lengths. Also, there are several methionines in each of the Pmo polypeptides: 15, 11 and 7 in PmoA, B, and C. However, while methionine-copper centers can be found in biology (exemplified by both some blue-copper metalloprotein centers, as well as the hydroxylase enzymes PHM and DβM) the sequence analysis of Pmo polypeptides reveals the shortcomings in this assignment. Using the available gene sequences for *pmo* and highly similar *amo* genes from ammonia oxidizing bacteria (a subject taken up again in further detail in Chapter 4), only five of

the thirty-plus methionine residues of *pmo* appear to be conserved. Thus, the five conserved methionines do not satisfy the requirements for the EXAFS data fits.

Efforts to identify the heavy ligand in the fully reduced enzyme will be a subject of future work. It is a subject of considerable interest as oxidation of pMMO by any means seems to eliminate the observed interaction (see below). The strongest conclusion that can be drawn at this time is that the existence of conserved, repeated motifs of binding copper ions in pMMO is not likely, regardless of the EXAFS data analysis.

Reaction with Dioxygen.

Moving about the simple scheme shown in Figure 1, we next consider the capacity for pMMO to interact with dioxygen. This was probed using three different protocols. The first allowed for simple, short-term re-oxidation of the enzyme after reduction with a chemical reductant (dithionite). Similarly, we examined pMMO membrane fragments that were isolated in air, presuming that such a condition would be similar to re-oxidation after total artificial reduction. And lastly, in order to test the upper limits of pMMO-dioxygen interactions, pMMO was treated under a pure dioxygen atmosphere. The ability of other chemical oxidants to generate a population of uniformly oxidized pMMO copper centers has been examined. However, each of those investigated has either proved inaffective, or have led to further complications. (For an example see Chapter 3, which discusses the pMMO chemistry of the oxidant ferricyanide.)

Generally, the copper ions of pMMO are not fully oxidized, regardless of the oxygen incubation conditions. This is not unprecedented when considering other copper enzymes, however. For example, multicopper oxidases such as laccase are isolated with ~25% of its type 3 active site coppers as Cu(I). PHM and DβM likewise contain a

significant fraction of Cu(I) when handled aerobically[13]. In the latter cases, the O_2-resistant Cu has been associated with an electron transfer function. By analogy, K-edge absorption reveals that as isolated in air, or after turn-over in oxygen, ~70% of the copper ions of pMMO appear air-insensitive. Further, we have postulated that these copper ions function in electron transfer (E-clusters), while those coppers readily oxidized in air (~30%) participate directly in O_2/hydrocarbon catalysis (C-clusters). With extended exposure to air or pure O_2, a larger fraction of the membrane associated copper can be oxidized (~60%). The oxidation is irreversible, however, rendering the protein inactive. Inactivation is frequently accompanied by acidification of the membrane preparations. It has been proposed that the damaging effects of extended O_2 exposure are due to irreversible oxidation of E-cluster coppers, namely that "forced" oxidation increases the lability of the copper site, and leads to the degradation of the copper center.

XAS data measured for fully-reduced, as-isolated in air (or reduced and re-exposed to air), and O_2-inactivated membranes demonstrate changes associated with increasing exposure to O_2 (Figure 6). Cu K-edges for these samples illustrate the gradual conversion from an all-Cu(I) population to a Cu(II)/Cu(I) mixture, as Cu(I)-specific edge features are replaced by features more characteristic of Cu(II). Prior estimations of the Cu(II):Cu(I) ratio made according to the edges for these samples were supported by EPR spin-quantitation data (Table 1). Dramatic changes in the FTs for these samples illustrate a concomitant structural conversion from a Cu(I)-like to a more Cu(II)-like average Cu coordination environment (Figure 6). The large first peak in the FT for the fully-reduced sample becomes less intense and broadens in the direction of shorter radial distances in the as-isolated FT. Identical EXAFS and FT were measured on samples which were first

reduced and then re-exposed to air. These changes reflect the broader spread of Cu-ligand distances spanned in this heterogeneous sample, including shorter, Cu(II)-like bond lengths. The first peak narrows and moves completely to a significantly shorter radial distance in the FT for the O_2-inactivated pMMO. At the same time, increasing O_2 exposure is accompanied by a diminishing of the large outer-shell peak at 2.4 Å in the FT for fully-reduced pMMO.

Fits to the EXAFS data elucidate qualitative observations made from the FTs. The Cu···S/Cl interaction observed in fits to data for the fully-reduced pMMO contributes less to fits for as-isolated membranes, and least to fits for O_2-inactivated pMMO, as illustrated by the reduced number of S/Cl backscatterers required for the fits. At the same time, the average distance to near-neighbor O/N ligands measured by fits to these data progressively shortens: 2.09 Å (fully-reduced), 2.06 Å (as-isolated), 1.99 Å (O_2-inactivated). In structural terms, reaction with O_2 apparently results in the movement of the ~2.3 Å and ~2.7 Å ligands away from the coppers and out of range of detection. Regarding the 2.3 Å scatterer, it is not uncommon for sulfur, a good ligand for Cu(I) but a poorer one for Cu(II), to move out of bonding distance or to be displaced by O/N ligands after metal oxidation. The loss of some of the structural features in the EXAFS data may be due to an increase of inhomogeneity in the copper population. Loss of bonding or bridging interactions on oxidation would in turn result in increased uncorrelated thermal motion, contributing to the disappearance of the backscattering atoms from the EXAFS. As the ~2.3 Å and ~2.7 Å ligands recede with increasing O_2 exposure, scattering contributions from carbon ligands at ~3.0 and 3.9 Å begin to grow in. These distances, as well as the two-peaked structure observed at 3-4 Å in the non-phase corrected FT, are

suggestive of imidazole rings. It is possible that contraction of Cu-ligand distances in the more oxidized protein positions imidazole ligands such that they contribute more strongly to the EXAFS. Stronger evidence for imidazole ligation comes from analysis of the pMMO after reaction with both O_2 and suicide hydrocarbons, and from prior ESEEM spectroscopic studies (Figures 11-13).

Reaction with Substrate Analogs – Anaerobic.

The interaction of pMMO with substrates was analyzed by using two different substrate analogs, the suicide substrates acetylene and 3-bromopropyne, in hopes of irreversibly and specifically trapping a state of pMMO C-clusters. An initial experiment was to test whether the addition of substrate **without** the addition of dioxygen had any effect. And as expected, in contrast to the analogous experiment with O_2-exposure (see below), anaerobic exposure of membranes to the suicide substrates acetylene or 3-bromopropyne has no effect on the Cu K-edge or EXAFS data (Figure 9).

This is to be expected, for in studies of the inhibition of pMMO by acetylene, it has been shown that acetylene, reductant, and dioxygen are required for maximal irreversible inhibition. As acetylene (and its methylbrominated analog) acts as a mechanism-based inhibitor, it binds at the active site and is irreversibly attacked by an activated oxygen species, the actual pMMO hydroxylating agent. As there is no oxygen present in this sample, acetylene does not irreversibly modify the protein, and the failure of the substrate to modify the K-edge and EXAFS is due to weak substrate binding.

Reaction with Substrate Analogs – Aerobic.

However, when acetylene or 3-bromopropyne are applied aerobically, Cu K-edge and EXAFS data are significantly altered (Figure 10) as compared to any of the

previously considered samples. K-edge data are consistent with near-complete (≥ 70%) oxidation of the membrane coppers. This is in stark contrast with the control sample which was exposed to air alone, in which only ~20% of the coppers are oxidized (Table 1). Air oxidation alone therefore cannot account for the high proportion of Cu(II) in the acetylene/O_2 samples. Oxidation of these coppers appears to result from an oxygen-dependent acetylene reaction. This result indicates that both the O_2-labile and the more O_2 inert coppers are capable of participating in O_2/acetylene chemistry, either directly or through electron-transfer to the site of substrate activation. As only PmoA 26kDa polypeptide is found to bind radio-labeled acetylene irreversibly, its seems unlikely that all (or indeed most) of the copper ions are interacting directly with acetylene. Thus, we conclude that the majority of coppers in the pMMO can serve a redox-active role, suggesting a chemical rather than a solely structural function.

Alternative interpretations are feasible for this finding. It may be the case that irreversible inhibition of the protein allows for the other active-site copper ions to act as an oxidase exclusively, such that the electron equivalents can be drained from the otherwise bound Cu(I) centers. Inhibition with acetylene might more dramatically affect the protein matrix of pMMO, however. Acetylene inhibition may in fact trap pMMO into a conformation in which the other Cu(I) clusters can react directly with dioxygen. Essentially, it is not clear whether the use of acetylene leads to the loss of electrons from a naturally occurring electron transfer pathway (presumably involving many of the copper ions of pMMO), or if some novel event (such as an unprecedented direct reaction between sheltered E-cluster copper ions and dioxygen) is responsible for the overall oxidized state of the pMMO copper ions. The former hypothesis is very attractive, as it

links substrate binding and reactivity directly into the re-reduction of the enzyme active site. In this model, the action of substrate reactivity and subsequent product release gates electron transfer back into the enzyme active site. Therefore, irreversible inhibition locks the gate open, and electrons flow into the active site as long as there are electrons to transfer. An elaboration of this model takes note that there are two hypothesized C-clusters, which is to mean that there appear to be two different sites which are reactive toward dioxygen. It seems quite possible that acetylene only inhibits one such cluster, and the other unaffected site continues to react with dioxygen, allowing for continued removal of the electrons from pMMO. Either way, the vast majority of the protein-based copper ions are oxidized. The latter hypothesis does invoke the lability of enzyme activity that is often observed. Specifically, it suggests that the Cu(I) centers from the isolated-in-air preparations (the E-clusters) are labile, and can be subjected to degradation and interaction with dioxygen. Loss of activity has been observed to coincide with an increase in the Type 2-like EPR signal of the protein (data not shown). It is possible that the increase in the EPR signal is related to a structural lability of the E-clusters. However, there currently is no clean way to determine between these two hypotheses.

In terms of the EXAFS for these samples, the fits for the acetylene/O_2 sample are most consistent with a per-Cu average 2 O/N ligands at 1.94 Å plus 2 O/N ligands at 2.03 Å. These distances are typical of Cu(II) in an O/N environment. There is no evidence for or against the formation of Cu-C bonds, as carbon and nitrogen should not be distinguishable by EXAFS. There are also no detectable Cu···(heavy atom) (Cu···S) scattering interactions. Unlike reaction with O_2 alone, reaction with O_2 and acetylene results in near *complete* elimination of both the 2.3 Å and 2.7 Å interactions associated

with the reduced state. These ligands likely move to longer radial distances where they can no longer be detected or are displaced by other ligands. Additionally, the bond distances to the coordinated O/N ligands are on average considerably shorter in the O_2/acetylene case, than in the case of the O_2-aged sample, suggesting complete conversion to a Cu(II)-like geometry in the former.

Fits including more distant ligands suggest 1-2 (data fit with 1.5) imidazole rings per Cu, with no detectable Cu···heavy atom interactions (Table 4). Additionally, there were no significant differences in fits to the data when 3-bromopropyne was used as a substrate instead of acetylene. The absence of Cu···Br interactions in the data might suggest that the bromine label is too distant from the coppers to be detected by EXAFS, or that the 3-bromopropyne binds in multiple, competing modes.

Summary and Conclusions

The above study is by no means considered to be the definative XAS study of particulate methane monooxygenase, although several important conclusions can be drawn from the K-edge absorption and EXAFS data. First, pMMO can be isolated directly from *M. capsulatus* (Bath), with a nearly full compliment of reduced Cu(I) ions, without using the strong reductant dithionite. The EXAFS from the fully reduced structure indicate that the copper ions must exists in uniform populations, and that some degree of heavy-atom, likely sulfur, ligation is present. Reaction of this fully reduced state with ambient levels of dioxygen over a short time-scale oxidizes ~20% of the copper ions of pMMO, and the resulting changes in the EXAFS correspond to the shift from entirely Cu(I) ions, to a mixed-valence population of Cu(I) and Cu(II) ions. The Cu(II) component loses the proposed S-ligand, as sulfur is a poorer ligand for Cu(II) than

for Cu(I), and the first coordination sphere draws closer. Final conclusions involve the interaction of acetylene (and presumably, all 1-alkyne suicide substrates) with pMMO. The use of much larger analog of acetylene (3-bromopropyne) did not affect our findings, and the alkynes studied only affected the reduced pMMO in the presence of dioxygen. Further, alkyne-based inhibition results in a undetermined modification of pMMO which unexpectedly initiates the loss (leakage) of electrons from the otherwise reduced copper centers of the proteins. This leakage may be due to an irreversibly opened conformational "gate," or another event which renders the Cu(I) centers directly exposed to dioxygen.

References Cited

1)Cook, S. A.; Shiemke, A. K. *J. Inorg. Biochem.* **1996**, *64*, 273-284.

2)Burrows, K. J.; Cornish, A.; Scott, D.; Higgins, I. J. *J. Gen. Microbiol.* **1984**, *130*, 3327-3333.

3)Prior, S. D.; Dalton, H. *Journal of General Microbiology* **1985**, *131*, 155-163.

4)Stanley, S. H.; Prior, S. D.; Leak, D. J.; Dalton, H. *Biotechnology Letters* **1983**, *5*, 487-492.

5)Nielsen, A. K.; Gerdes, K.; Murrell, J. C. *Mol. Microbiol.* **1997**, *25*, 399-409.

6)Brantner, C. A.; Buchholz, L. A.; McSwain, C. L.; Newcomb, L. L.; Remsen, C. C.; Collins, M. L. P. *Canadian Journal of Microbiology* **1997**, *43*, 672-676.

7)Chan, S. I.; Nguyen, H.-H. T.; Shiemke, A. K.; Lidstrom, M. E. *Studies Toward Characterization of Methane Monooxygenase*; Murrell, J. C. and Kelly, D. P., Ed.; Intercept: Andover, Hampshire, U.K., 1993, pp 93-107.

8)Semrau, J. D.; Zolandz, D.; Lidstrom, M.; Chan, S. I. *J. Inorg. Biochem.* **1995**, *58*, 235-244.

9)Nguyen, H. H. T.; Elliott, S. J.; Yip, J. H. K.; Chan, S. I. *Journal of Biological Chemistry* **1998**, *273*, 7957-7966.

10)Takeguchi, M.; Miyakawa, K.; Okura, I. *JOURNAL OF MOLECULAR CATALYSIS A-CHEMICAL* **1998**, *132*, 145-153.

11)Prior, S. D.; Dalton, H. *Fems Microbiology Letters* **1985**, *29*, 105-109.

12)Nguyen, H. H. T.; Nakagawa, K. H.; Hedman, B.; Elliott, S. J.; Lidstrom, M. E.; Hodgson, K. O.; Chan, S. I. *Journal of the American Chemical Society* **1996**, *118*, 12766-12776.

13)Reedy, B. J.; Blackburn, N. J. *J. Am. Chem. Soc.* **1994**, *116*, 1924-1931.

Chapter 3: Chemical Modification of pMMO

Abstract

In order to probe our ability to distinguish between the copper ions of particulate methane monoxyganse, a series of chemical- (EDTA and ferricyanide) and proteolytic-treatments were developed. Using EDTA depletes the enzyme of all but 4 of the copper ions associated with the protein, suggesting that many of the copper ions of the protein are in soluble domains and that the residual copper ions are quite likely housed in a membrane-localized domain of the protein. Similarly, proteolysis of pMMO isolated in membrane-fragments was carried out to determine the ability of proteolytic enzymes to remove or at least damage such soluble domains.

Introduction

The study of the pMMO problem can be thought of as a dilemma of numbers: as-isolated, there are a large number of copper ions associated with the pMMO system. Each of the centers is of interest, whether it is directly involved in catalysis, or plays a role in the electron-transport pathways of the protein. Further, while the exact function(s) of the many centers is not clear, it has been well established that most of the centers can access multiple oxidation states[1]. However, in terms of the ability of pMMO to oxidize methane, determining the nature of the novel catalytic site of the enzyme is of paramount interest above all others. The numeric complication of a protein with 15 copper centers is all too apparent, as designed experiments must tackle the problem of observing characteristics of a single sub-set of copper sites that are to be studied in a given experiment. The chemistry of copper does not aid this pursuit, as few biologically known copper centers have truly distinctive spectroscopic characteristics[2,3]. It seems then, that short of a crystal structure might reveal all of the copper centers and their environments, any attempts at trying to understand the arrangement and coordination chemistry of the many copper ions of pMMO will likely have shortcomings. This will be addressed in

Chapter 5, wherein difference ESEEM experiments are required to validate proposed copper-histidine interactions were solely attributed to the copper ions of pMMO that react with dioxygen. Further, with those experiments it was apparent that all spectroscopic techniques sample a large population that will suffer from inhomogeneity. EPR characterization is difficult with the large number of copper ions: the existence of Type II signals have been well-established, and the reliance of ferricyanide to generate a new "cluster signal" has also been utilized, though the nature of the species giving rise to this signal has come under question. In this chapter, we approach the issue of trying to distinguish the sites of pMMO by any means necessary; and in this case, we opt for chemical modification.

Many of the copper ions are known to be reduced in the as-isolated state, as shown in Chapter 2. Thus, it has always been presumed that the interaction of pMMO with ferricyanide involves an electron transfer reaction from pMMO to the oxidant ferricyanide[1,4], thereby generating copper(II) in the protein which can be detected by EPR, as well as a reduced ferrocyanide species. However, the precise nature of the products and the nature of the reaction have been unknown to date. X-ray Absorption Spectroscopy (XAS) and Extended X-ray Absorption Fine Structure (EXAFS) studies, discussed in Chapter 2, indicate some kind of copper(II)-ferrocyanide adduct formed as a result of the ferricyanide treatment. This species is akin to a "Prussian Blue" compound, of which many have been prepared in the literature, although only a few have been structural characterized[5-9]. Therefore, it is of great interest to assess the identity of the proposed adduct, and identify its contribution to the EPR spectra from ferricyanide

oxidation experiments. In order to elucidate the nature of the species generated in the reaction, two types of model compounds were synthesized as part of the present study. The copper(II)-iron(III) ferricyanide-bridged compound $[Cu(dien)]_3[Fe(CN)_6]_2 \cdot 6H_2O$ as studied by Morpugo, *et al.*, was used to model a potential product of the ferricyande interaction with oxidized coppers in pMMO (dien = bis-2-aminoethylamine)[6]. The presumed product of the reaction of reduced pMMO-based copper and ferricyanide is a copper(II)-iron(II) species, and this was modeled by $[(Cu(dien))_2(NC)_2Fe(CN)_4] \cdot 4H_2O$ and $[(Cu(dpt))_2(NC)_2Fe(CN)_4] \cdot 4H_2O$ as prepared and characterized by Suzuki and Uehara (dpt = bis-3-aminopropylamine)[10].

Experimental Procedures.

General Methods.

EPR Spectroscopy was conducted essentially as described in Chapter 2. All samples were prepared as frozen solutions, and were stored at liquid nitrogen temperature until the time of analysis. All EPR experiments were performed at liquid helium temperature, using an ESR-900 Oxford Instruments (Oxford, England) liquid helium cryostat. EPR spectra were recorded on a Varian E-line Century X-band spectrometer. For each sample, spectra covering the entire X-band EPR spectrum was acquired, with particular attention paid to the region around g=2.0. Protein quantification and elemental analysis was conducted as described in Chapter 2, *via* the Lowry method and ICP-MS, respectively.

Model Compound Synthesis.

The synthesis of the model compounds $[Cu(dien)]_3[Fe(CN)_6]_2 \cdot 6H_2O$, $[(Cu(dien))_2(NC)_2Fe(CN)_4] \cdot 4H_2O$ and $[(Cu(dpt))_2(NC)_2Fe(CN)_4] \cdot 4H_2O$ were carried out essentially as described by Morpurgo, *et al.*[6], and Suzuki and Uehara[10], with the following modifications. $[Cu(dien)]_3[Fe(CN)_6]_2 \cdot 6H_2O$ was synthesized by dissolving 0.676g of $K_2S_2O_8$ and 1.64 g $K_3[Fe(CN)_6]$ were dissolved together in 40 ml H_2O with stirring. An aqueous solution (20 ml) of 0.622 g $CuSO_4 \cdot 5H_2O$ and 0.35 ml dien was then added, along with 10 ml methanol. This mixture was allowed to stand at 4°C, and the green solution yielded sharp dark-green crystals. The crystals were collected by filtration and carefully washed with ice-cold water and acetone. $[(Cu(dien))_2(NC)_2Fe(CN)_4] \cdot 4H_2O$ and $[(Cu(dpt))_2(NC)_2Fe(CN)_4] \cdot 4H_2O$ were prepared in a similar fashion: 1 mmol of $K_4[Fe(CN)_6]$ was taken in 20 ml H_2O and was stirred while an aqueous solution (20 ml) of 2.0 mmol of $Cu[NO_3]_2 \cdot 6H_2O$ and 2.5 mmol of ligand were added. To this, 5 ml of acetone was added, and the mixture was allowed to stand at room temperature, without stirring, for 2 h, and was then placed at 4°C. After standing in the cold overnight, a crop of dark green cystals were collected, which turned blue-purple in air upon standing.

Chemical Treatments.

pMMO-containing membrane fractions were freshly prepared as described previously and 0.5 ml of such a preparation was treated with *N,N,N',N'*-Ethylenediamine-tetraacetic acid (EDTA) at a final concentration of 12.3 mM. Incubations were carried out on ice, for exactly 30 minutes. The preparations were centrifuged in a bench-top microfuge for 8 minutes at 4°C, and the supernatant was removed for further analysis. Pelleted membranes were then resuspended to the original volume, and centrifuged and

resuspended a second time. Treatment of membrane fractions were typically carried out as follows: $K_3Fe(CN)_6$ solutions in 50mM PIPES (pH = 7.0) buffer were prepared, and added to membrane preparations to a final concentration of either 5, 0.5, or 0.05 mM ferricyanide. The treated samples were then incubated on ice for 12 hours, after which time they were centrifuged and resuspended in 50mM PIPES (pH = 7.0) without ferricyanide. This washing procedure, to remove any soluble ferricyanide, was carried out twice more.

Proteolytic Treatments.

Proteolysis was achieved by incubation of pMMO-containing membrane fractions with proteolytic enzymes as follows. In the case of either Trypsin or Chymotrypsin (Roche-Boehringer-Mannheim, sequencing grade) ~1 mg of the solid, lyophilized enzyme was re-hydrated in a minimal amount of 50mM PIPES buffer (pH 7.0) and this was directly added to 0.4 ml of the pMMO-preparation, giving a ratio of protein:protease of approximately 50:1. These preparations were incubated at 37°C for four hours, with periodic mixing using a vortex mixer. In the case of Papain treatment, Calbiochem Papain (10mg) was taken in 50mm NH_4Acetate buffer (pH 5.0), to which 40 µl of 10% L-cysteine is added. This solution is mixed well, and incubated at room temperature briefly, before centrifuging an aliquot of the protease in bench-top microfuge. The resulting solution is removed from the pellet (which contains unactivated and denatured Papain) and the solution is added to a membrane preparation, 3:1 (vol:vol). This is incubated at 37°C for hour hours, with periodic mixing using a vortex mixer. Digests are then quenched on ice and centrifuged to remove the soluble fragments. They are re-suspended in 50 mM PIPES, and centrifuged and suspended a final time to further remove peptide fragments. For some experiments, pellets were washed in a high-salt

wash (250mM NH_4Cl in 5mM Phosphate buffer, pH=7.0), pure water and stripped with 1N NaOH to remove any exogenous peptide fragments. These further steps were not found to play a significant role in the results described below.

Results and Discussion

(Note that throughout the text, we will make use of "apparent *g*-values" for spectral features. The feature observed at g=2.12 is such a value, where the spectrum is formally indicated by the cross-over point of the derivative spectrum. However, for the ease in comparison, maxima and minima in the derivative spectrum are used instead.)

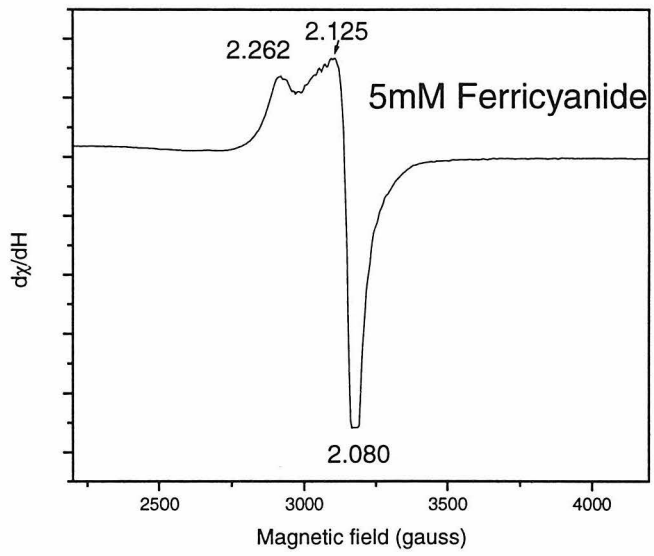

Figure 1. EPR spectrum of pMMO-containing membranes treated with 5mM ferricyanide. 10mW power, 2G modulation amplitude, 4.2K.

Ferricyanide Treatments of pMMO.

The treatment of pMMO with ferricyanide ion has been used widely in our group to generate a novel, quasi-isotropic signal that is analogous to the one shown in Figure 1[1]. Beginning with as-isolated pMMO-containing membrane fragments, the experiment

begins with incubation and mixing of the membranes with millimolar (5-20mM) concentrations of ferricyanide. Excess ferricyanide is removed by multiple centrifugation-resuspension cycles, wherein the concentration of ferricyanide is monitored by UV/Visual absorption (λ_{max}=410nm). The spectrum shown in Figure 1 is typical for incubation of pMMO-containing membrane fragments with millimolar concentrations of ferricyanide, and it demonstrates the strong features at g=2.24 and 2.12. This preparation has been used to represent the "all oxidized" form of pMMO to date, as X-ray Edge Absorption Spectroscopy (XAS) of such a preparation shows that the copper ions are ~100% copper (II), in comparison with 30% copper (II) found in the as-isolated preparation.

Alteration of the ferricyanide concentration used in the incubation yields distinct spectroscopic features. Shown in Figure 2, varying the concentration of ferricyanide over two orders of magnitude demonstrates that a g=2.175 feature develops initially, and that other features in the $g_{\|}$ region (and less obviously, in $g_{\perp}$) persist throughout the lower concentrations. These smaller contributing signals (g=2.496 and 2.047 in Figure 2) can be saturated at increased microwave powers (data not shown) which indicated that this portion of the signal is likely due to residual Type II copper centers. Examination of the line-shape of the spectrum from the incubation at 5mM ferricyanide, as compared to the lower (0.5mM) concentrations, is shown in Figure 3. The difference spectrum of standard ferricyanide treatments, which is normalized by the protein concentrations (all spectra are of equal magnitude), reveals that there is some loss of the g=2.175 component, as presumably that is transformed into the species that give rise to the other components in the spectrum. Of particular interest is the very narrow feature at g=2.12 which is clearly

observable in the difference spectrum, and not readily visible from the original spectra. Further, the difference spectrum is also useful for removing any components due to residual Type II copper ions that persist. Also the g=2.24 signal is quite clear in the difference spectrum. Previous work by Antholine and co-workers has demonstrated that this feature is due to a non-specific, long-time scale transformation of a copper-ferricyanide adduct[11].

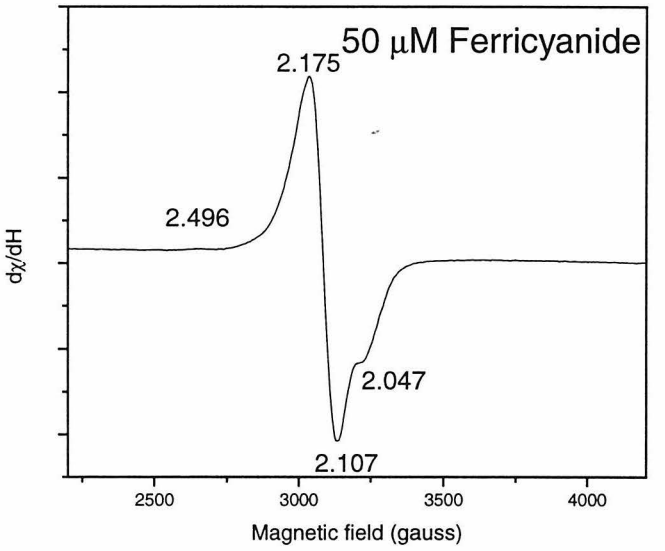

Figure 2. EPR spectrum of pMMO-containing membranes treated with 50μM ferricyanide (data collection as in Figure 1).

The nature of the signals have been assessed by the synthesis and EPR characterization of the model compounds $[Cu(dien)]_3[Fe(CN)_6]_2 \cdot 6H_2O$ (**1**), $[(Cu(dien))_2(NC)_2Fe(CN)_4] \cdot 4H_2O$ (**2**) and $[(Cu(dpt))_2(NC)_2Fe(CN)_4] \cdot 4H_2O$ (**3**). Compound **1** is a Fe(III)-Cu(II) complex which has been crystallographically characterized by Morpurgo and co-workers, while compound **2** and **3** are Fe(II)-Cu(II)

species. The EPR spectra for t compound **1** and **3** are given in Figure 4. Two features are of note immediately: the first is that compound **1** does have an EPR signal, albeit at a much smaller intensity than the ferrocyanide-based alternative. The weak intensity is likely due to the fast-relaxing properties of Fe(III). The second point is that the maximum of the derivative spectrum observed for **3** is at exactly g=2.175. Thus, we assign the feature observed in the low ferricyanide regime of pMMO to a ferrocyanide-copper (II) adduct.

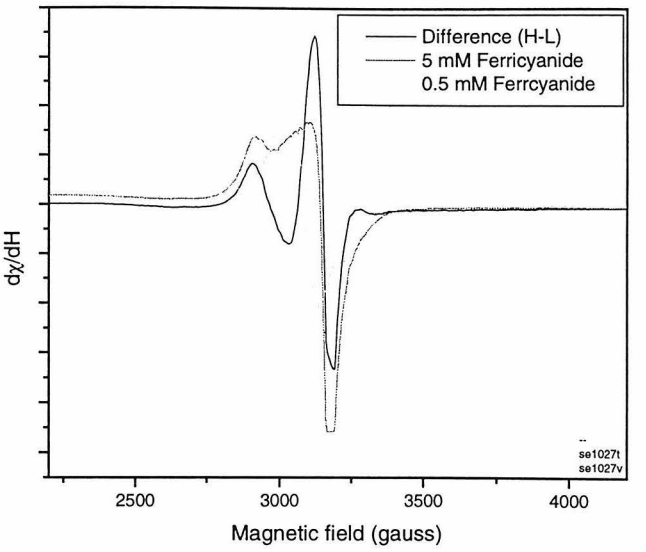

Figure 3. Difference EPR spectrum of the spectra shown in Figures 1 and 2.

Proteolytic Enzymes.

As observed, the ability of ferricyanide ion and proteolytic enzymes have given rise to the following general scheme shown in Figure 5. These experiments all start with as isolated pMMO, which for the ease of depiction is shown as a two sub-unit system with soluble and membrane-anchored domains only. Experiments then proceed with either addition of the oxidant ferricyanide (at either high or low concentrations) or a protease to cleave soluble-domains within the protein. Then, the membrane fraction is isolated (either to remove excess ferricyanide, or to remove the cleaved soluble domains)

and the other reagent (protease or ferricyanide, respectively) is applied. Individual experiments can examine the soluble-cleaved domains, the membrane-specific domains, and do so with either high or low concentrations of ferricyanide. For example, the experiment indicated by the uppermost path of Figure 5 begins with the initial application of a protease (Trypsin, Chymotrypsin, or Papain) which frees the soluble domain, and cleaving it into a number of smaller fragments. The soluble domains are removed from the protein domains and treated with a low concentration (50 μM) of ferricyanide for subsequent EPR analysis.

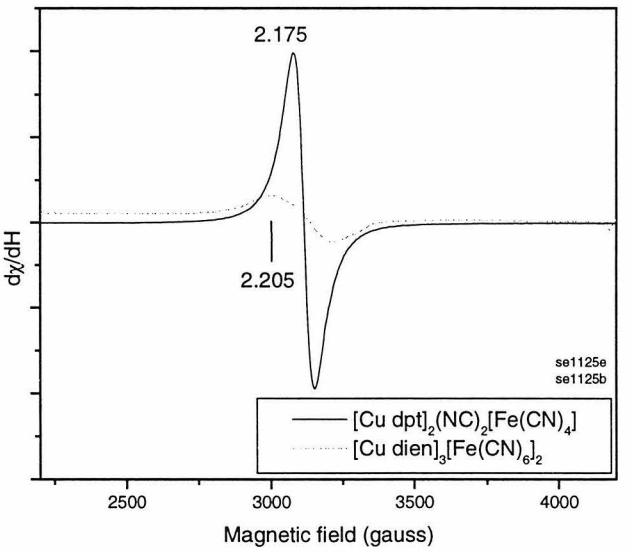

Figure 4. EPR spectra for the ferricyanide-copper compound *1* (dashed line) the ferrocyanide-copper compound *3* (solid). The gain of the spectrum for *1* is x40 of that for *3*. 1 mW power, 1.0 G modulation amplitude, 4.2K.

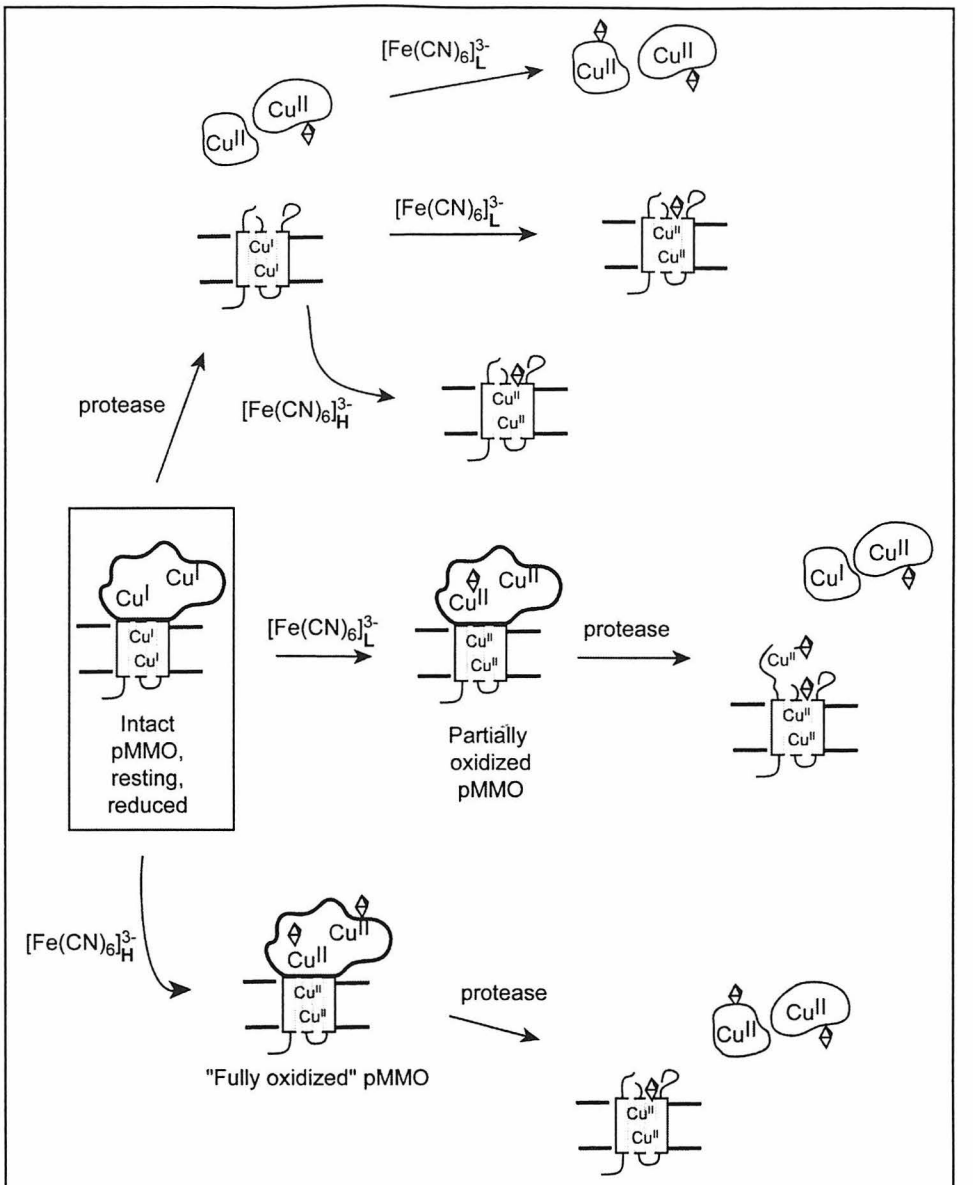

Figure 5. Schematic of the use of proteolytic enzymes and ferricyanide to "selectively" probe ferricyanide-oxidized copper ions.

At this point, ferricyanide treatment of either the soluble protein-copper complexes or the residual membrane-bound domain may proceed, using either a low (50 μM) or high (5 mM) concentration of the oxidant. All four resulting preparations for each of the three proteases can then be studied by EPR to determine the ability of the preparation to interact with ferricyanide. In a similar fashion, one can follow the middle or lower path shown in Figure 5, wherein the as-isolated pMMO is first treated with

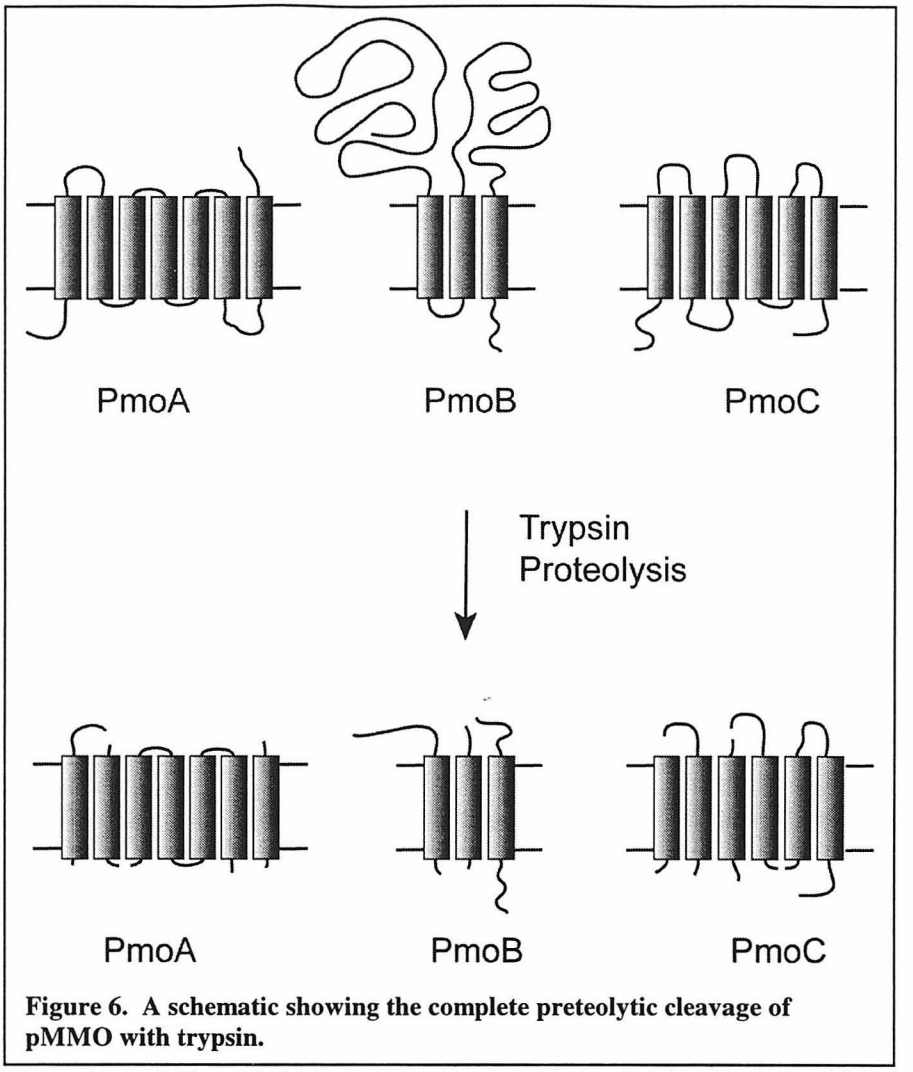

Figure 6. A schematic showing the complete preteolytic cleavage of pMMO with trypsin.

50μM ferricyanide, followed by protease, or the preparation is treated with 5 mM ferricyanide, then protease. Again, in each case soluble and membrane-bound fractions result, each of which can be examined *via* EPR.

The homogeneity of this cleavage is not entirely uniform, depending on the enzyme and the reaction conditions used. Immediately following cleavage of the membrane fragments, from our model of pMMO, it is assumed that a large portion of the copper ions associated with the protein will then be liberated into a soluble fraction, and may in fact retain their native *in protein* ligands. The choice of protease plays considerably in this regard. Figure 6 shows a cartoon depiction of the cleavage process,

which can either cut a soluble loop domain twice, thereby removing a piece of the protein entirely, or it may nearly nick the loop domain, which may effect the ability to bind metal ions in that domain of the protein.

Generally, it was found that the ferricyanide-dependent EPR signals evolved over time, slowly increasing with intensity. The spectra shown in Figures 1 and 2 represent the end-points of these treatments, namely, the maximal concentration of the species involved. There are several general features observed in the experiments depicted in the figures below, although each individual protease gave unique results in specific cases. As such, the exceptional results shall be described in the context of the general findings. Data will be presented and discussed in the order of the lower concentration (50 μM) ferricyanide treatment followed by the higher concentration (5mM) experiments. Within each section, the data corresponding to the soluble domains are presented first, followed by the data for the membrane domains. The samples initially proteolytically cleaved are discussed first (soluble domains, followed by membrane domains), and the samples treated with ferricyanide initially are dealt with next (again, soluble domains, followed by membrane domains.)

Low concentration treatment - *soluble domains*. Generally, it was found that all of the proteolytically cleaved domains of pMMO could interact with ferricyanide subsequent to proteolysis in order to generate the g=2.175 signal (uppermost pathway, Figure 5). This is shown as Figure 7. However, the intensity was not nearly so great as the standard treatment achieved at the site of the membranes. This may be due to an incomplete proteolysis of the soluble domains, or proteolytic damage to the ferricyanide

binding site. However, since the intensity decreases, it does suggest that the interaction of ferricyanide with the pMMO copper-ions is not entirely adventitious in nature. Figure 8 shows the results of proteolytic cleavage after the ferricyanide treatment (Figure 5 soluble fraction of middle pathway). This also gives the same g=2.175 feature, and again this is observed at a decreased intensity. Of note, it seems that Trypsin and Chymotrypsin (in comparison with Papain) are particularly well suited for the cleavage of intact Type II copper ions, which are clearly present in the soluble fraction of this treatment. This latter finding is quite likely due to the general nature of papain cleavage.

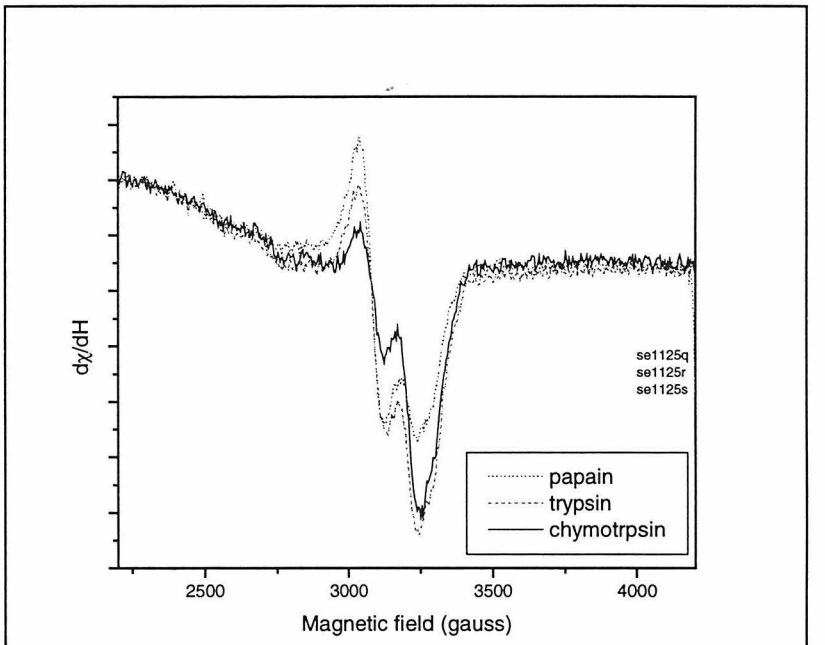

Figure 7. Interation of 50μM ferricyanide with soluble domains of pMMO prepared by proteolytica cleavage. 1mW power, 1.0G modulation amplitude, 4.2K.

This clearly indicates that a subset of pMMO copper ions exist in primarily soluble domains, and that these copper ions can be removed differentially with the utilization of different proteolytic enzymes.

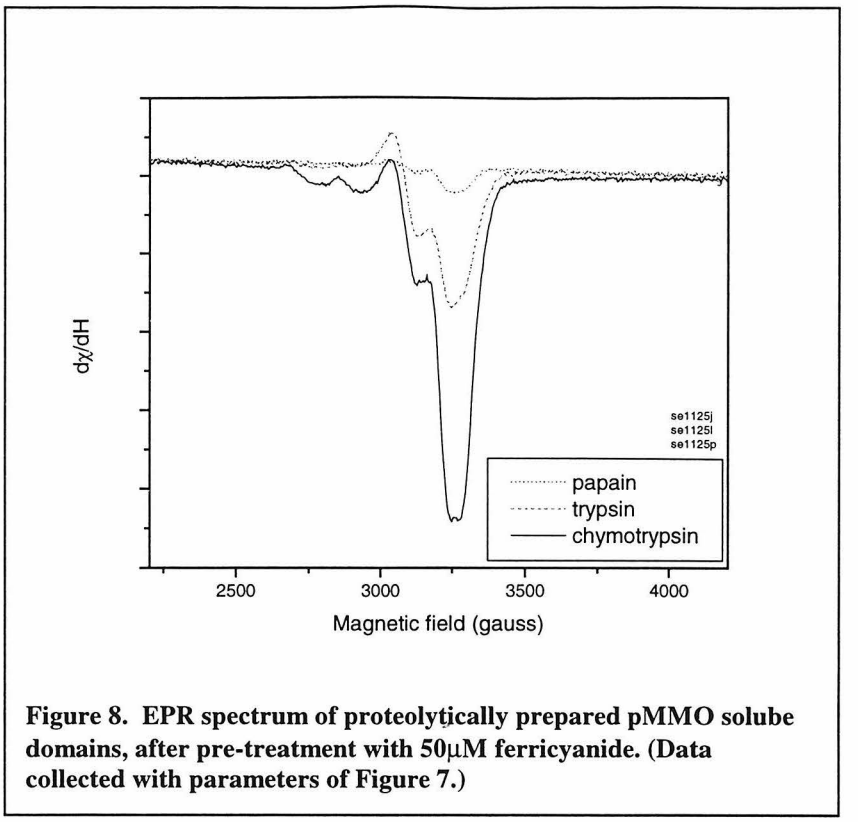

Figure 8. EPR spectrum of proteolytically prepared pMMO solube domains, after pre-treatment with 50μM ferricyanide. (Data collected with parameters of Figure 7.)

Low concentration treatment - membrane domains. The corresponding membrane-bound preparation are shown as Figures 9 and 10. As Figure 9 shows, treatment with protease prior to treatment with ferricyanide severely hinders the ability to bind ferricyanide for any of the proteases used. Papain allows for less than half of the previously observed g=2.175 signal to form, Trypsin prevents all but ~20% of the signal from forming, and Chymotrypsin totally removes the ability of the ferricyanide to form an adduct. In the case of the former two enzymes, the slight deviation in the line-shape in the g=2.06 feature is due to the change in intensity: as the ferricyanide concentration decreases, the contribution due to unmodified Type II copper centers becomes easier to observe. In the case of Chymotrypsin, the evidence is quite striking, as there is no discernible development of the adduct signal. Thus, we can conclude that the remaining

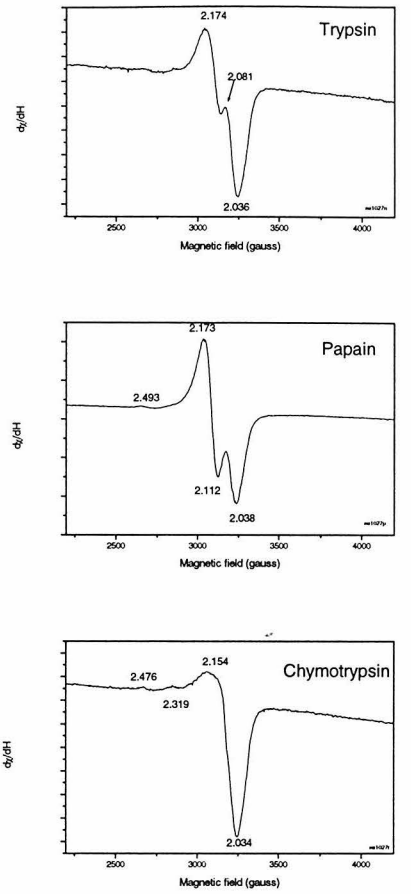

Figure 9. EPR spectrum of ferricyanide (50mM) treatment of pMMO membrane domains, after pre-treatment with the proteases trypsin (top), papain (middle), or chymotrypsin (bottom). (Data collected as in Figure 7.)

Type II centers from the initial preparation are retained, and therefore must be buried deep within the protein structure.

However, those spectra for the proteolytic cleavage after ferricyanide treatment (Figure 10) are all quite similar, and they mirror the appearance of the non-proteolytically cleaved standard quite remarkably. Apparently, in the low concentration regime, initial treatment with ferricyanide protects the soluble domain from cleavage, or the adduct that

forms during the ferricyanide treatment is buried within the protein (as might be suspected if ferricyanide were binding deep within the membrane, or at the active site itself).

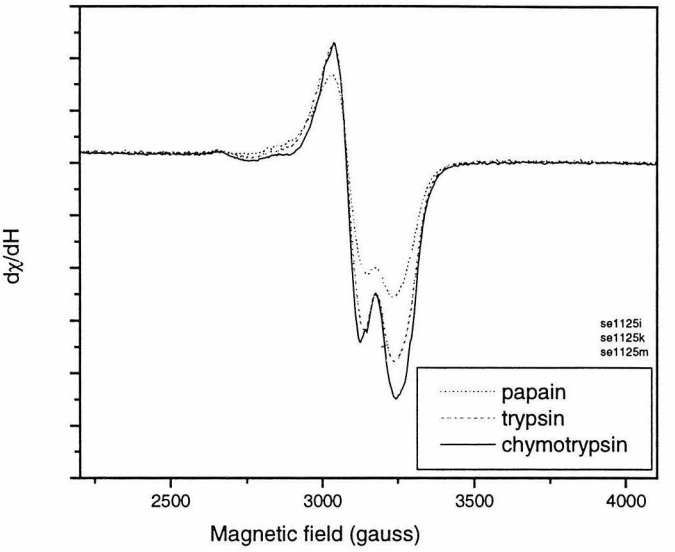

Figure 10. EPR spectra of proteolytically prepared membrane domiains after pre-treatment with 50μM ferricyanide. (Data collected as in Figure 1.)

High concentration treatment-soluble domain. Within the high concentration regime, the background EPR signal from ferricyanide itself inhibits the ability to resolve any signal due to a copper-ferrocyanide adduct. As such, no data is reported herein for the soluble fractions generated by proteolytic treatments.

High concentration treatment-membrane domains. However, the multiple steps of centrifugation and resuspension in ferricyanide-free buffer were found to efficaciously remove the oxidant from the membrane fractions, and such preparations can be readily studied by EPR. Data for proteolyzed, then ferricyanide-treated preparations are shown as

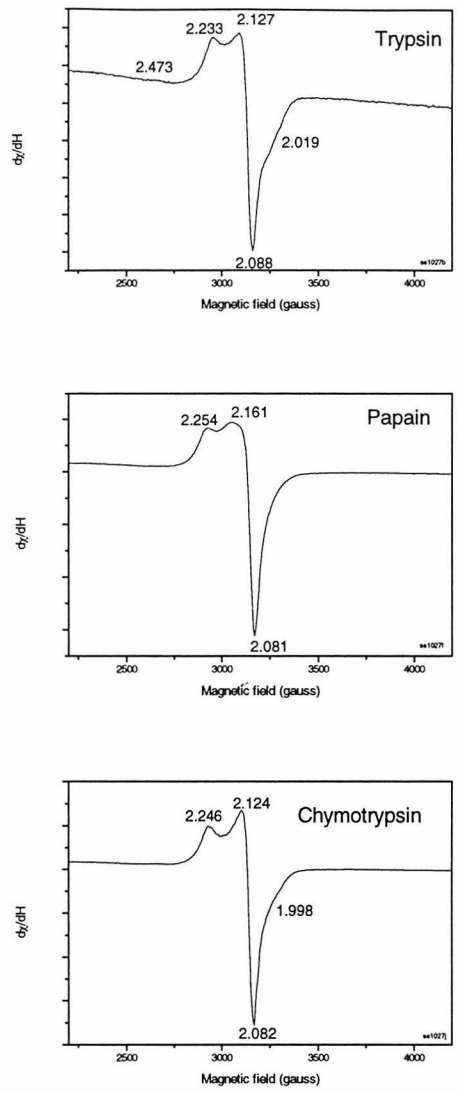

Figure 11. EPR spectra displaying the interaction of ferricyanide (5mM) upon membrane domains of pMMO first prepared by proteolytic treatment with trypsin (top), papain (middle), or chymotrypsin (bottom). (Data collected as in Figure 1.)

Figure 11. The spectra for Trypsin and Chymotrypsin treatment appear quite similar to each other and to that of the standard shown as Figure 1.

Spectra corresponding to ferricyanide-treated, then proteolyzed membrane domains from pMMO are given as Figure 12. Again, Trypsin- and Chymotrypsin-treatments have similar appearances (likely due to their generally similar specificities)

and the Papain-treatment appears different. However, none of the data mirror that of the standard 5mM ferricyanide treatment.

A novel feature is found at ~g=2.24 for the standard (non-proteolyzed) case, as well as for all of the protease plus high concentration ferricyanide samples (with a single exception). Antholine and co-workers have found that this spectrscopic feature is not unique to pMMO and can be generated by the interaction of ferricyanide with several copper-containing proteins (some membrane bound, and some soluble) in what appears to be a non-specific manner. Their findings also suggest that this species only develops over a long time scale, e.g., several days at low temperature, as if it is the product of some kind of conversion of the initial copper-ferrocyanide adduct that gives rise to the g=2.145 signal. In all of our experiments, this signal is found to be generated in a much shorter time scale, though obviously there is a requirement for millimolar ferricyanide concentrations.

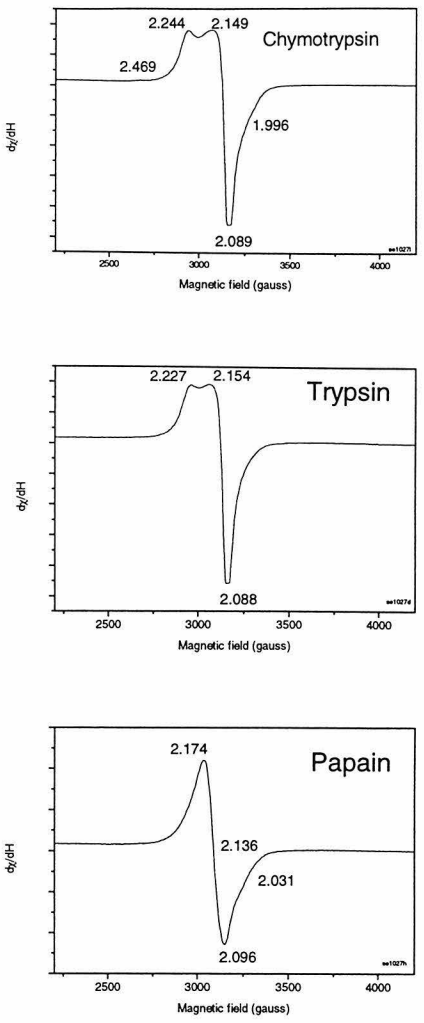

Figure 12. EPR spectra of proteolytically preapred membrane domains of pMMO, after pre-treatment with 5mM ferricyanide.

Most of the preparations generated have the general appearance of the standard 5mM ferricyanide treatment shown in Figure 1. However, the application of Papain,

prior to ferricyanide treatment, as well as the usage of Trypsin and Chymotrypsin after ferricyanide treatment, give spectra that have a subtly altered line shape in the g=2.145 region, when compared to the standard spectra. Whereas the standard has a much sharper feature that is shifted to g=2.12, these preparations seem to be primarily composed of the g=2.145 feature. The generation of these similar signals using different proteases is most unusual, and does not correspond with the specificity of the enzymes. Most interesting is the application of Papain after treatment with 5mM ferricyanide. In this case, the ability to generate either the g=2.12 signal, or the g=2.24 is hindered. Instead, only the g=2.145 signal persists, indicating that all EPR active metal centers, other than a copper(II)-ferrocyanide adduct, have been removed. Again, it is not clear how Papain is capable of being very effective in this one example, while not dramatically affecting other preparations. The apparent shift in the g=2.145 feature to g=2.12 is better revealed by considering difference spectra for the various proteolytic and standard samples, always subtracting the 50 μM ferricyanide treatment from the 5 mM ferricyanide treatment. For the standards, these are shown in Figure 3. For the cases of proteolytic treatment (before and after treatment with ferricyanide), this is shown in Figures 13 and 14. As Figure 12 shows, the further oxidation of pMMO by the usage of the ferricyanide gives rise to a sharp feature whose maximum is a g=2.12. This feature is the true "cluster signal" of pMMO, that is found only when the protein is fully oxidized.

The overlap of the closely situated signals make quantifying this feature very difficult, and it is difficult to assess the percentage of the EPR-detectable copper that can be attributed to this signal. However, the intensity of the signal must be less than that shown in the component 5mM ferricyanide sample, a preparation which had previously been used to assess the percentage of copper bound by pMMO which gives rise to the previously reported cluster signal[1]. It was found that the signal intensity could account for 41% (± 7%) of the copper associated with pMMO. Previously this assessment was used in conjunction with the model that all the copper of pMMO was arranged into homologous tri-nuclear copper clusters, and that as such, the 41% value required a correction for the intensity anomaly expected from the intensity of the $|-1/2\rangle \rightarrow |+1/2\rangle$ transition within the S=3/2 quartet manifold (as described by the tri-nuclear copper cluster)[1,12]. However, we have subtracted the component signal which is now correctly assigned to a copper(II)-ferrocyanide adduct,

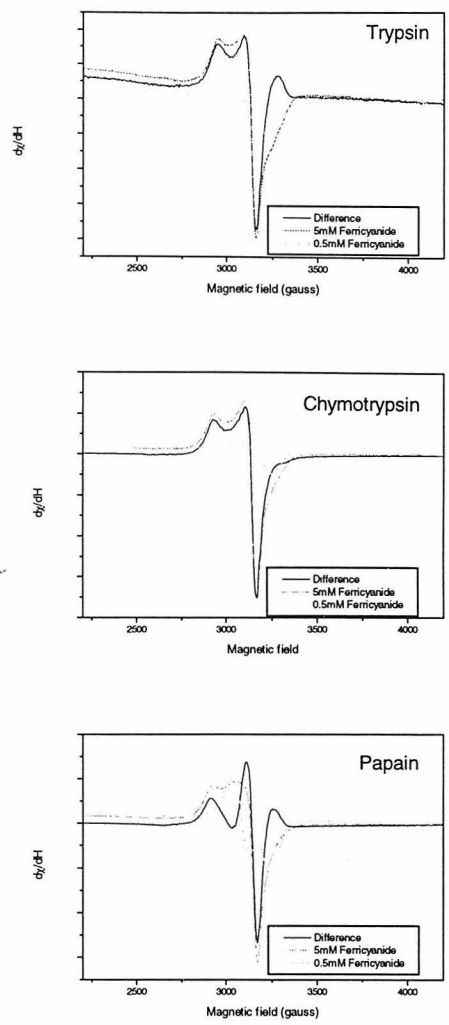

Figure 13. EPR difference spectra for the spectra shown in Figure 11.

and therefore the resultant signal (~1/2 of the original intensity after subtraction) must represent less than 50% of the total copper ions associated with the protein. Therefore, it can now be stated that all of the copper ions of pMMO cannot be arranged in tri-nuclear copper clusters, though certainly the feature found at g=2.12 indicates some component that when fully oxidized, is represented by such a cluster. A caveat to this point is that partial oxidation of clusters may lead to EPR silent species. (For example, a trinuclear cluster that has a composition of Cu(I)-Cu(II)-Cu(II) may have antiferromagnetic coupling between the two Cu(II) ions, and therefore would not be detected by EPR). This potential complication is impossible to assess fully without using another complimentary technique such as XAS to determine the Cu(II)/Cu(I) composition of these samples. However, the realization that all of pMMO coper clusters are likely not as uniform as

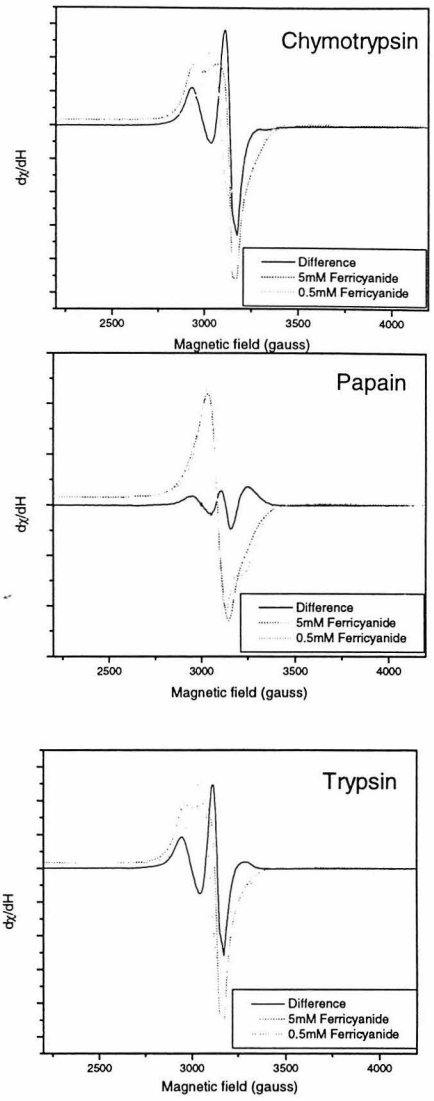

Figure 14. EPR difference spectra for the spectra shown in Figure 12.

previously suggested seems an appropriate finding, though the exact quantitation is beyond our grasp currently.

As a final comment on the difference data, it appears that proteolysis after ferricyanide treatment for Trypsin and Chymotrypsin is much less effective at removing the copper ions that give rise to the copper(II)-ferrocyanide adduct found in the low ferricyanide concentration regime. Thus, the difference spectra for these have very little contribution from the g=2.145 feature. Reversing these steps still leaves a substantive contribution at g=2.145 in the difference data, as pretreatment with protease removes the ability to generate the adduct at low ferricyanide concentration.

EDTA Treatment.

The treatment of pMMO with EDTA results in the loss of most of the copper ions

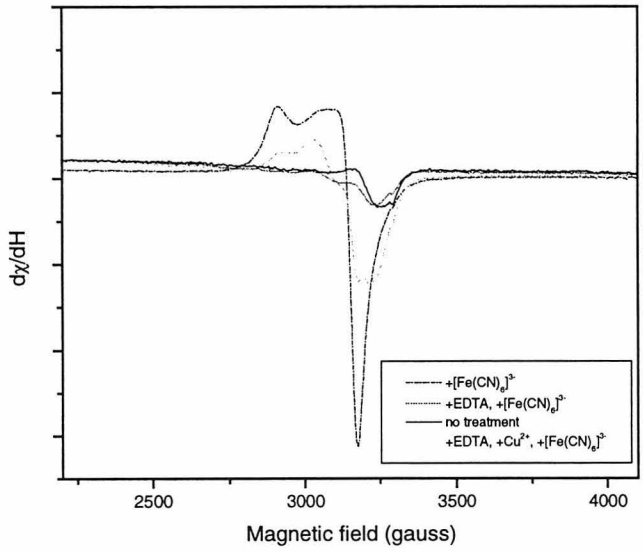

Figure 15. EPR spectra demonstrating the effect of 11.3mM EDTA on pMMO. Treatment of pMMO with EDTA, followed by 5mM ferricyanide (middle dotted lined); reconstitution with 0.1 mM copper sulfate (dashed line); and the standard 5mM ferricyanide treatment (top dot-dash line).

of the protein. Incubation in 11.3 mM EDTA was found to efficiently remove all but forty percent of the copper ions of the protein, after an incubation time of 30 minutes. The soluble fraction from these preparations can account for the copper lost from the membrane-bound protein. Moreover, the copper-EDTA complex that results does not respond to ferricyanide treatment, either at 50 μM or 5mM, unlike what was observed for the soluble, proteolyzed fractions generated above. It would appear that the copper bound in the proteolyzed fractions must be coordinately unsaturated, unlike the copper-EDTA complex described here.

Figure 15 shows the effect this treatment has on the EPR spectrum of pMMO. Treatment with EDTA reduces the Type II copper signal inherent to the as-isolated preparation. Upon treatment of this new copper-depleted form of pMMO with high (5mM) concentrations of ferricyanide, a spectrum similar to those observed in Figure 1 is not observed. As compared to a standard membrane preparation (no EDTA treatment) that is exposed to 5mM ferricyanide, the EDTA-treated sample is only capable of generating the g=2.145 signal, and then, it does so at a very low intensity (data not shown). However, incubation with a low concentration of copper sulfate (100 μM) re-generates that ability, though the spectrum does not appear like the "fully-oxidized" spectra reported above (and also in Figure 15). Thus, EDTA appears to remove a sub-set of the copper ions that are excessible in a soluble-domain. The removal of these copper ions prevents the electron-transfer steps that have been observed above which give rise to the sharp g=2.12 feature, the "cluster signal." It therefore seems quite likely that the soluble-domain copper ions (in some part) play a role in electron transfer through the pMMO system.

Moving to higher copper concentrations in the reconstitution of EDTA-treated pMMO improved the ability to generate the signals observed above. Figure 16 shows the effect on the sample when 2mM copper sulfate is used in the reconstitution process. The spectrum shown displays the features previously associated with the copper(II)-ferrocyanide adduct, as well as a small contribution of the feature at g=2.12. However, the ferricyanide treatment in this sample is at the high (5mM) concentration, and clearly this is not identical to the spectra observed in Figure 1. The concentration of copper used in this step (2mM) should be sufficient to replenish any depleted copper-binding sites, yet clearly the "reconsituted" protein is not identical to the as-isolated form. Therefore, the removal of copper ions from the soluble domain disrupts the ability to extract electrons efficiently from the membrane-localized copper ions.

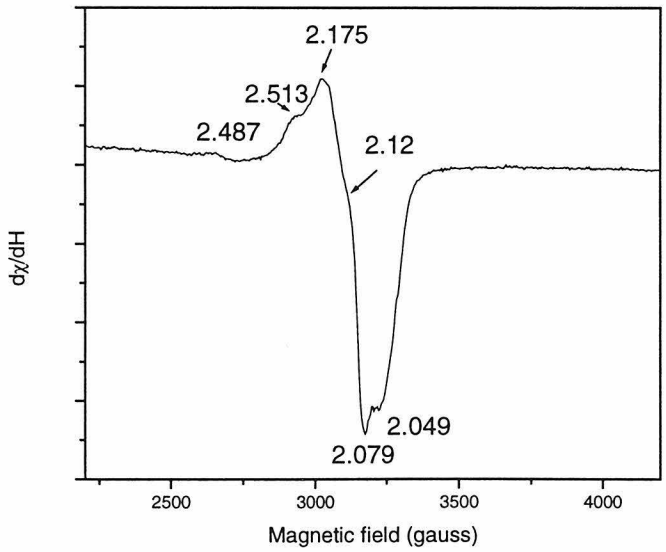

Figure 16. EPR spectrum of EDTA treated pMMO, reconstituted with 2mM copper sulfate, and then subjected to 5 mM ferricyanide. (Data collected as in Figure 7.)

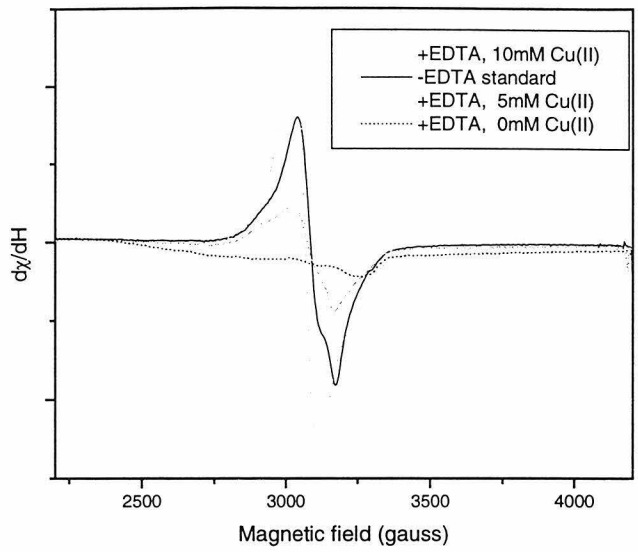

Figure 17. EPR spectrum of EDTA treatment of pMMO, followed by reconstitution with varying concentrations of copper sulfate, and subsequent ferricyanide (5mM) treatment.

A final point of note is observed in Figure 17 which shows spectra acquired using 5mM ferricyanide treatment after a variable about of reconstitution with copper sulfate. It is apparent that the copper sulfate concentration gives rise to a variable concentration of the g=2.145 signal due to the copper(II)-ferrocyanide adduct, and that it is possible to add excess copper to the system, which yields an increase in intensity at g=2.145 due to adventitious copper ions bound to the surface of protein molecules and membrane fragments. The sharpening of the EPR spectrum when moving from 5mM to 10mM copper sulfate concentration also masks the contribution of the g=2.12 signal which is observed in the lower-concentration reconstitution and the standard, which both display the feature as a slight inflection, as above.

Summary

Many findings have been described above, which when taken together paint a new picture of the different copper ions of particulate methane monooxygenase. It is now quite clear that there are copper ions located within the soluble domain of the protein, and those that are not accessible to proteolytic cleavage, nor the chelator, EDTA. In the latter case, removal of copper ions with the retention of the soluble-domain architecture hinders the ability to generate the copper(II)-ferrocyanide adduct seen previously, as well as the ability to visualize the g=2.12 cluster signal. Reconstitution of this preparation with re-addition of copper ions is difficult, due to the possibility of adventitious copper binding.

The use of proteolytic enzymes cleaves these solvent-accessible regions of the protein, and demonstrates that there must be unique cleavage and binding sites within the soluble domain. Chymotrypsin incubation in particular seems to remove a subset of copper ions that initially yield a copper(II)-ferrocyanide adduct when pMMO is treated with low concentrations of ferricyanide. Papain and Trypsin achieve this as well, but to a lower extent. And lastly, the observation of the g=2.12 signal, when separated from the g=2.145 component, indicates that the "cluster signal" must only be derived from a sub-population (<7 copper ions approximately) of the copper ions of pMMO. And therefore, the EPR signal due to a tri-nuclear copper cluster would appear to come from two of such clusters at most. It cannot be determined whether or not ferricyanide disrupts the other clusters entirely or partially, however, but it does appear that two of such clusters could be buried deeply within the protein-membrane complex.

References Cited

1)Nguyen, H. H. T.; Nakagawa, K. H.; Hedman, B.; Elliott, S. J.; Lidstrom, M. E.; Hodgson, K. O.; Chan, S. I. *Journal of the American Chemical Society* **1996**, *118*, 12766-12776.

2)Karlin, K. D.; Tyeklar, Z. *Bioinorganic Chemistry of Copper*; Chapman and Hall: New York, 1993.

3)Solomon, E. I.; Sundaram, U. M.; Machonkin, T. E. *Chemical Reviews* **1996**, *96*, 2563-2605.

4)Nguyen, H.-H. T. *The Bioinorganic Chemistry of the Particulate Methane Monooxygenase from Methylococcus capsulatus(Bath) and Methane Activation from a Biological Perspective*; Caltech: Pasadena, CA, 1997. Ph.D. Thesis.

5)Morpurgo, G. O.; Mosini, V.; Porta, P.; Dessy, G.; Fares, V. *J. Chem. Soc. Dalton Trans.* **1980**, 1272-1276.

6)Morpurgo, G. O.; Mosini, V.; Porta, P.; G., D.; Fares, V. *J. Chem. Soc. Dalton Trans.* **1981**, 111-117.

7)Scott, M. J.; Holm, R. H. *J. Am. Chem. Soc.* **1994**, *116*, 11357-11367.

8)Scott, M. J.; Lee, S. C.; Holm, R. H. *Inorg. Chem.* **1994**, *33*, 4651-4662.

9)Smekal, Z.; Brezina, F.; Sindelar, Z.; Klicka, R.; Krausova, D.; Nadvornik, M. *SYNTHESIS AND REACTIVITY IN INORGANIC AND METAL-ORGANIC CHEMISTRY* **1996**, *26*, 1537-1549.

10)Suzuki, M.; Uehara, A. *Bull. Chem. Soc. Jpn.* **1984**, *57*, 3134-3138.

11)Yuan, H.; Collins, M.; Antholine, W. *JOURNAL OF INORGANIC BIOCHEMISTRY* **1998**, *72*, 179-185.

12)Nguyen, H. H. T.; Shiemke, A. K.; Jacobs, S. J.; Hales, B. J.; Lidstrom, M. E.; Chan, S. I. *Journal of Biological Chemistry* **1994**, *269*, 14995-15005.

Chapter 4: Homology Analysis of the Primary Structure of PmoA Reveals Potential Ligands for the pMMO Active Site

Abstract

To determine the possible ligands for the copper centers of particulate methane monoooxygenase, a study of the homology of the PmoA protein from a series of 12 methane oxidizing bacteria and 6 ammonia oxidizing bacteria was conducted. The generation of double-stranded DNA sequences of PmoA from *Methylomonas rubra* S1, *Methylomonas methanica* Sh15, and *Methylomicrobium album* BG8, as well as several methanotrophic isolates from Lake Washington, Washington, U.S.A., were completed, and compared to the scant number of previously reported sequences available from *pmoA* and *amoA*. The homology that results strongly identifies several key regions in PmoA which are likely candidates for copper binding, particularly three His residues, and an acid-rich region that is thought to exist at the interface of the periplasm.

Introduction

Bacteria that oxidize ammonia (ammonia oxidizers) and bacteria that oxidize methane (methanotrophs) are important components of the global cycling of nitrogen and carbon, respectively. Both types of bacteria are composed of Gram negative species, though ammonia oxidizers are predominantly of the β branch of the proteobacteria, and methanotrophs are of the α and γ branches[1,2].

All methanotrophs currently studied utilize methane as their sole carbon and energy source and are obligate aerobes[3]. Methane is first oxidized to methanol, and in individual steps, the methanol is converted to formaldehyde (which is used for the generation of biomass) and then to formate and carbon dioxide. Methanotrophs are further differentiated into two types, based on (a) the metabolic pathway they anabolize formaldehyde, (b) the type of intracytosolic membrane they produce, and (c) what kinds of phospholipids they produce[4,5]. Type I methanotrophs are exemplified by the genera

Methylobacter, Methylomonas, Methylomicrobium, Methylococcus, and most recently, *Methylothermus*[6], utilize the ribulose 5'-phosphate pathway for carbon assimilation, and have intracytosolic stacked membranes and C_{16} fatty acids, primarily. Type II methanotrophs (*Methylosinus* and *Methylocystis*) utilize the serine pathway for carbon assimilation, have intracytosolic membranes that form concentric circles to the outer membrane, and have C_{18} fatty acids[3]. Ammonia oxidizers have no such sub-divisions.

In terms of metabolism, methanotrophs and ammonia oxidizers possess a very similar gene product that is responsible for the analogous first step of their energy-generating metabolic pathways. Ammonia oxidizers are all obligate aerobes which oxidize ammonia (NH_3) to hydroxylamine (NH_2OH) using the membrane-bound protein ammonia monooxygenase (AMO). The reducing equivalents generated in this process, along with those generated by the subsequent oxidation of hydroxylamine to nitrite partitioned between AMO (to regenerate AMO activity), as well as to a terminal oxidase[3].

The AMO protein has been shown to be quite similar to particulate methane monooxygenase (pMMO) which is found in all methanotrophs, and is responsible for the oxidation of methane to methanol[7]. In terms of primary sequence, behavior towards inhibitors, and genetic organization of their respective *amo* and *pmo* operons, these two systems have considerable similarity, even though they have different roles in the overall biochemistry in their environment. Both systems are now accepted to be comprised of three polypeptides; e.g., for methane oxidizers, PmoA, PmoB, and PmoC, of approximately 27, 45 and 23kDa in size. Specifically, initial comparisons of the available pMMO sequences (for *pmoA* and *pmoB* from *Methylococcus capsulatus* (Bath)) revealed

that the sequence was very similar (over *pmoB*, a 42.9% identity to *amoB* from *Nitrosomonas europeae*, while over *pmoA*, a 46.7% identity to *amoA* was found)[8]. AMO and pMMO have been found to be affected by very similar inhibitors such as acetylene, EDTA, and the reduced copper chelators[9]. The genetic arrangements of the operons are also very similar[10-12]. The *pmoA* (*amoA*) gene is found upstream a very short distance from *pmoB*. A third gene, *pmoC*, is found at a variable distance upstream from *pmoA*. Within a given strain, the copies of *pmo* and *amo* genes are nearly identical, and an additional copy (or copies) of either *pmoC* or *amoC* are found elsewhere on the genome, without copies of *pmoAB* downstream[12]. More recently, primers designed to clone the 532 bp fragment of *pmoA/amoA* and to compare the homology of this internal segment from five methanotrophs and four ammonia oxidizers, and to describe the phylogenetic relationship between the strains under study[13]. The phylogenetic relationship between the strains indicated that ammonia oxidizers and methanotrophs are evolutionarily related. Finally, both *pmo* and *amo* code for proteins whose activity is intimately tied to copper concentration. Moreover, in both systems, the 27kDa membrane bound protein (PmoA or AmoA) is specifically labeled by [^{14}C]-acetylene, an irreverisble inhibitor of the enzymes[14,15]. Yet, for all the similarity reported for the *amo* and *pmo* systems, the corresponding proteins perform different biological functions.

The ubiquity of copper in both systems is singularly significant, and in particular, the eminent goal of this study is to elucidate the features of the protein sequence responsible for the binding and chemistry of the protein-bound copper ions. Specifically, we have chosen to expand the available *pmoA* gene sequences by completing the sequencing of those strains listed in Table 1. This sequencing effort will lead to the

construction of a library of sequences, which in turn might give insight as to the potential ligands for the copper ions of these proteins.

Species	Type
Methylomonas rubra S1	I
Methylomonas methanica Sh15	I
Methylosinus trichosporium OB3b	II
Methylococcus capsulatus (Bath)	X
Methylomicrobium album BG8	I
Lake Washington (LW) –2	II
LW-3	II
LW-4	II
LW-5	II
LW-13	I
LW-15	I
LW-21	I

Table 1. Strains and isolates used in this study

As described below, in order to determine which residues in the primary sequence of PmoA, the polypeptide apparently responsible for containing the active site of the protein, an entire homology search over the entire PmoA sequence is required. This could reveal potential metal-binding side chains, such as those found in histidine and acidic amino acid side chains. Therefore, the subsequent assembly of contiguous fragments, and their sequence analysis, can help demonstrate the overall similarity in *pmoA* from a variety of organisms (Type I and Type II methanotrophs) and reveal a sense of the similarity between methanotrophs and ammonia oxidizers. Further, the existence of

identical copper binding residues throughout the sequences examined will allow for new insights into potential copper-binding sites within PmoA.

Experimental Procedures

Primer Design.

Primers were designed initially by visual inspection of the relevant partial sequences that were made available in the laboratory of Dr. Mary E. Lidstrom (University of Washington), or were from the laboratory of Dr. Colin Murrell (Warwick, U.K.) in the case of *M. trichosporium* OB3b. Previously cloned and partially sequenced *pmoA*-containing DNA from Lake Washington isolates have been described by Costello and Lidstrom[16]. The identities of the primers used in this study are summarized in Table 2. The primer S189R was used for sequencing previously cloned and partially sequenced *pmoC-pmoA* regions from *M. methanica*, *M. rubra*, *M. album* BG8, as well as LW-21, LW-15 and LW-13. For the other Lake Washington isolates (LW-2, LW-3, LW-4, LW-5) specific primers localized to the *pmoC* and *pmoA* region were designed and utilized to generate a double-stranded sequence. The primers A342 and B456 were designed to hybridize with the downstream (C-terminal) region of *pmoA* and the upstream (N-terminal) region of *pmoB*, respectively, for a wide range of methanotrophs.

DNA Sequencing Reactions.

DNA sequencing was carried out by the University of Washington Sequencing Facility, with an Applied biosystems automated sequencer.

Cloning of 3'-End of pmoA.

To facilitate sequencing of the C-terminal PmoA region, a new section of pmoA was cloned. A new primer (B456) was designed from aligned sequences of pmoB from M. capsulatus (Bath), M. trichosporium OB3b, and M. album BG8. B456 was used in conjunction with a well- used primer for PmoA, A189, to generate an approximately ~1.0 kb PCR product. PCR reactions were carried out as follows: reactions were all carried out on a 50 µl scale using, 1.5 µl 1.5 mM $MgCl_2$, 1 µl template (chromosomal DNA, ~200 ng) DNA, 1 µl primer DNA (50 pmol of each primer), and 1 µl of 10mM dNTP, 5 µl Gibco reaction buffer, and 2.5 U of Gibco Taq polymerase. In some reactions, addition of 5 µl DMSO was found to be useful in PCR yield. The B456-A189 product was prepared from *M. rubra*, *M. methanica*, as well as all of the Lake Washington isolates, and a trial from *M. capsulatus* (Bath) as a control. The PCR reactions were performed in a Perkin-Elmer model 9600 GeneAmp PCR System thermal cycler, carried out using 25 cycles consisting of 92°C for 1 min, 55°C for 1.5 min, and 72°C for 5 min.

The PCR products were transfected into *E. coli* using a TopoTA Cloning Kit (Invitrogen), following the manufacturer's instructions. Cloning reactions were prepared using 2 µl of the PCR reaction product, 2 µl of sterile water and 0.7 µl of pCR-TOPO vector. The mixture was carefully mixed and incubated for 5 minutes at room temperature, and then placed on ice. Competent cells were transformed and after transformation, aliquots were plated onto agar containing X-gal (40 µl of 40 mg/ml) and IPTG (40 µl of 100 mM), and were incubated at 37°C overnight. White homogenous clones containing inserts were transferred into 2.0 ml of Luria Broth using toothpicks and the resulting cultures were grown overnight at 37°C. Aliquots from each overnight

culture were pelleted by centrifugation and plasmid DNA was prepared according to the method of Dollie and Birnboim. Plasmid DNA was then restriction enzyme digested with *Eco*RI and analyzed by agarose gel electrophoresis. Positive clones were identified by observation of a ~1.0 kB fragment that corresponded to the PCR product. This visualized band was excised and purified using a QIAquick gel extraction kit (Qiagen). Purified DNA was then submitted for sequencing using the A342 primer.

Primer	Sequence	Reference
A189	GG(C/G)GACTGGGACTTCTGG	Holmes, et al.
S189R	CCA(A/G)AA(A/G)CCACTCACC	This work
LW2R1	GAACCACCAGAGCCGACGG	*Ibid.*
LW2F1	CGCTTATTCACCAAGGAC	*Ibid.*
LW3R1	GAACACCAGGCTGATCGGG	*Ibid.*
LW3F1	GTTTCGGAGAGGGATCG	*Ibid.*
LW4R1	GAAGGTCGCGCCGAACG	*Ibid.*
LW4F1	GAATGCTCTCGGAACGAAG	*Ibid.*
LW5R1	GATCGGGAAGTAGGTCCAGC	*Ibid.*
LW5F1	GGAGCGTGATTGTCTGG	*Ibid.*
A342	CTTCTGGGG(A/C/T)TGGAC(A/C/T)TA(C/T)TTCC	*Ibid.*
B456	GAT GAT (C/T)GG (A/G/T)CC (A/G)CC C	*Ibid.*

Table 2. The primers used in the current study

Sequence Data Analysis.

Assembly of contiguous sequences ("contigs") and translation of DNA sequences were carried out using Genetic Computer Group programs (Genetics Computer Group, Madison, WI). The development of hydropathy plots and the assignments of transmembrane helices were achieved by use of internet-based web tools. The hydropathy analysis was performed on-line at http://www.bmb.psu.edu/ (Department of Biochemistry and Molecular Biology, Penn State University), and the transmembrane domain predictions were carried out similarly using the PredictProtein tool at http://www.embl-heidelberg.de/ (European Molecular Biology Laboratory, Heidelberg, Germany).

Phylogenetic Analysis.

Translated PmoA and AmoA sequences were aligned manually and/or by using the ClustalW alignment algorithm as a part of the SeqPup package. Based on the alignments, dendrograms were constuctured for translated PmoA sequences using the PROTDIST, PROTPARS, NEIGHBOR, and SEQBOOT programs from PHYLIP, version 3.5c[17], and tree files were analyzed using TreeView[18].

Results

Sequencing of Strains and Isolates.

The initial sequencing of the 5'-region of the *pmoA* gene was achieved readily through the design of primers appropriate to the strains listed in Table 1. Both the more general primer S189R (used for *M. methanica*, *M. rubra*, *M. album* BG8, as well as LW-21, LW-15 and LW-13), and the specific primers designed for sequencing the C-terminal region of *pmoC* through the N-terminal region of *pmoA*, gave excellent results with sufficient overlap in the resulting contigs to resolve any potential discrepancies. These individual sequences were taken and compiled with partial sequences of *pmoA* generated in the laboratories of Professor Mary E. Lidstrom (University of Washington, Seattle, U.S.A.) and Dr. Colin Murrell (University of Warwick, Coventry, U.K.). However, most of the reported partial sequences were for a 532 bp internal fragment of *pmoA* , and many of the sequences represented single-strand data for a portion of the *pmoA* sequence.

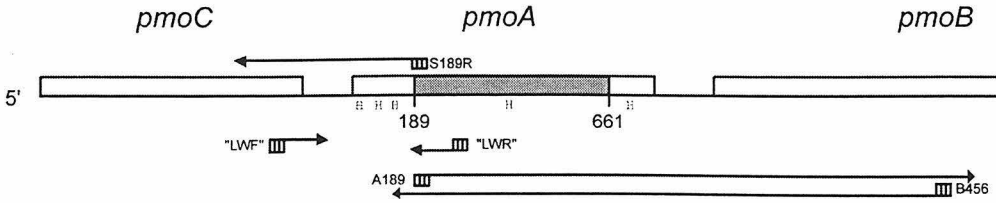

Figure 1. A general scheme for the *pmo* operon, indicating the sites for primers used in this study. The physical position of the histidine residues of PmoA from *M. capsulatus* (Bath) are indicated by H. Either S189R was used to sequence the second strand of several of the strains used in this study, or the combination of LWF- and LWR-primers were used to generate both strands. The 3'-end of *pmoA* was targeted by cloning the region between A189 and B456.

Due to errors that can occur in sequencing, a second strand sequence was required before utilizing these sequences in a homology study. Further, inspection of the entire sequence available for *Methylococcus capsulatus* (Bath) shows that the internal fragment might not contain several of the potential copper ligands, since the putatitve histidine residues are absent. As Chapter 5 clearly shows, histidine residues can be detected at the active site of pMMO, and therefore are likely copper ligands for PmoA. As such, the assembly and generation of second-strand data for the strains in the collection was required to give a full interpretation of the resulting PmoA protein sequence.

The contigs in their fully assembled form are given in Figures 2 and 3. In all cases, the sequences utilized complete the desired N-terminii of the protein.

Cloning of 3'-pmoA Region.

In order to finish the entire PmoA sequence for as many strains as possible, the sequencing described above was followed by an attempt to clone a fragment of *pmoAB* that would contain the C-terminal domain of *pmoA*. This region is not of interest specifically for histidine residues, as such, but is still desired for the sake of completeness. The A189 primer was utilized along with a designed primer for *pmoB*,

B456, which was designed based on the sequences from *M. capsulatus* (Bath), *M. trichosporium* OB3b, and *M. album* BG8. These primers were first used to amplify the desired fragment from chromosomal DNA from all of the strains listed in Table 1 *via* PCR. Based on the observed success of these PCR reactions, the PCR product prepared from *M. rubra* and *M. methanica* was prepared for direct sequencing by excision and purification using a QIAquick gel extraction kit. However, attempts to perform direct

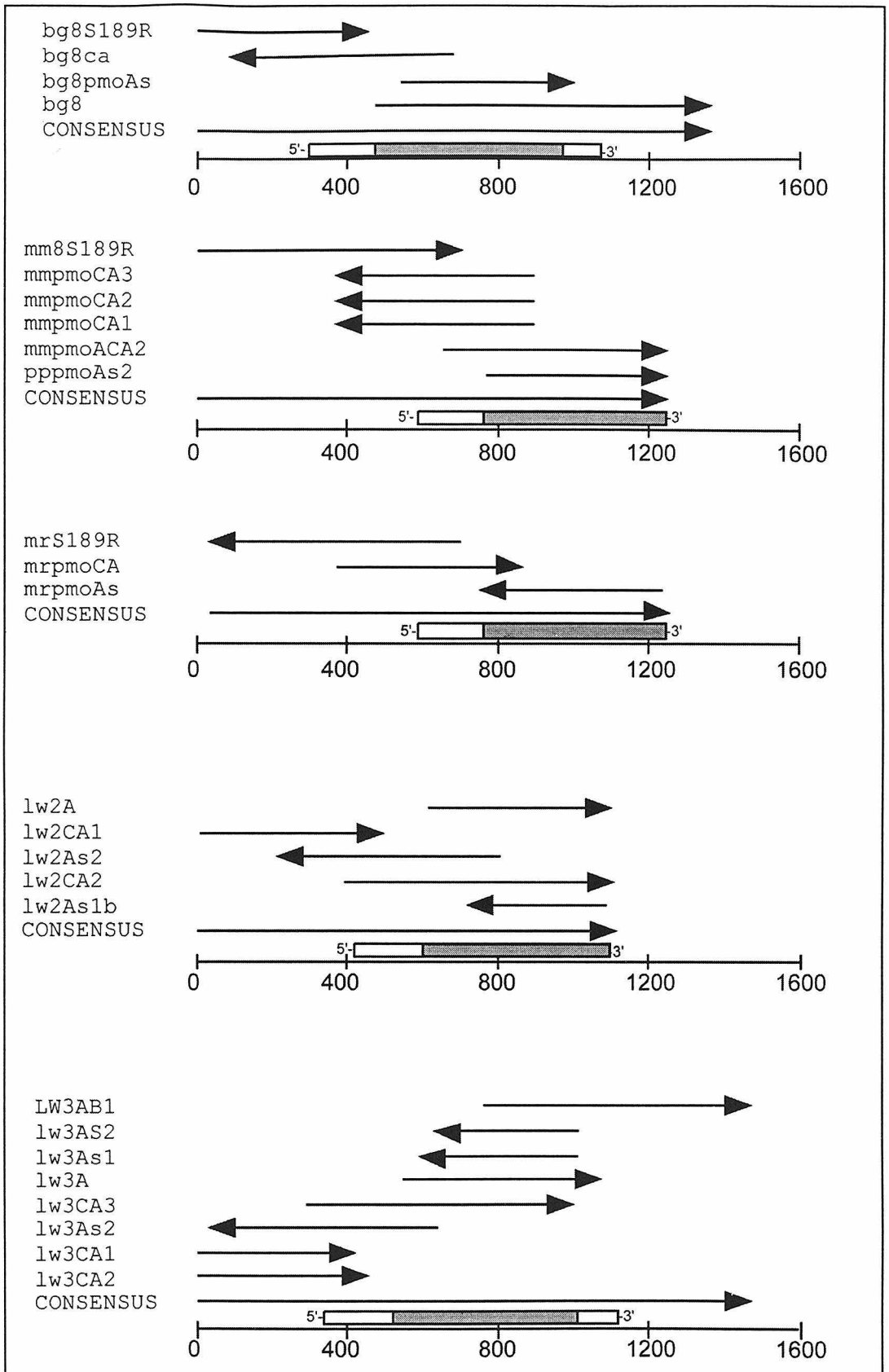

Figure 2. An example of the assembly of contiguous single stranded sequences.

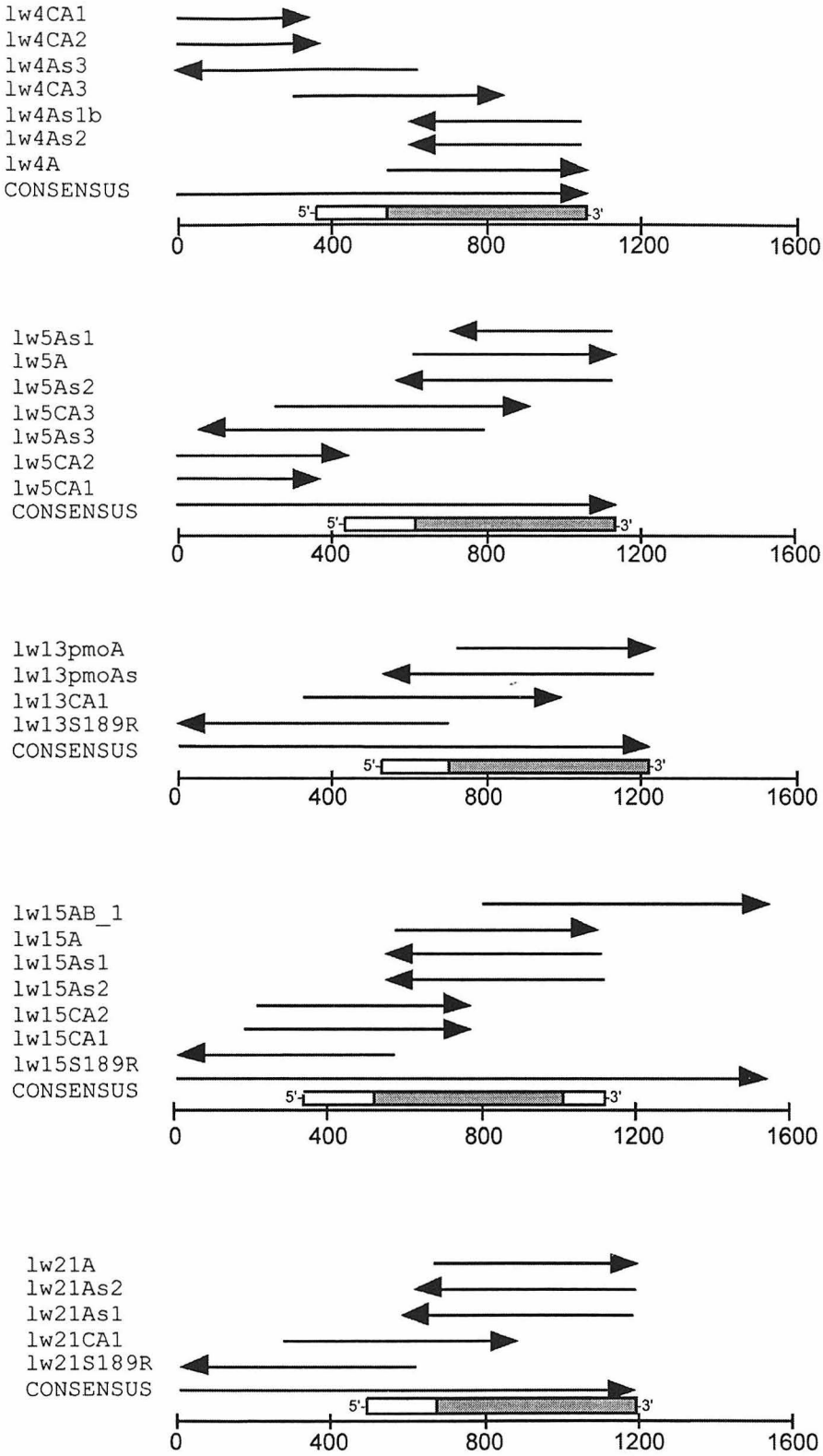

Figure 3. The assembly of remaining contiguous nucleotide sequence fragments.

sequencing using the A342 as a sequencing primer all failed. Therefore, the PCR

products were instead inserted into the pCR.2 vector provided (TopoTA kit, Invitrogen), which was monitored by subsequent digestion with *EcoR*I, as shown in Figure 4. Initial transfection into *E. coli* and blue/white selection on X-gal/ITPG yielded positive clones for *M. methanica*, *M. rubra*, and LW-3 and LW-15. Twelve positive colonies from each strain were used to inoculate overnight liquid cultures, giving cells that were used for the preparation of plasmid DNA. Figure 4 shows the insertion pattern of the resulting plasmids, and those colonies that were deemed to contain the insert. Plasmid DNA corresponding to the positive lanes was then submitted for sequencing using the A342 primer. LW-3 and LW-15 yielded useable sequence data, and the subsequent design of primers based on those sequences enabled the acquisition of the second strand sequence. Thus, C-terminal domain sequences for LW-3 and LW-15 were achieved.

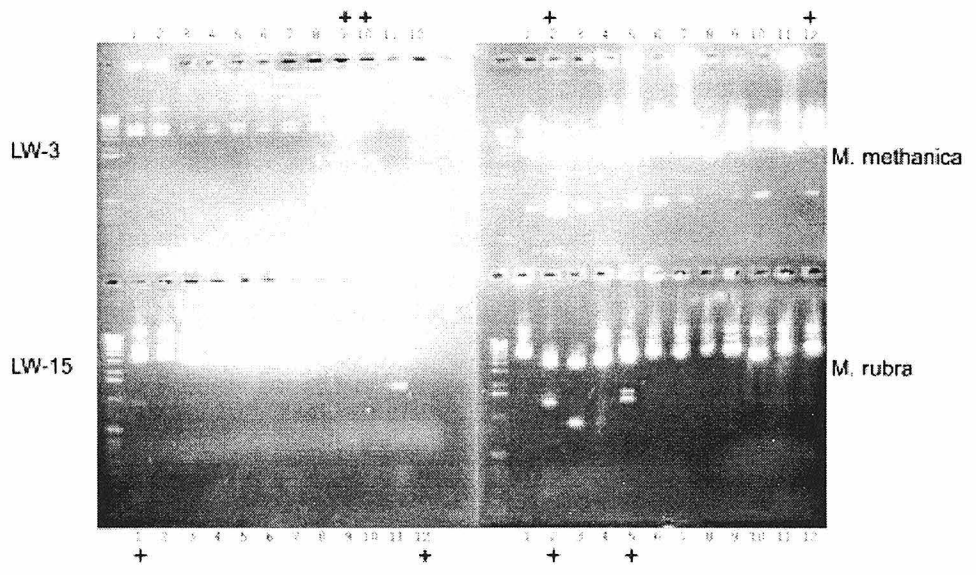

Figure 4. Suessful cloning of ~1.0 kb insert of the A189-B456 for LW-3, LW-15, *M. methanica* and *M. rubra*. Those lanes marked with a (+) indicate individual clones positive for insertion. Plasmid DNA prepared from the positive clones was then used in sequencing reactions as described.

Sequences.

The DNA sequences assembled from contiguous fragments generated previously and in this study were taken and loaded into the sequence analysis software SeqPup. Using the ClustalW alignment tool, a multi-sequence alignment was achieved. The alignment is shown in Figure 5 and subsequent alignment file was truncated to remove any gaps and then taken into the PHYLIP software package for phylogenic analysis. Utilizing PROTPARS, PROTDIST, NEIGHBOR and TreeView, a basic phylogram was constructed for the sequence between positions 22 through 214, and bootstrap values for the strains were acquired by running SEQBOOT. The phylogram is shown as Figure 6.

In terms of the potential chemistry of PmoA and AmoA, the sequence information reported in Figure 5 is most useful when considered in terms of absolute identity between sequences. As an arbitrary level of "identity," those residues which are identical between all strains, allowing for a single exception only, are depicted in white on a black background. There is considerable similarity between all sequences, and as such, a high level of homology is required in order to be significant. Alternatively, the entire sequence would appear to be of significance due to the high degree of similarity.

Regarding the potential ligands for metal ions in pMMO and AMO, the histidines residues (excellent ligands for metal ions) are found to be mostly, though not uniformly, conserved throughout the sequence. Histidines found in position 43, 45 and 173 are identical, and therefore are likely involved in metal-binding, or another important role in protein function. (Here the position number refers to the relative position in Figure 5, and not the actual position of the residue in the amino acid sequence for the particular strain.) Other histidine residues similarly implicated previously (such as those found at

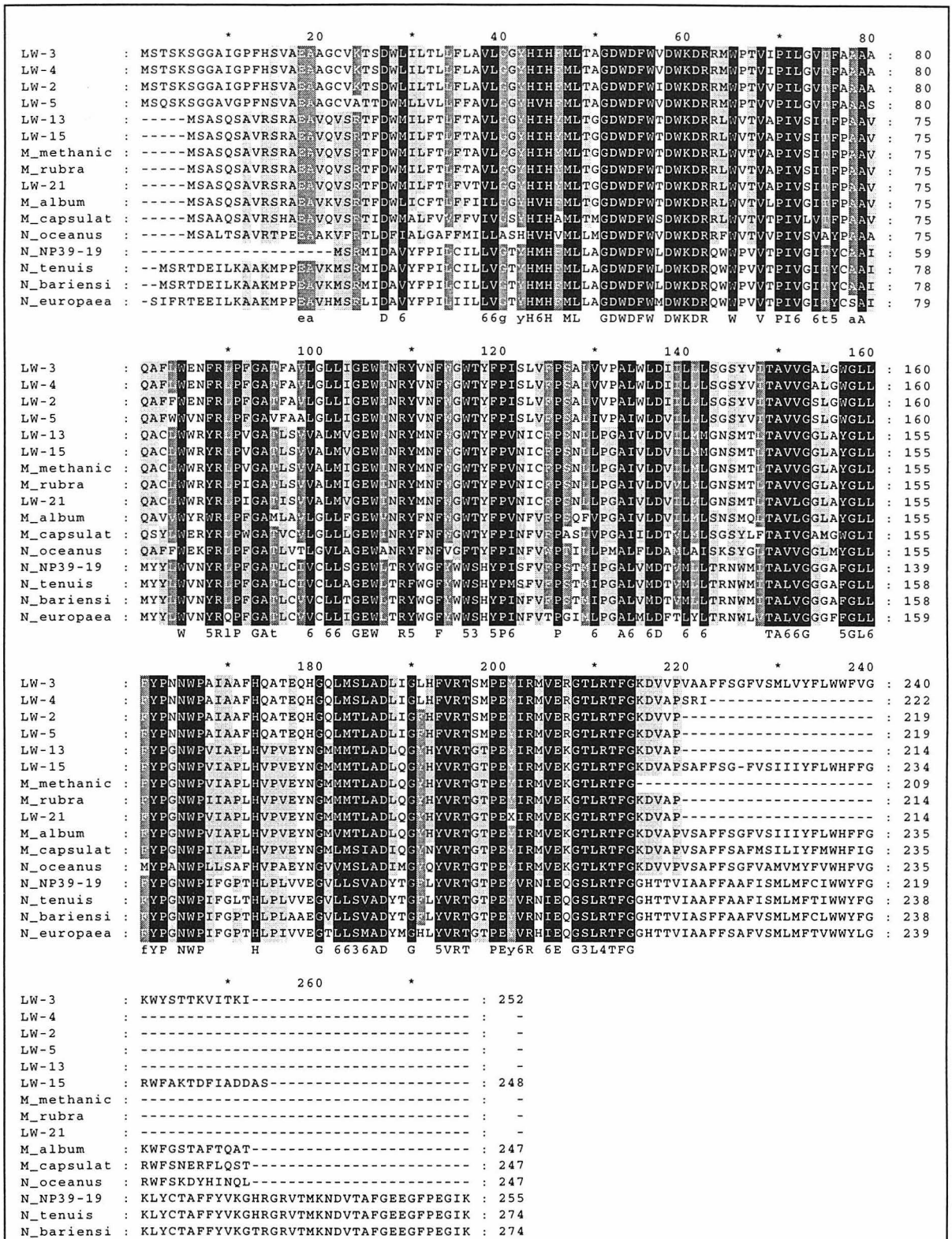

Figure 5 Sequence alignment for PmoA from the strains studied currently, as well as the PmoA sequences from *Methylococcus capsulatus* (Bath), and the AmoA from four ammonia oxidizers: *Nitrosococcus oceanus, Nitrosospira* NP39-19, *Nitrosospira briensis*, *Nitrosovibrio tenuis,* and *Nitrosomonas europaea.*

positions 16 and 237 in the sequence of *M. capsulatus* (Bath)) are typically substituted for by either hydrophobic or polar residues, such as valine, proline, and tryptophan. However, there are positions that contain histidine residues which may indeed have a role in metal binding, as the substitutions that are observed involve other potential ligands (unusual ones). For example, position 192 is a histidine in all of the methanotrophs but *M. capsulatus* (Bath), where it is asparagine.

Other regions within the PmoA sequence are identical over several residues. In particular, the region between position 51 and 62 contains four aspartic acid residues that are conserved, and the entire sequence is identical with the sole exception of position 57, which only shows modest substitutions between non-polar residues.

Aside from these examples of identical residues, it is not clear which PmoA amino acids might be involved in metal binding. All of the sequences display a dearth of cysteine residues that might be expected due to the propensity of pMMO to bind reduced copper ions. No cysteine residue is identical throughout the sequences, nor is any specific cysteine uniformly replaced by a different metal-binding residue. Therefore, we conclude that cysteine is not likely involved in copper binding in PmoA. Methionine has been found to act as a metal-ligand occasionally, particularly for copper centers. Here, the methionine in position 47 is identical throughout all sequences, and is found within a cluster of identical residues, including the histidines mentioned above. As such, it seems quite possible that this methionine might act as an available copper ligand. All other methionines are un-identical throughout the sequences, and many (such as those in position 102, 140 and 183) are substituted for by leucine, a non-polar homologue of similar shape and size. The methionine in position 204, however, is substituted for by

possible ligands (histidine and asparagine), possibly indicating its involvement in metal binding.

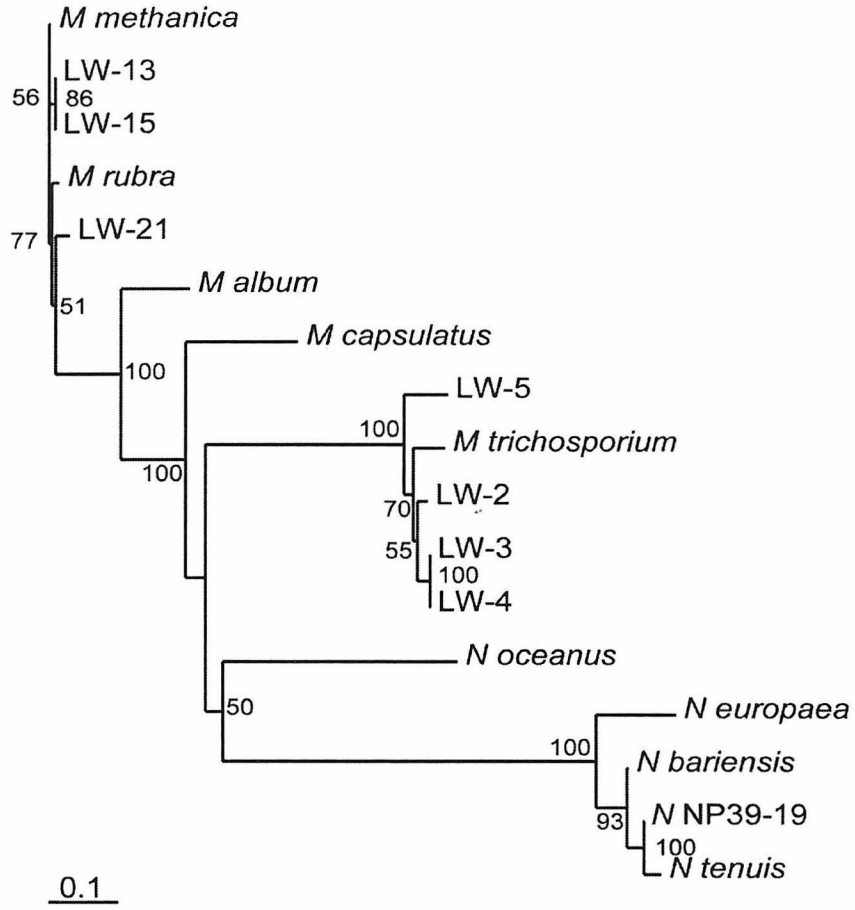

Figure 6. Phylogenetic analysis of the derived amino acid sequences encoded by the *pmoA* genes. Bootstrap values greater than 50% based on 100 replicates are shown near the branch points. The bar represents 10% sequence divergence as determined by measuring the lengths of the horizontal lines connecting two species.

Phylogeny and Conserved Domains.

The phylogram displayed in Figure 6 demonstrates the relative sequence divergence of the PmoA peptide sequences displayed in Figure 5. The phylogram mirrors those found previously for the 253 bp internal fragment sequenced by Holmes

and co-workers, and Costello and Lidstrom, although considerable variation is observed in the N- and C-teminal regions. Because of the appearance of gaps, these regions are excluded from phylogenetic analysis. As found in the latter of those studies, utilzing either the nucleotide or the peptide sequences for phylogenetic analyses appears to yield identical results. Also of particular note for our studies, previous phylogenetic study of the 16S RNA for these strains demonstrated that Lake Washington isolate LW-3 and LW-4 were previously found to fall under the genera *Methylosinus*, and LW-15 is considered a part of the *Methylomonas* genus. This is also shown in the phylogram produced by the comparison of PmoA. In terms of the sequence information presented in Figure 5, this implies that complete, double-strand sequences are now completed for the major genera *Methylosinus*, *Methylococcus*, *Methylomicrobium*, and *Methylomonas*.

Using the complete sequences of PmoA now in hand, and sequences of AmoA from three ammonia oxidizers, the general topology of the PmoA/AmoA protein was investigated by examining transmembrane domain prediction, as determined by PredictProt, a computation tool available through the European Molecular Biology Laboratory. The predictions of transmembrane domains are depicted in Figure 7 as a list of the complete sequences, where the transmembrane helices predicted for the methanotrophs are shaded in light gray, and those for the ammonia oxidizers are shaded in dark gray. Generally, there appears to be two different possibilities for the arrangement of transmembrane helices in this system, either yielding six or seven transmembrane domains. The placement of the first three (and arguably, four) of the domains appear nearly identical throughout, and indeed the final domain is in nearly exactly the same position for all sequences. The placement of the fifth helix , and the existence of a sixth

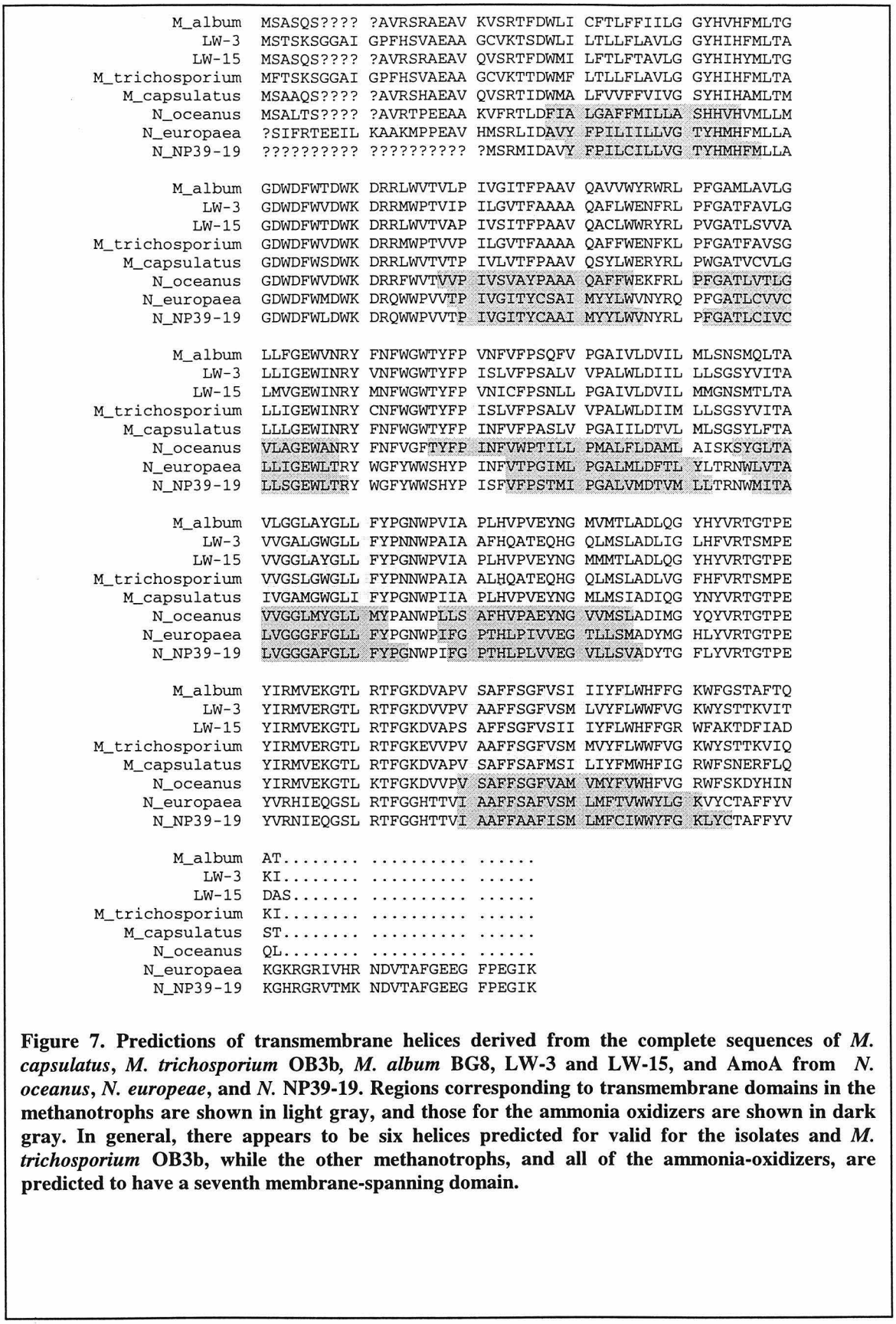

Figure 7. Predictions of transmembrane helices derived from the complete sequences of *M. capsulatus*, *M. trichosporium* OB3b, *M. album* BG8, LW-3 and LW-15, and AmoA from *N. oceanus*, *N. europeae*, and *N.* NP39-19. Regions corresponding to transmembrane domains in the methanotrophs are shown in light gray, and those for the ammonia oxidizers are shown in dark gray. In general, there appears to be six helices predicted for valid for the isolates and *M. trichosporium* OB3b, while the other methanotrophs, and all of the ammonia-oxidizers, are predicted to have a seventh membrane-spanning domain.

helix for some sequences, is not precisely predicted, however. While this computational ambiguity suggests that different PmoA proteins may have different folds, this seems intuitively unlikely. While it does limit our ability to assess a potential general topology for PmoA and AmoA, it does seem that the overall similarity in the protein sequences would lead to a homologous fold and topology. Consulting a hydropathy analysis for this region within the sequences (data not shown) does reveal that the entire region is hydrophobic.

Discussion

To put the above results in terms of what is known about pMMO, the findings are most useful in terms of the potential identification of the ligands for (at least) some of the copper ions that are known to be associated with the protein. As will be shown in Chapter 5, more than one histidine residue must be associated with a site of dioxygen chemistry for the enzyme, which is presumed to be the active site. Therefore, as there are three histidines found to be identical within all the sequences, at least two of these three are likely to be involved in copper binding at the active site of the pMMO system.

This general model is further enhanced by the consideration of the transmembrane domains predicted for the PmoA and AmoA sequences. Figure 8 shows a comparison of the two different models for the general topology of the protein, both using the sequence of *M. capsulatus* (Bath) to illustrate the breadth of change between the two models. The six-helix model (top, Figure 8) places one of the identical histidines in a soluble domain, whereas the seven-helix model (bottom, Figure 8) places all of the identical residues in transmembrane helices. As both models agree on the topology for the first several

helices, as well as the final helix, histidines 38 and 40 are likely buried in the membrane domain (note here we refer to the specific residues in terms of the absolute position within the PmoA sequence from *M. capsulatus* (Bath). Visual inspection of Figure 7 shows that all sequences agree on the location of these histidine residues, therefore they should exist close to the membrane-periplasm interface. Further, in either model the third

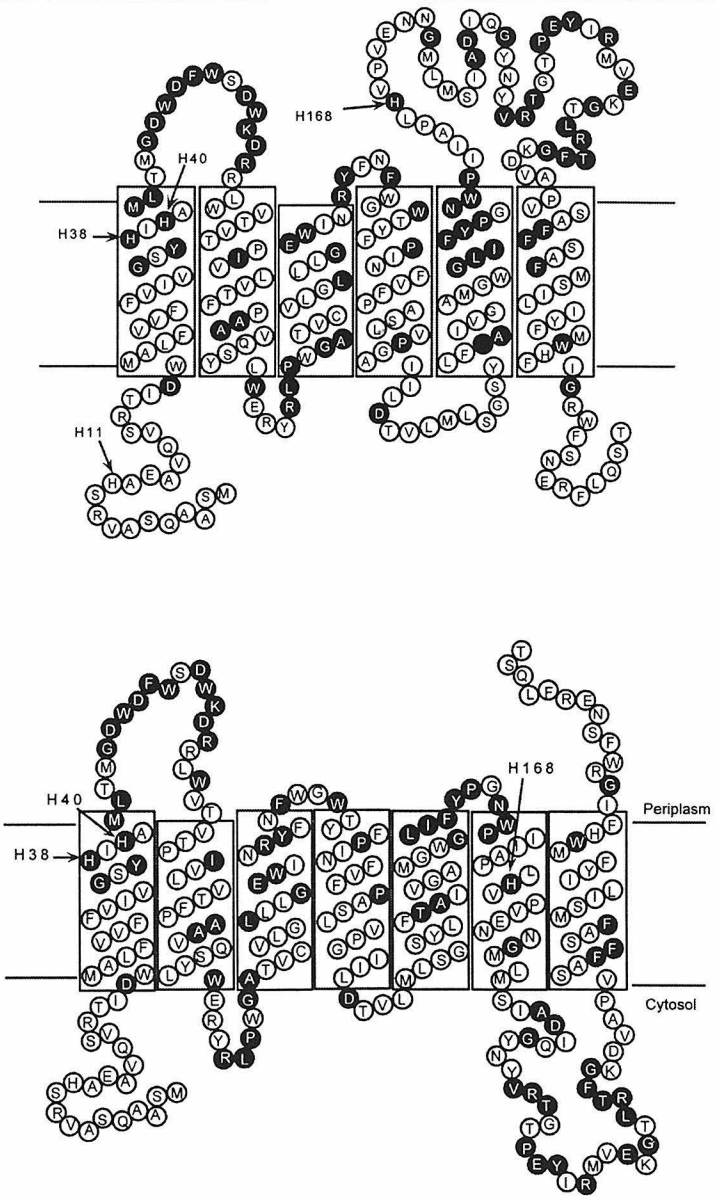

Figure 8. Predicted transmembrane domains modeling potential topologies for PmoA from *M. capsulatusI* (Bath). Identical positions are shown as white-on-black.

identical histidine is located on the same face of the membrane as the other histidine residues, whether in a loop domain or a transmembrane helix. Therefore, the models allow for folding of PmoA and AmoA such that all three of the identical histidine residues (His-38, -40, and -168) can be in close proximity to one another, as might be required for the assembly of a membrane-associated copper cluster. Together these models suggest that the active site of pMMO and AMO is likely located close to the periplasm-membrane interface.

However, the overall number of available, identical ligands is small as compared to the number of copper ions bound by pMMO. Specifically, aside from the identical histidines, there are five identical aspartate residues and three identical glutamate residues that are potential ligands for copper. Four of the aspartates appear to be specifically oriented toward the periplasmic side of the membrane, and closely follow after His-38 and –40. However, the other acidic residues either will be found on the periplasmic or cytosol side of the membrane depending on which transmembrane prediction is correct. Regardless of their exact location, the additional eight acidic residues can account for additional copper ligands, although obviously they are not sufficient to bind all of the fifteen copper ions anticipated to be associated with the complete protein. This is further confirmation that the protein-based copper sites must exist throughout the enzyme, as described in Chapter 3, and while a subset of copper ions are bound within the membraneous domains of pMMO, the bulk of the copper ions are bound in soluble domains. Further sequencing studies of *pmoB* and *pmoC* will further elucidate potential copper ligands for the various copper-binding sites of pMMO and AMO.

References Cited

1)Koops, H.-P.; Moller, U. C. *The Lithotrophic Ammonia-Oxidizing Bacteria*; Balows, A., Truper, H. G., Dworkin, M., Harder, W. and Schleifer, K.-H., Ed.; Springer-Verlag: New York, 1992; Vol. III, pp 2625-2637.

2)Hanson, R. S.; Netrusov, A. I.; Tsuji, K. *The Obligate Methanotrophic Bacteria Methylococcus, Methylomonas, and Methylosinus*; Balows, A., Truper, H. G., Dworkin, M., Harder, W. and Schleifer, K.-H., Ed.; Springer-Verlag: New York, 1992; Vol. III, pp 2350-2364.

3)Hanson, R. S.; Hanson, T. E. *Microbiol. Rev.* **1996**, *60*, 439-471.

4)Whittenbury, R.; Phillips, K. C.; Wilkinson, J. F. *J. Gen. Microbiol.* **1970**, *61*, 205-218.

5)Green, P. N. *Taxonomy of Methylotrophic Bacteria*; Murrell, J. C. and Dalton, H., Ed.; Plenum Press: New York, 1992, pp 23-62.

6)Bodrossy, L.; Holmes, E.; Holmes, A.; Kovacs, K.; Murrell, J. *ARCHIVES OF MICROBIOLOGY* **1997**, *168*, 493-503.

7)Arp, D. J.; Hommes, N. G.; Hyman, M. R.; Juliette, L. Y.; Keener, W. K.; Russell, S. A.; Sayavedra-Soto, L. A. *Ammonia Monooxygenase from Nitrosomonas europaea*; Lidstrom, M. E. and Tabita, F. R., Ed.; Kluwer: Dordrecht, The Netherlands, 1996, pp 159-166.

8)Semrau, J. D.; Chistoserdov, A.; Lebron, J.; Costello, A.; Davagnino, J.; Kenna, E.; Holmes, A. J.; Finch, R.; Murrell, J. C.; Lidstrom, M. E. *J. Bacteriol.* **1995**, *177*, 3071-3079.

9)Bedard, C.; Knowles, R. *Microbiol. Rev.* **1989**, *53*, 68-84.

10)Klotz, M. G.; Alzerreca, J.; Norton, J. M. *Fems Microbiology Letters* **1997**, *150*, 65-73.

11)Sayavedra-Soto, L. A.; Hommes, N. G.; Alzerreca, J. J.; Arp, D. J.; Norton, J. M.; Klotz, M. G. *Fems Microbiology Letters* **1998**, *167*, 81-88.

12)Stolyar, S.; Costello, A. M.; Peeples, T. L.; Lidstrom, M. E. *Microbiology-Uk* **1999**, *145*, 1235-1244.

13)Holmes, A. J.; Costello, A.; Lidstrom, M. E.; Murrell, J. C. *Fems Microbiology Letters* **1995**, *132*, 203-208.

14)Hyman, M. R.; Wood, P. M. *Biochem. J.* **1985**, *227*, 719-725.

15)Prior, S. D.; Dalton, H. *Fems Microbiology Letters* **1985**, *29*, 105-109.

16)Costello, A. M.; Lidstrom, M. E. *Applied and Environmental Microbiology* **1999**, *65*, 5066-5074.

17)Felsenstein, J. *Cladistics* **1989**, *5*, 164-166.

18)Page, R. D. M. *Comput. Applic. Biosci.* **1996**, *12*, 357-358.

Chapter 5: Pulsed EPR Studies of Particulate Methane Monooxygenase from *Methylococcus capsulatus* (Bath): Evidence for Histidine Ligation

Abstract

The membrane-bound particulate methane monooxygenase (pMMO) from *Methylococcus capsulatus* (Bath) is a multi-copper protein. Two distinct subsets of copper ions have been proposed: a set that activates dioxygen and serves as the active site for the oxidation of methane to methanol (C-clusters); and a second set that has either a structural or an electron transfer role (E-clusters.) This report presents a preliminary electron spin-echo envelope modulation (ESEEM) and electron-nuclear double resonance (ENDOR) study of pMMO, using the g = 2.06 signal(s) detected in samples reduced with dithionite, followed by oxidation at 4°C with either ambient atmosphere or ferricyanide. Both treatments give similar 3-pulse ESEEM spectra with modulations at 0.6, 0.8, 1.6, 2.2 and ~4.5 MHz (e^2qQ = 1.60; η =0.98; A=1.70 MHz), characteristic of the ^{14}N nuclear quadrupolar interaction (nqi) of non-ligated ^{14}N nuclei in the imidazole ring of a histidine residue ligated to Cu(II). Similar ENDOR measurements on pMMO samples prepared with ^{14}N and ^{15}N provided evidence for a strongly coupled nitrogen from a histidine bound to the same Cu(II) ions in the active site. Based on these results and sequence homology analysis, a location of the pMMO active site within the membrane-bound 27 kDa pMMO subunit PmoA is proposed.

Introduction

Particulate methane monooxygenase (pMMO), a membrane-bound metalloenzyme found in all obligate methanotrophs, catalyzes the 2 electron, dioxygen-dependent oxidation of methane to methanol[1-3]. We have previously proposed that the catalytic site of pMMO is a copper cluster based on the observed dependence of cellular growth and catalysis with copper ion concentration[4,5]. The number of copper ions strongly bound by pMMO is large, up to 15 copper ions per pMMO unit, and we have suggested that they are primarily arranged in multinuclear clusters that are unlike other multinuclear copper centers found in metallobiochemistry[2,6]. pMMO has three subunits that are encoded by the genes *pmoA*, *pmoB*, and *pmoC* [7]. The 27kDa *pmoA* gene-product is irreversibly modified by acetylene, indicating that this polypeptide alone contains the

active site of the enzyme.[4,8] In a recent report characterizing the X-ray K-edge and CW-EPR spectroscopic features of pMMO poised in a series of redox states, we presented a model that differentiated the pMMO copper content into subsets of copper ions that are associated with catalysis (termed C-clusters), which are readily susceptible to oxidation by air from the Cu(I) to the Cu(II) state, and those copper ions that can only be oxidized by ferricyanide[6], which probably participate in electron transport only (termed E-clusters). Exploiting the differing reactivities of the copper ions of the C- and E-clusters toward dioxygen, we have elucidated the ligand structure of the copper ions within the pMMO active site.

Electron spin-echo modulation spectroscopy (ESEEM) has been a useful tool for the identification and characterization of nitrogenous ligands in copper(II) complexes and copper(II)-containing metalloproteins[9-23]. In this paper we present our initial characterization of the copper(II) ions of oxidized pMMO from *Methylococcus capsulatus* (Bath) by ESEEM spectroscopy, including the identification of potential histidine ligands at the C-cluster; and we incorporate these findings into a model for the location and composition of the enzyme active site.

Materials and Methods

Dithionite-reduced pMMO-containing membranes were oxidized by exposure to air at 4°C for 20 minutes or by treatment with ferricyanide (as a 10 mM solution). All ESEEM and ENDOR experiments were performed at liquid helium temperature, on a laboratory-built instrument[24], using a three-pulse ($\pi/2 - \tau - \pi/2 - T - \pi/2$) stimulated echo pulse sequence and a Davies pulse sequence[25] for the ESEEM and ESE-ENDOR experiments, respectively. Figure 1 presents representative Fourier transforms[26] of the time domain ESEEM patterns obtained from pMMO samples oxidized by either air or ferricyanide, and collected at a frequency of 10.280 GHz with applied magnetic field

values that correspond to fields below, above, and directly at the maximal ESE-EPR intensity for the observed signal at g =2.06 (see Figure 1 caption for details).

Results and Discussion

The spectra shown in Figure 1, as well as similar spectra obtained with other values of τ, all indicate a consistent set of features at 0.6, 0.8, 1.6, and 2.2 MHz, with a fifth transition of greater intensity and width at approximately 4.25 MHz. Such spectral features are characteristic in shape, frequency and intensity of weakly hyperfine coupled ^{14}N-nuclei in close proximity to an EPR active species, such as Cu(II), near the "exact cancellation" limit. At this limit, in one of the M_S= ±1/2 sub-manifolds, the ^{14}N nuclear Zeeman and hyperfine interactions cancel[27], giving three intense low-frequency transitions at 0.6, 0.8 and 1.6 MHz. These transition frequencies are controlled by the ^{14}N nuclear quadrupole interaction (nqi), and are invariant with applied magnetic field. Moreover, the sum of the frequencies of the first two transitions should equal the frequency of the third. A fourth transition, often referred to as the double quantum transition, υ_{dq},

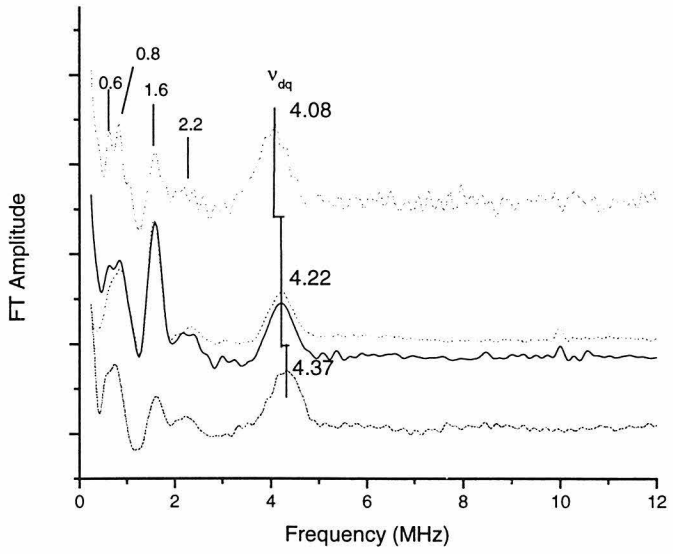

Figure 1.Three-pulse ESEEM spectra of air- (solid line) and ferricyanide-oxidized (dashed lines) pMMO-containing membrane samples. The applied magnetic field varies from 3600G (upper), 3560G (middle spectra), and 3400 G (lower) with the other conditions being τ= 198 ns (upper and lower), τ= 132 ns (middle); microwave frequency, 10.28 GHz; pulse width, 20 ns; pulse sequence repetition rate, 3ms; temperature, 4.2K.

arises from the $\Delta M_I = 2$ transition of the other $M_S = \pm 1/2$ sub-manifold[27]. It is expected to exhibit a broad lineshape, and to shift in frequency linearly with the applied magnetic field. As clearly shown in Figure 1, only the transition at ~4.25 MHz shifts with varying field, indicating that it is indeed υ_{dq}. The remaining nqi feature observed in Figure 1, the weak 2.2 MHz feature, can be assigned to υ_C, a combination of the nqi components observed at 0.6 and 1.8 MHz. The presence of such a feature indicates multiple magnetically equivalent ^{14}N nuclei with the Cu(II) center[16,17,19,27].

Whereas the ESEEM experiments can detect coupling between the paramagnetic copper center and weakly hyperfine coupled nitrogens, such as a proximal, unbound, amide backbone or protein side-chain nitrogens, or the distal nitrogen atom of a Cu(II)-bound histidine imidazole ring, ESE-ENDOR can identify nitrogen nuclei more strongly coupled to a paramagnetic center. Figure 2 shows Davies ESE-ENDOR spectra for air-oxidized samples of pMMO that have been cultured from either natural abundance nitrogen isotopes (^{14}N, solid line) or globally-labelled ^{15}N nitrogen (dashed line)[28]. Spectra were collected using a short microwave pulse length (15 ns) to minimize the contribution from strongly coupled protons and enhance the contribution of hetero-atomic nuclei. In the natural abundance sample, the data show a blue copper-like hyperfine coupling that shifts appropriately to higher frequency[29] upon incorporation of the ^{15}N isotope, indicating the presence of a strongly hyperfine-coupled nitrogenous ligand in addition to the

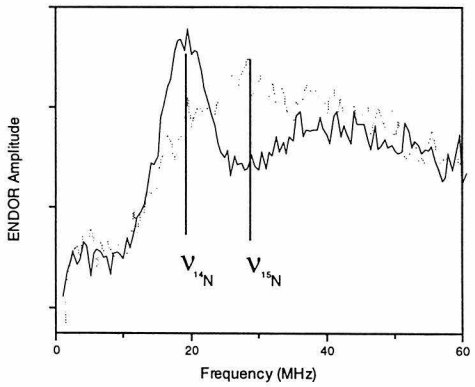

Figure 2. Davies ESE-ENDOR spectra of air-oxidized natural isotopic abundance (solid) and globally labeled ^{15}N (dashed) pMMO-containing membrane samples. Experimental parameters: microwave fequency = 10.203 GHz; magnetic field = 3543 G; τ=200 ns; *T*= 5μs; RF power = 100W; temperature = 4.2K.

weakly coupled ^{14}N nuclei observed in the ESEEM experiments. Such signals typically demonstrate multiple features, which are not resolved in the case of the present study due to poor angle selection at the magnetic field where the experiments were performed. However, the expected Larmor (and quadrupole, for the ^{14}N case) splitting is well within the bandwidth of the observed transitions. Further, while the ESEEM findings indicate multiple equivalent nitrogen nuclei *via* υ_C, the ENDOR does not allow resolution of multiple equivalent $^{14/15}N$ nuclei.

In assigning the chemical identity of the ^{14}N nuclei detected in the FT-spectra shown in Figure 1, we note that the ferricyanide-oxdized sample contains oxidized C- and E-clusters whereas the air-oxidized sample only contains C-clusters that do not contain the S=3/2 ground-state

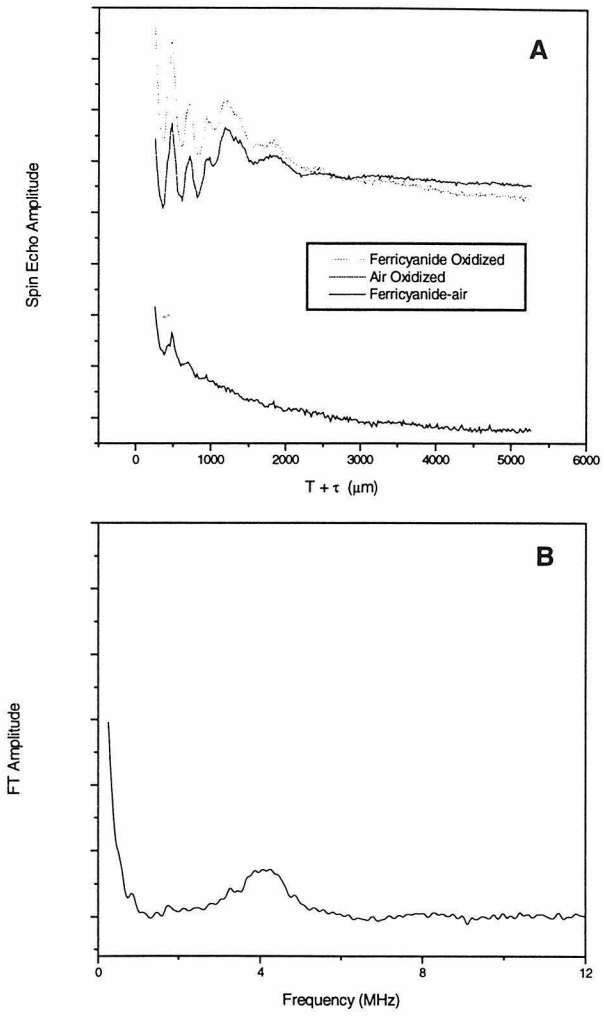

Figure 3. Time domain (A) and frequency domain (B) three-pulse ESEEM spectra for ferricyanide and air-oxidized pMMO-containing membrane sample, and their difference spectrum (A, lower trace, and B). Experimental parameters: magnetic field = 3560G; t=198 ns; pulse width = 15 ns; repetition rate = 5 ns; temperature = 4.2K.

observed for E-clusters[6]. Considering the time-domain 3-pulse ESEEM experiments for ferricyanide versus air-oxidized preparations (Figure 2), we note that the overall echo intensity for the ferricyanide-oxidized sample is larger, though not as great as would be intuited by the oxidation of the three E-clusters thought to be present per protein unit. This is due to the anomalously low signal intensity for the ferricyanide-oxidized sample, resulting from observing only the $|\pm 1/2\rangle$ levels of the S=3/2 manifold at the g -value used.[6] Moreover, a great portion of the decay is expected to occur during the deadtime of the experiment because of the expected shorter T_2 for fully oxidized E- and C-clusters. The contribution from the C-clusters should remain about the same (a 20% increase is expected) between the two preparations. In any case, the difference spectrum (and corresponding Fourier transform) should reveal the presence of additional modulation components that are inherent to the ferricyanide-oxidized sample regardless of the difference in overall echo intensity. Yet, as shown in Figure 3, such a difference spectrum does not yield the set of modulations that correspond to ^{14}N nuclei. While the very broad feature at ~4 MHz is consistent with ν_{dq}, the $\Delta M_I = 1$ transitions in the other M_S manifold which should be of equal magnitude to ν_{dq} are absent. We take this result as evidence that the copper ions in pMMO that are solely oxidized by ferricyanide (*i.e.*, E-clusters) are not magnetically coupled to remote nitrogen nuclei. Thus, the C-clusters of pMMO, which are the apparent active site(s) of pMMO, contain the only multiple weakly coupled ^{14}N nuclei, in addition to at least one strongly coupled ^{14}N. This is the first spectroscopic finding that directly distinguishes the ligand environment (and therefore the chemical properties) of the two distinct sets of pMMO copper-sites.

The nqi for the $I = 1$ ^{14}N nucleus is parameterized by the quadrupolar coupling constant, e^2qQ and the asymmetry parameter, η, both of which can be directly computed from the nqi frequencies, and used to indicate the type of ^{14}N nuclei involved in the coupling.[30,31] Table 1 summarizes ^{14}N ESEEM-derived nqi parameters for several copper(II)-containing proteins, as well as the nqi parameters derived here for pMMO.

The remote ^{14}N of ligated His ligands exhibit a distinctively small e^2qQ. The parameters for pMMO are quite similar to those observed for other proteins that are known to exhibit copper coordination by histidine(s) (notably other multi-copper proteins such as laccase and ascorbate oxidase). Further, the observed ESE-ENDOR features yield a hyperfine coupling of ~38 MHz for the ^{14}N -labeled sample, which agrees with literature values for imidazole nitrogens from histidine residues bound to Cu(II) centers in metalloproteins and model compounds.[32-35] Thus, we conclude the existence of histidine coordination for at least one of the copper ions in the active site of pMMO.

Sample	e^2qQ (MHz)	η	ref.
pMMO	1.60	0.98	--
dopamine ß-hydroxylase	1.44	0.98	17
amine oxidase[a]	1.73	0.48	15
stellacyanin	1.49	0.94	18
$Ag^{I}_2Cu^{II}_2$-superoxide dismutase	1.44	0.94	21
T2-laccase	1.47	0.83	20
T2-ascorbate oxidase[a]	1.56	0.83	13
Cu(II)-hemocyanin	1.52	0.92	22
galactose oxidase[a]	1.70	0.65	12
phenylalanine hydroxylase	1.68	0.55	16
coalbumin[a]	1.53	0.91	14

[a] As quoted in reference 18.

Table 1. Summary of ^{14}N nqi parameters for copper(II) proteins, and the nqi parameters from pMMO ESEEM shown in Figure 1.

The presence of histidine(s) at the pMMO active site has not been previously observed spectroscopically and considering the small number of histidine residues present in the protein overall[7], the above findings further specify the location of the active site of pMMO within the overall structure of the protein. PmoA, a 27 kDa subunit of pMMO, contains five histidine residues[7]. This subunit is hypothesized to contain the

active site as it is radio-labelled irreversibly by the suicide substrate ^{14}C-acetylene.[7] Kyte-Doolittle hydropathy analysis of this pMMO subunit, and the analogous subunit of the evolutionarily related ammonia monooxygenase[36] (AMO) from *Nitrosomonas europaea,* suggest that both polypeptides are comprised of transmembrane helices primarily (Figure 3)[37]. This is discussed in great detail in the preceding Chapter.

References Cited

1)Bédard, C.; Knowles, R. *Microbiol. Rev.* **1989**, *53*, 68-84.

2)Nguyen, H.-H. T.; Shiemke, A. K.; Jacobs, S. J.; Hales, B. J.; Lidstrom, M. E.; Chan, S. I. *J. Biol. Chem.* **1994**, *269*, 14995-15005.

3)Nguyen, H.-H. N. T.; Zhu, M.; Elliott, S. J.; Nakagawa, K. H.; Hedman, B.; Costello, A. M.; Peeples, T. L.; Wilkinson, B.; Morimoto, H.; Williams, P. G.; Floss, H. G.; Lidstrom, M. E.; Hodgson, K. O.; Chan, S. I. *Microbial Growth on C_1 Compounds*; Lidstrom, M. E. and Tabita, F. R., Ed.; Kluwer Academic Publishers, 1996, pp 150-158.

4)Prior, S. D.; Dalton, H. *J. Gen. Microbiol.* **1985**, *131*, 155-163.

5)Semrau, J. D.; Zolandz, D.; Lidstrom, M. E.; Chan, S. I. *J. Inorg. Bioch.* **1995**, *58*, 235-244.

6)Nguyen, H.-H. T.; Nakagawa, K. H.; Hedman, B.; Elliott, S. J.; Lidstrom, M. E.; Hodgson, K. O.; Chan, S. I. *J. Am. Chem. Soc.* **1996**, *118*, 12766-12776.

7)Semrau, J. D.; Chistoserdov, A.; Lebron, J.; Costello, A.; Davagnino, J.; Kenna, E.; Holmes, A. J.; Finch, R.; Murrell, J. C.; Lidstrom, M. E. *J. Bact.* **1995**, *177*, 3071-3079.

8)Shiemke, A. K.; Cook, S. A.; Miley, T.; Singleton, P. *Arch. Biochem. Biophys.* **1995**, *321*, 421-428.

9)Mims, W. B.; Pesiach, J. *Biochemistry* **1976**, *15*, 3863-3869.

10)Mondovi, B.; Graziani, M. T.; Mims, W. B.; Oltzik, R.; Peisach, J. *Biochemistry* **1977**, *16*, 4198-4202.

11)Kosman, D. J.; Peisach, J.; Mims, W. B. *Biochemistry* **1980**, *19*, 1304-1308.

12)Avigliano, L.; Davis, J. L.; Graziani, M. T.; Marchesini, A.; Mims, W. B.; Mondovi, B.; Peisach, J. *FEBS Lett.* **1981**, *136*, 80-84.

13)Zweier, J. L.; Peisach, J.; Mims, W. B. *Biochemistry* **1982**, *257*, 10314-10316.

14)Mondovi, B.; Morpurgo, L.; Agostinelli, E.; Befani, O.; McCracken, J.; Peisach, J. *Eur. J. Biochem.* **1987**, *168*, 503-507.

15)McCracken, J.; Peisach, J.; Dooley, D. M. *J. Am. Chem. Soc.* **1987**, *109*, 4064-4072.

16)McCracken, J.; Pember, S.; Benkovic, S. J.; Villafranca, J. J.; Miller, R. J.; Peisach, J. *J. Am. Chem. Soc.* **1988**, *110*, 1069-1074.

17)McCracken, J.; Desai, P. R.; Papadopoulos, N. J.; Villafranca, J. J.; Peisach, J. *Biochemistry* **1988**, *27*, 4133-4137.

18)Jiang, F.; McCracken, J.; Peisach, J. *J. Am. Chem. Soc.* **1990**, *112*, 9035-9044.

19)Lu, J.; Bender, C. J.; McCracken, J.; Peisach, J.; Severns, J. C.; McMillin, D. R. *Biochemistry* **1992**, *31*, 6265-6272.

20)Gurbiel, R. J.; Peoples, R.; Doan, P. E.; Cline, J. F.; McCracken, J.; Peisach, J.; Hoffman, B. M.; Valentine, J. S. *Inorg. Chem.* **1993**, *32*, 1813-1819.

21)Bubacco, L.; Magliozzo, R. S.; Wirt, M. D.; Beltramini, M.; Salvato, B.; Peisach, J. *Biochemistry* **1995**, *34*, 1524-1533.

22)Peisach, J. *Bioinorganic Chemistry of Copper*; Karlin, K. D. and Tyeklàr, Z., Ed.; Chapman & Hall: New York, 1993, pp 21-33.

23)Magliozzo, R. S.; Bubacco, L.; McCracken, J.; Jiang, F.; Beltramini, M.; Salvato, B.; Peisach, J. *Biochemistry* **1995**, *34*, 1513-1523.

24)Sturgeon, B. E.; Britt, R. D. *Rev. Sci. Instrum.* **1992**, *63*, 2187-2192.

25)Davies, E. R. *Phys. Lett.* **1974**, *47A*, 1-2.

26)Mims, W. B. *J. Magn. Res.* **1984**, *59*, 291-306.

27)The correct assignment of M_S=+1/2 or M_S=-1/2 cannot be achieved with knowing the sign of the hyperfine tensor *A*, which is not known currently.

28)Samples globally labeled with ^{15}N were prepared by using $K^{15}NO_3$ (Cambridge Isotope Labs) in the nitrate mineral salts medium, instead of the natural abundance compound, as described in reference 2.

29)For $^{14/15}N$ ENDOR, the signals are centered at a frequency of one-half the hyperfine coupling, $A(^{14/15}N)/2$, and follow the relation: $|[A(^{15}N)/ A(^{14}N)] = 1.403$.

30)The nuclear quadrupole coupling constant e^2qQ and the asymmetry parameter η are related to the nqi frequencies by $\nu_{\pm} = 3/4e^2qQ(1 \pm \eta/3)$ and $\nu_0 = 1/2\ e^2qQ\eta$.

31)Mims, W. B.; Peisach, J. *J. Chem. Phys.* **1978**, *69*, 4921-4930.

32)Roberts, J. E.; Brown, T. G.; Hoffman, B. M.; Peisach, J. *J. Am. Chem. Soc.* **1980**, *102*, 825-829.

33)Van Camp, H. L.; Sands, R. H.; Fee, J. A. *J. Chem. Phys.* **1981**, *75*, 2098-2107.

34)Cline, J.; Reinhammar, B.; Jensen, P.; Venters, R.; Hoffman, B. M. *J. Biol. Chem.* **1983**, *258*, 5124-5128.

35)Scholl, H.-J.; Hüttermann, J. *J. Phys. Chem.* **1992**, *96*, 9684-9691.

36)Holmes, A. J.; Costello, A.; Lidstrom, M. E.; Murrell, J. C. *FEMS Microbiol. Lett.* **1995**, *132*, 203-208.

37)Vannelli, T.; Bergmann, D.; Arciero, D. M.; Hooper, A. B. *Microbial Growth on C_1 Compounds*; Lidstrom, M. E. and Tabita, F. R., Ed.; Kluwer Acadmeic Publishers: the Netherlands, 1996, pp 80-87.

Chapter 6: The Reaction of pMMO with Nitric Oxide: A Ferrous Question Resolved?

Abstract

The reaction of nitric oxide (NO) with particulate methane monooxygenase (pMMO) has been investigated by EPR spectrscopy. When NADH-reduced, or as-isolated anaerobic pMMO preprations from intracytosolic membranes from *Methylococcus capsulatus* (Bath) were treated with either NO gas or one of two different chemical delivery systems, novel features in the EPR spectrum were detected in the g=4.0 region of the spectrum. These features are rigorously determined to be linked to the presence of reduced iron in the samples. The ability to generate the NO adduct is found to be independent of whether or not pMMO has been inhibited with acetylene, and is sensitive to the proteolytically-cleaved state of the protein. Implications for the role of iron in pMMO chemistry are discussed, and it is suggested that the iron found to be associated with pMMO is adventitious in nature.

Introduction

The investigation of the biological activation of kinetically inert dioxygen has proven to be an intensely important problem in bioinorganic chemistry. Hydroxylases that exhibit either dioxygenase or monooxygenase chemistry, as well as other enzymes and proteins that bind and/or activate oxygen have become important subjects of research. The use of the dioxygen mimic nitric oxide (NO) has been adopted as a particularly useful paramagnetic spin-probe. Nitric oxide is less-reactive than dioxygen, and will bind to metal centers with limited reactivity (in contrast to dioxygen, which often forms "activated dioxygen intermediates"). As NO carries an unpaired electron, and monitoring NO itself, or the metal centers that may alternatively interact with dioxygen or NO, allow for a new set of experiments using Electron Paramagnetic Resonance (EPR) spectrscopy.

Nitric Oxide is known to bind at *reduced* metal centers, thereby generating metal nitrosyls, which result in changes in the EPR spectrum for the metal center. NO has been

widely used in biological systems to probe the coordination chemistry of heme systems, non-heme iron systems and copper systems as the resulting metal-nitrosyl demonstrates significantly different EPR characteristics depending on the nature of the metal involved. In terms of copper chemistry, such as might be expected from a copper-containing metalloprotein such as pMMO, NO typically binds to Cu(I) sites yielding new signals in the g=1.8 to g=2.0 region of the EPR spectrum. Model compounds[1] as well as protein studies have demonstrated this[2-4]. One of the best characterized Cu-nitrosyls from a metalloprotein was found in the study of the interaction of reduced laccase with NO[3]. This study demonstrates that the oxidized form of the multi-copper oxidase laccase is reduced by NO, and in the reduced state, binds NO, forming an EPR detectable species near g=2.0. Iron-nitrosyls have also been studied extensively. In particular, the formation of an iron-nitrosyl upon the treatment of a reduced Fe(II) species with NO, has been used to characterize binuclear non-heme iron enzymes such as sMMO[5] and ribonucleotide reductase[6], and mononuclear enzymes like the extradiol dioxygenases[7-9], isopenicillin N-synthase[10] and lipoxygenase[11]. The interaction of non-heme iron with NO has been interpreted in terms of the odd electron from NO combining with a high-spin (S=2) Fe(II) site to yield an axial site with a S=3/2 electronic groundstate, thereby giving a feature in the EPR spectrum at ~g=4.0[12].

Considering particulate methane monooxygenase (pMMO) NO has also been used as a spin-probe. NO chemistry has been investigated to date by the Chan group at Caltech, as well as other groups either investigating pMMO or the similar AMO system from ammonia-oxidizing bacteria. As stated in Chapter 1 of this dissertation, DiSpirito and co-workers, studying pMMO from *M. capsulatus* (Bath) and the AMO of

Nitrosomonas europaea, have used the NO-chemistry of pMMO and AMO as evidence for a proposed iron-atom active site in the enzyme[13,14]. Treatment of the reduced protein with NO(g) results in the generation of the g=4.0 axial EPR signal which is typically ascribed to a non-heme iron-nitrosyl. Okura and co-workers have also observed similar signals from the purified pMMO from *M. trichosporium* OB3b[15], and have demonstrated some small reductions in the observed EPR spectra upon treatment with redox reagents, which they suggest indicates that iron plays a catalytic role[15]. They have yet to conclude that iron is the dioxygen binding site in the protein based solely on these findings.

The Chan group has also generated such a species from pMMO preparations from *M. capsulatus* (Bath), but initial characterization of the species was carried out in terms of two signals due to *syn*-[(Cu(I)NO)$_3$] and *anti*-[(Cu(I)NO)$_3$] species formed by the binding of NO to reduced copper clusters. In this analysis one signal was found to be a near-axial signal with $g_{\perp}$=3.997, and a rhombic signal with g_x=4.27 and g_y=3.74. A third EPR signal was also observed at g=2.02, which based on the decomposition of the g~4 signals, and the observed evolution of N_2O, was interpreted to be a residual [(Cu(I)NO)Cu(II)$_2$] species.

The matters are rendered somewhat more complicated when the proposed elemental analyses for the protein is considered. The DiSpirito group claims 2.5 iron atoms per pMMO unit, the Okura group 1 (or less than one) and the Chan group, less than 0.5. The potential for iron to act as a conserved, essential characteristic of pMMO seems less likely when considering the variability in the concentration of iron over the preparations. Indeed, adventitious iron is often found in biological systems, so called "junk iron" that is observed in the EPR-spectrum at g=4.3. Further, due to the proclivity

of non-heme iron to form an iron-nitrosyl, it seems that any iron site that may exist in pMMO could generate an NO-adduct, and not necessarily be an essential component of the active site.

In order to address the questions regarding the role of iron in pMMO oxygenation chemistry, and to positively identify the species responsible for the g=4.0 EPR spectra observed in our group, the following study pursued the interaction of NO with the pMMO metal centers.

Materials and Methods

General Methods.

pMMO was prepared as described in Chapter 2, from *Methylococcus capsulatus* (Bath) which was grown as previously reported, with two different concentrations of iron. In the low iron concentration regime, solid iron(III)-EDTA was added to the usual Nitrate Mineral Salts medium (NMS) to give a concentration of 5 μM. This was used to grow methanotrophs with minimal contribution of soluble methane monooxygenase. The "normal" iron regime utilizes a final iron concentration of 20 μM. Membrane preparations were prepared as described previously, without the addition of any exogenous reductants. Final membrane preparations were immediately degassed and were kept for any period of storage at 4°C, sealed and under argon or nitrogen gas. All dilutions of membrane preparations utilized degassed 50 mM Pipes buffer, pH=7.0.

Copper concentrations were determined chemically by induced-coupled plasma mass spectrometry (ICP-MS). An aliquot (~250 μl) of the sample was digested in neat, Redistilled Nitric Acid (GFS Chemicals) and digested at room temperature for 1 hr. This was then diluted to 0.1% nitric acid with ultra-pure water, and the resulting diluted

sample was assessed for copper content. Copper concentrations were determined with comparison to a reference curve constructed using standards of 2.5 mM to 150 mM in copper concentration (0.1% nitric acid), which were prepared by dilution a commercially available standard (GFS Chemicals). Measurements were repeated in order to ensure reproducibility.

EPR spectra were recorded on a Varian E-line Century X-band spectrometer. In the EPR experiments, sample temperature was maintained at 77 K with a liquid nitrogen dewar, and at 4.2 K with an ESR-900 Oxford Instruments (Oxford, England) liquid helium cryostat. The EPR samples were prepared by sealing 200 μL of membrane suspensions under an atmosphere of nitrogen in quartz EPR tubes at a total protein concentration of ~50 mg/mL (~0.53 mM in 94 kDa protein) in 20 mM Pipes (pH 7.2). All samples described below were prepared in a glove-box and transferred into quartz EPR tubes while still in the box. Typically, the tubes were sealed with suba-seal septa and then removed from the box, and were rapidly frozen in liquid nitrogen to minimize any chance of oxygen contamination. Quartz EPR tubes equipped with a septum port were used in experiments involving the anaerobic addition of reduced iron.

^{57}Fe Cell Growth.

Isotopically enriched *M. capsulatus* (Bath) was grown by taking 40 mg of ^{57}Fe (from Trace Sciences International, 94.69% enrichment, obtained as the foil) and dissolving the metal in 100 ul of 1:1 sulfuric:nitric acid. This acidified ^{57}Fe solution was diluted into 50 mM Pipes (pH=6.0) which contained 50 mM EDTA such that it could be used in cell growths, as described above.

Preparation and Handling of DEAN. Addition of Fe(II).

Diethylamine NONOate hydrochloride (DEAN) was obtained from Calbiochem and used as received. Solutions of DEAN were prepared by handing the compound in an anaerobic glove box, and freshly prepared solutions of known concentrations (ε_{250nm} =6500 M•cm) were made in degassed 10mM KOH before each experiment. Microliter additions of the basic reagent to neutral pH solutions leads to release of NO and the amine. Generally, the DEAN solution was made to 485 mM DEAN, and then 10 ul of this solution was added to a 250 ul volume of pMMO-containing membrane suspension in an EPR tube. The contents were rapidly mixed by syringe pumping, and the tube sealed, removed and frozen in liquid nitrogen.

Preparation and Handling of NO(g).

Reagent grade nitrous oxide gas was utlized by first scrubbing the gas through a tower of 10M KOH to remove any yellow-brown color from the gas-stream. The stream was allowed to blow until there was no detectable yellow coloration in the gas that bubbled through the tower, and out an exit port into a column of water open to the air. NO was utilized only when the headspace on the column was perfectly clear, indicating that no dioxygen was present in the exit gas stream.

In order to incubate small volumes (an EPR-sample volume) of pMMO-membranes, we constructed nested vials from a large serum vial that could be later stoppered with a suba-seal septum, and a small inner vial that could contain the preparation, as well as a small stir bar, for thorough mechanical mixing. Serum vials (40 ml size) were taken, and inside of each, a small 0.5 dram soft glass vial was glued in place using epoxy. The nested vials were then allowed to dry, and a microflea-sized,

Teflon-coated stir bar was placed inside the smaller vial, before the entire assembly was capped with a suba-seal. To charge the vials with NO, nested vials were evacuated for 10 minutes on a vacuum line, and back-filled with Ar gas. This procedure was repeated three times for each vial. After a final evacuation step, the vial was then filled with an atmosphere of scrubbed NO(g). Any yellow color observed in the headspace of the vial was taken as a sign of an oxygen leak and the vial was discarded immediately.

These vial-within-a-vials were then used as NO incubation chambers for all experiments involving NO incubation. Typically, a large (~5 ml, as might be required for a large set of experiments) volume of membrane preparation was degassed thoroughly, and that serum vial was placed in a cold-finger chamber previously frozen to –20°C. The membrane preparation and however many NO chambers were required for the experiments, were then transferred into a glove box. Within the glove box, 0.4 ml of membrane suspension would be introduced into the inner vial of the NO-chamber, and the suspension was then stirred *via* the included stirbar. After incubation under the NO-headspace at room temperature, the sample was removed, directly loaded into an EPR tube, removed and frozen.

Reaction with Acetylene.

Membrane preparations were pre-treated with acetylene gas to irreversibly inhibit pMMO. A 1-2 ml quantity of membrane preparation would be loaded into a 10 ml serum vial and made to 0.5 mM with NADH. This was first allowed to equilibrate with air while on ice, and then was sealed with a suba-seal septum. To this, 2 ml of acetylene gas was introduced via a syringe. The reaction was incubated at 42°C for 2h, and then quenched by venting the head-space with a nitrogen stream and placing the reaction on

ice until further use. Subsequent reaction with NO(g) was achieved by degassing the reaction mixture under vacuum, and then directly treating the now-anaerobic, inhibited preparation with NO(g). No additional NADH was added to this reaction mixture.

Proteolysis Experiments.

Proteolysis was achieved by incubation of pMMO-containing membrane fractions with proteolytic enzymes as follows. In the case of either trypsin or chymotrypsin (Roche-Boehringer-Mannheim, sequencing grade) ~1 mg of the solid, lyophilized enzyme was re-hydrated in a minimal amount of 50mM PIPES buffer (pH 7.0) and this was directly added to 0.4 ml of the pMMO-preparation, giving a ratio of protein:protease of approximately 50:1. These preparations were incubated at 37°C for four hours, with periodic mixing using a vortex mixer. In the case of papain treatment, Calbiochem Papain (10mg) was taken in 50mm ammonium acetate buffer (pH 5.0), to which 40 µl of 10% L-cysteine is added. This was mixed well, and incubated at room temperature briefly, before centrifuging an aliquot of the protease in bench-top microfuge. The resulting solution was removed from the pellet (which contains unactivated and denatured Papain) and the solution was added to a membrane preparation, 3:1 (vol:vol). This was incubated at 37°C for four hours, with periodic mixing using a vortex mixer. Digests are then quenched on ice and centrifuged to remove the soluble fragments. They were re-suspended in 50 mM PIPES, and centrifuged and suspended a final time to further remove peptide fragments. For some experiments, pellets were washed in a high-salt wash (250mM NH_4Cl in 5mM Phosphate buffer, pH=7.0), pure water and stripped with 1N NaOH to remove any exogenous peptide fragments. These further steps were not found to play a significant role in the results described below.

Results

NO-delivery Systems.

Initial experiments focused on developing a satisfactory, reproducible system for the delivery of nitric oxide into pMMO-containing membranes. This was initially investigated using the reagent diethylamino-NONOate (DEAN), a commercially available reagent that decomposes spontaneously at neutral pH, generating NO *in situ*. In our hands, the use of DEAN was found to give highly variable results. This is exemplified by Figure 1 which depicts the low-temperature, X-band EPR spectra for two

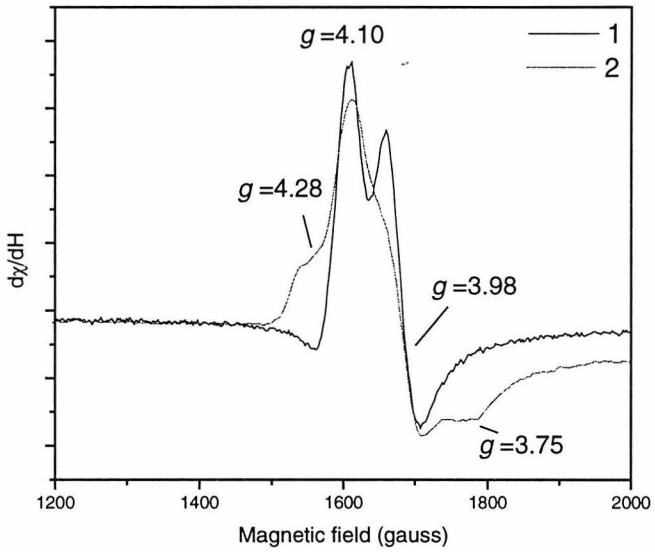

Figure 1. Liquid helium temperature EPR of pMMO treated with DEAN (19.4mM) over the course of two different trials. Samples were incubated for 10 minutes at room temperature. The differences between the trials are discussed in the text. (Data collected with 1 mW, 10G modulation amplitude, 4.2K.)

different preparations of pMMO-containing membranes. The spectra correspond to the g=4.0 region, and show pronounced differences between them. Using identical DEAN concentrations and identical incubation times (incubation allows for the decomposition of the reagent) the spectra labeled **1** and **2** were acquired for two different preparations of

pMMO. Both spectra show similar features: a prominent feature in the derivative spectrum with a maximum at g=4.1, and what would appear to be a near-axial signal with a cross-over point at g=3.98. Generally it appears that each spectrum has some contribution from each of these two features, though the intensity of the g=3.98 feature is more pronounced in the spectrum **1**. Spectrum **2** also has contributions from what would appear to be g_x = 4.28 and g_y=3.75 rhombic signals, which previously have been associated with the axial g=3.98 signal (see below). However, in the case of spectrum **1**, the g=3.98 signal is quite clear and the rhombic signals are not observed.

The variation between the spectra reported in Figure 1are representative of what was found with the DEAN reagent. Different samples from within the **same** membrane preparation gave similar variability.

The DEAN reagent clearly undergoes a number of steps in its reaction chemistry. As Figure 2 shows, an initial preparation of pMMO, as isolated from intracytosolic membranes (dashed line) reveals no EPR signal in the g=4.0 region. Immediate freezing of an aliquot of this sample after being mixed with DEAN, gives the spectrum shown as the solid line. This does show very small contributions from features at g=4.102 and g=3.924, but is initially dominated by a g=4.3 signal, which is typical of adventitious, non-heme iron, and not related to NO-chemistry. Only after anaerobic incubation are the customary signals (g=4.1 and g=3.9) observed.

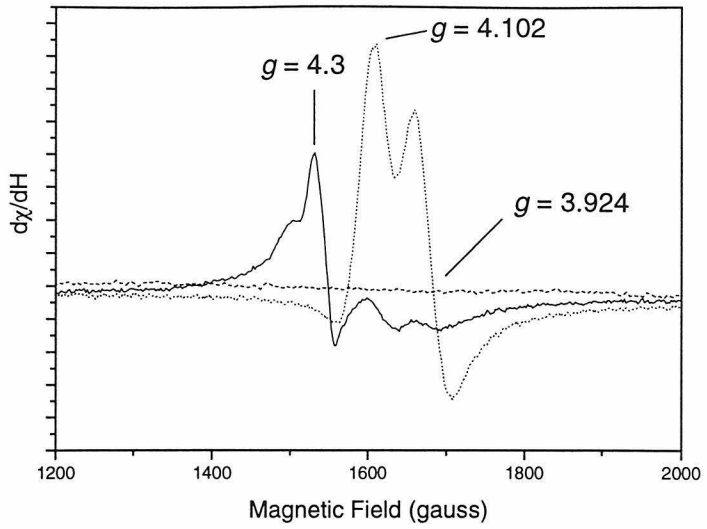

Figure 2. EPR spectra for a preparation of pMMO (dashed line) with no DEAN added, the injection of DEAN and immediate freezing of the sample (solid line) primarily yields a product with a *g*~4.3 feature, suggestive of non-specific, oxidized iron. Only after a 15 minute incubation time (dotted line) are features similar to those found in Figure 1 observed. (Data collected with 0.1 mW power, 10G modulation amplitude, 4.2K.)

With the above findings in hand, we sought to use NO(g) itself as a more efficacious alternative, in hopes it would yield greater reproducibility and less troublesome reaction chemistry. NO(g) was first cleaned by bubbling through a KOH tower, and the colorless exit-gas of the tower was used to back-fill evacuated incubation vessels which could readily hold a small volume of sample (such as a membrane preparation aliquot) under a de-oxygenated NO-atmosphere. The resultant method proved to be highly reproducible, both between preparations, and within multiple trials for a given preparation. All further results described below utilize this technique.

Figure 3 shows a typical spectrum of pMMO reduced with NADH and degassed, followed by incubation under an atmosphere of NO(g). The spectrum (solid line)

displays the near-axial signal at g=3.98, and very small contributions from the rhombic signals observed previously. (A spectrum from Figure 1 (dotted line) generated from incubation of pMMO with DEAN is included for comparison.) It should be noted that the g=4.1 component associated with all DEAN treated samples is lacking in all samples treated with NO(g).

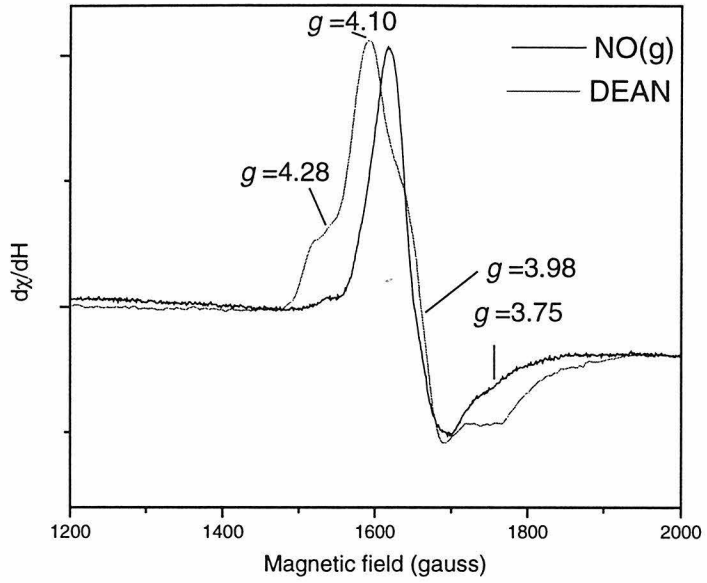

Figure 3. EPR spectra for the same preparation of pMMO but treated with either DEAN or NO gas. (Data collection as in Figure 2).

Effect of Iron in the Growth Medium.

The generation of pMMO-NO adducts analagous to those found by DiSpirito, Okura, and other members of the Chan group was found to be a matter of some difficulty, initially. Initial attempts to generate the intermediate were unsuccessful, until the issue of the growth conditions of *Methylococcus capsulatus* (Bath) had been considered. The initial cell growths were carried out using lower concentrations of ferric-EDTA than had been used previously, with no deliterious effects upon cell growth or the resultant activity

of pMMO preparations. Thus, it was found that when "low-iron" NADH-reduced, pMMO-containing membranes from *M. capsulatus* (Bath) were treated with either NO(g) or the NO-delivery reagent DEAN, no changes were observable in the liquid helium temperature EPR spectrum. However, growth of *M. capsulatus* (Bath) at 20 μM ferric-EDTA resulted in a membrane preparation that was capable of generating new features in the EPR signal upon NO treatment. The resulting features were generally similar to those found by our group previously, and by DiSpirito and co-workers, and Okura and co-workers. This cross-over is shown in Figure 4. Further increases in the ferric-EDTA concentration were found to be detrimental for cell growth; thus, for further experiments 20 μM ferric EDTA was used exclusively.

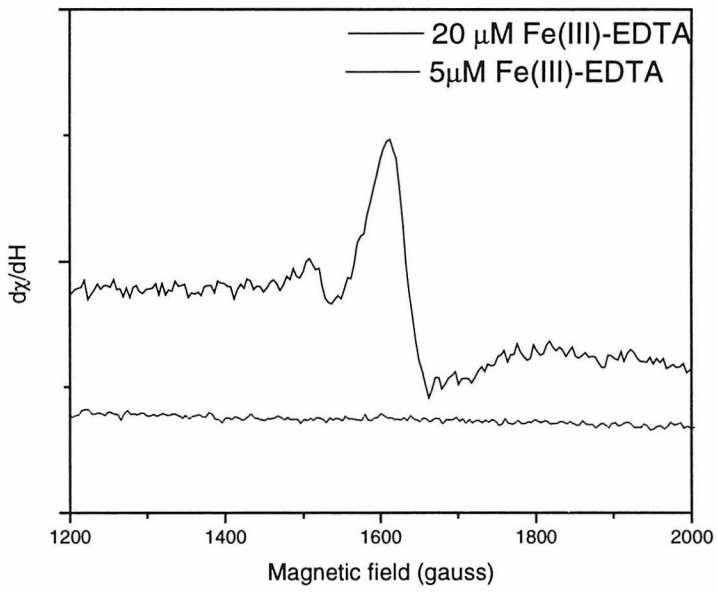

Figure 4. Alteration of the growth conditions of *M. capsulatus* (Bath) results in the ability to generate EPR signals in the *g*=4.0 region, following NO(g) treatment. Specifically, increasing the amount of ferric iron-EDTA added to the cellular growth medium allows for the evolution of the signal. Here it is attained by treatment of an alliquot of pMMO-enriched membranes with NO(g). (Data collected with 1mW power, 10G modulation amplitude, 4.2K).

The Identity of the g=4.0 NO-signal.

As the above experiments indicated that the NO-chemistry associated with pMMO preps could be somewhat variable (at the least) and did have a correlation to the iron-content of the growth conditions of *M. capsulatus* (Bath), an experiment to confirm the identity of the NO-species observed in the g=4.0 region of the spectrum was conducted. *M. capsulatus* (Bath) was grown in the presence of 20 μM ^{57}Fe-EDTA, which had been prepared by dissolving the (~95% enriched) elemental foil in acid. The enrichment of iron in the resultant pMMO-containing membranes was determined by Induced-Coupled Plasma Mass Spectrometry, which is sensitive to isotopic information. Membrane fragments from these ^{57}Fe-enriched cells were taken, treated with NADH, degassed and incubated under NO(g) as described previously. The resulting EPR spectra comparing the enriched sample to a sample with natural abundance iron is shown in Figure 5. The line-broadening that results from the interaction of NO with the I=1/2 nucleus of ^{57}Fe is overwhelmingly apparent. In fact, the signal that corresponds to g_y in the Chan group model (the derivative minimum at 1753 gauss in the Standard sample shown in Figure 5) is no longer observable. The magnitude and significance of the observed broadening will be discussed below.

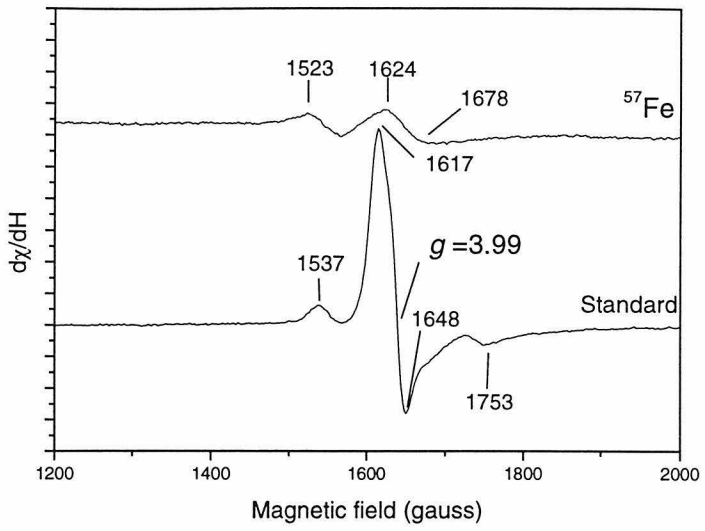

Figure 5. The effect of ^{57}Fe enrichment on the ability to generate EPR spectra in the g=4.0 region. Line broadening occurs due to two phenomena, the first is due to the presence of the I=1/2 nucleus of ^{57}Fe, illustrated here, and the second is discernible broadening that is concentration dependent (data not shown). Here, the data are normalized to protein concentration. (Data collected with 1mW power, 10G modulation amplitude, 4.2K.)

Acetylene Chemistry and NO-Chemistry.

As acetylene acts as an irreversible inhibitor of pMMO (see Chapters 2 and 5), it was hypothesized that monitoring the ability of acetylene-inhibited membrane preparations to generate the g=4.0 EPR signal may lead to some insight as to the nature of the species giving rise to the observed NO-chemistry. In order to assess whether acetylene inhibition blocks the generation of the NO-based EPR signal, we prepared one experimental sample, and two controls. Inhibited membranes were generated through the standard pre-treatment with acetylene (described previously in Chapter 2, as well as in this chapter). This inhibited preparation was thoroughly degassed to remove any dioxygen, and without the addition of further NADH, it was subjected to NO-incubation

as described. Dioxygen was specifically excluded due to the potential for generation NO_x *in situ*. A control experiment was also carried out, in which a membrane aliquot was subjected to the same length of incubation at 40°C as the acetylene-labeled sample, but without the acetylene. (This too was then degassed before subsequent treatment with NO.) This was done to rule out any possibility that 40°C incubation in the presence of NADH (both are required for acetylene inhibition) has no affect on the NO-chemistry observed. A second control experiment was also conducted: pMMO-membranes were degassed, reduced with NADH and directly treated with NO; no incubation at 40°C, nor exposure to acetylene was used. The findings of this experiment are shown in Figure 6. It is quite clear from the spectra that the control experiment involving no pre-incubation of any kind (lower trace) demonstrates the same features in the EPR spectrum. The control which had been incubated at 40°C, but had not been exposed to acetylene (upper, dotted line), also shows the same features, though not with the same intensity, indicating that there does seem to be some thermal-decay of the center that gives rise to the NO-based EPR signal. However, the sample that had been exposed to acetylene (upper, solid line) only shows a very small reduction in the magnitude of the signal, as compared to both control spectra.

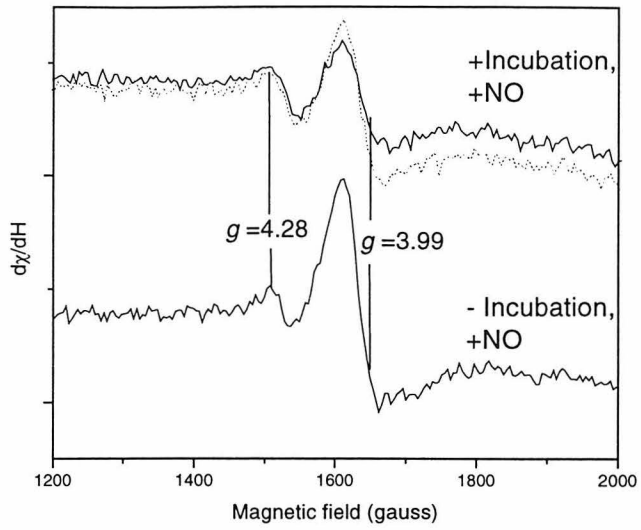

Figure 6. The effect of acetylene oxidation is demonstrated by the upper traces, as compared to the lower trace. The lower trace (solid line) is standard preparation of pMMO-containing membranes treated with NO(g) as described in the material methods. Pre-treatment of pMMO with acetylene (upper, solid line) as described in the materials and methods section is shown along side a blank spectrum (upper, dotted line) that has been appropriately incubated (0.5 mM NADH and air at 40°C for 2h) without **acetylene, prior to standard degassing and exposure to NO. All samples are of identical protein concentrations.**

These results strongly indicate that acetylene binding and the irreversible inhibition of pMMO does not hinder the ability of NO to interact with whatever metal center gives rise to the EPR spectra in the g=4.0 region of the spectrum. On very general grounds this intuitively indicates that NO-binding is not likely to be truly mimicking the binding of dioxygen by pMMO, as precisely the same signals are generated by defunct enzyme.

Proteolysis as a Means of Removing Metal Ions.

Continuing along the same approach to determining the significance of the observed pMMO-NO chemistry in the EPR spectra, we utilized the ability of proteolytic enzymes to cleave the soluble domains of pMMO. Membrane fragments were treated

with the general protease Papain, as well as the more specific protease Chymotrypsin, and the yet more specific protease Typsin. The success of these cleavage reactions were monitored by their ability to remove protein from pelleted membranes, as well as by the concomitant loss of both iron and copper. The details of the metal depletion as a function of proteolysis is given in Table 1.

Sample	% Fe retained (#)	% Cu retained (#)
Blank	100 (<1)	100 (14.5)
Trypsin	73	90
Chymotrypsin	64	53
Papain	26	43

Table 1

As presumed by the specificities of the proteases, the more specific the protease, the less metal ions were lost in the proteolytic treatment.

After cleavage, membrane pellets were taken and treated with NO(g), and the resulting EPR spectra are shown in Figure 7. Much like the trend in the loss of metals from the membrane preparations, the EPR intensity of the g=4.0 region signals observed is diminished as well. However, no protease is sufficient to utterly remove the demonstrated ability to interact with NO. This may be due to adventitious binding of protein fragments that continue to bind metal ions, and defy our attempts to wash them away with high salt and low ionic-strength alike. It also may indicate that some small amount of the NO-reactive species is simply protected from proteolytic cleavage. However, if the NO-reactive species were due to a buried metal-site, as the C-clusters of pMMO are proposed to be, then certainly the ability to generate the tell-tale EPR signal should not be hampered. Thus, we conclude that the EPR signal is due to a moiety that is close to the surface of the protein, and not entirely protected from proteolysis.

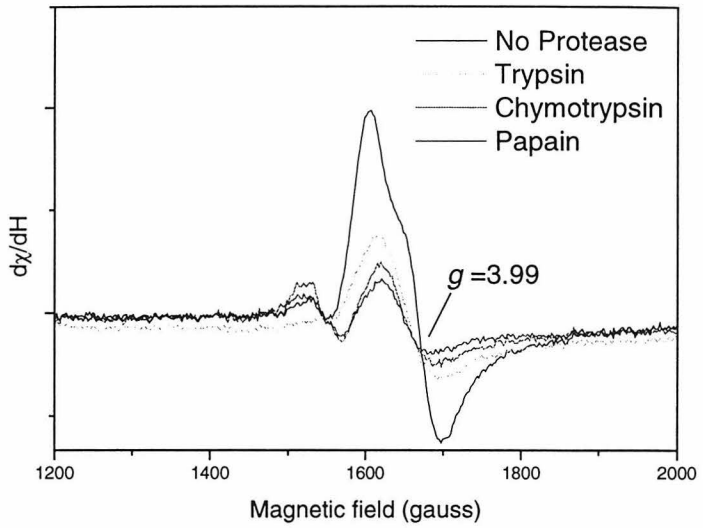

Figure 7. Proteolytically cleaved pMMO-containing membranes demonstrate the ability to reduce the formation of the EPR signals in the *g*=4.0 region of the spectrum. All data are normalized to protein concentration.

Discussion

Identification of Iron-NO Chemistry.

The EPR data for the interaction of pMMO with NO was initially reported by DiSpirito and co-workers for pMMO from *M. capsulatus* (Bath)[13], and for the AMO protein from *Nitrosomonas europaea*[14], as well as by Okura and co-workers for pMMO from *Methylosinus trichosporium* OB3b[15]. In these three separate studies, the treatment of the enzyme results in new EPR-detectable signals in the *g*=4.0 region of the spectrum, and these have been uniformly attributed to mononuclear non-heme iron centers. Further, in each case, the existence of the signal has been taken to inherently imply that the iron atom identified is a part of the active site of the protein. However, in the studies previously published, the report of the signal and its assignment are based solely on

comparisons with known mononuclear non-heme enzymes and their reaction with NO. Very little direct evidence exists to suggest that the iron atom observed must be related to catalysis. To address these issues, we have pursued several separate threads of evidence to demonstrate that a non-heme iron atom is responsible for the reported EPR signal found in the g=4.0 region after treatment of pMMO with NO(g), yet, this iron atom does not appear to be a significant co-factor in catalysis.

The most significant evidence for an iron atom yielding the observed NO-adducts is the demonstration that iron concentration in the initial growth medium of *M. capsulatus* (Bath) directly influences the observation of any EPR signal in the g=4.0 region (Figure 4). The evolution of EPR signals over the time-course of the reaction of DEAN with pMMO also reveals the role of iron, by virtue of the g=4.3 signal observed. These DEAN-initiated EPR signals (g=4.30, 4.10, 3.98) are highly similar to analogous findings of Thomson and co-workers, which examined the interaction of NO with the non-heme iron centers of Bacterioferritin from *Escherichia coli.*[16] In this study, the workers found that multiple mono-nitrosyl adducts formed, yielding several EPR signals in the g=4.0 region. Also, the oxidation of iron (II) to iron (III), giving rise to an increase in the g=4.3 EPR signal, was also observed. A final piece of evidence in our study which conclusively identifies iron as the source of the g=4.0 EPR signals, is the observed effect of ^{57}Fe enrichment on the observed spectra (Figure 5). Examination of the data quickly shows that the line-broadening observed in a comparison between the natural abundance standard and the isotopically enriched sample is very large. In fact, the ^{57}Fe line-broadening is larger than what has been reported for analogous experiments studying the effect of enrichment upon the NO-reactivity of catechol 2,3-dioxygenase and

protocatechuate 4,5-dioxygenase, as reported by Lipscomb and co-workers[9]. In that study, the ^{57}Fe line-broadening of the non-heme iron enzymes was found to be approximately 7 gauss. Here, the width at half-height for the central near-axial signal is approximately twice that. Clearly, there is an affect, and it is a strong affect. It is possible that excessive line-broadening is representative of inhomogeneity in the iron population: if the observed EPR spectra are due to slightly different species (as might be found if iron is binding non-specificially) with overlapping EPR signals, the line-broadening observed would be the sum of the broadening of each feature. Regardless of the nature of the explanation, the effect is dramatic, and clearly diagnoses the observed NO-adduct as being derived from iron.

The NO-Iron Adduct and Reactivity.

While it is clear that iron is responsible for the formation of the EPR-active NO-adduct, it is not clear what (if any function) this iron center plays in pMMO chemistry. As mentioned above, it has been previously suggested that as NO is thought to act as a dioxygen mimic, binding at locations that dioxygen would bind to reduced metals (such as Fe(II) or Cu(I)) yielding NO-adducts that are EPR-detectable. Considering the possibility that the iron detected as an iron-nitrosyl in the above experiments might be located at the active site of pMMO, we probed this possibility by examining the ability of acetylene to prevent the ability of pMMO to interact with NO. As Figure 6 shows, the ability of pMMO to form the NO-adduct detected at g=4.0 in the EPR spectrum is only very slightly inhibited by treatment with acetylene. Initially this merely suggests that acetylene binds in such a way that any dioxygen binding sites are still accessible to gaseous molecules. If the active site of pMMO has two distinct channels for the two co-substrates (dioxygen and hydocarbon), this finding does not yield any insight into pMMO

catalysis and the role of iron. However, as has been convincingly shown in Chapter 2 of this dissertation, acetylene inhibition of pMMO results in the overwhelming oxidation of the copper ions of the protein. The true significance of this being that electron equivalents within the various cofactors of pMMO have been drained away due to redox processes with acetylene itself, and/or dioxygen. If NO still binds to such a preparation and reveals an NO-adduct, then clearly it is binding to a center that did not undergo a redox-change after pMMO was inhibited by acetylene. Therefore, it holds that the iron center bound by pMMO (which clearly is still reduced after acetylene inhibition, otherwise no NO-adduct would form) is not involved in turnover of genuine substrates, such as the suicide substrate acetylene.

This finding is supported by the proteolysis experiments depicted in Figure 7 as well. The treatment with proteases (which can result in a retained iron content of <0.25 atoms/pMMO) affects the ability to generate the NO-adduct, indicating that NO does not bind at a buried site, as is thought for the pMMO active site. We take these combined findings to indicate that iron is likely not bound in a specific fashion, which is supported by the general finding that reproducibility of NO-based chemistry is difficult at best (as was found, for example, in the use of DEAN).

Conclusions

In this course of this chapter, we have examined the lingering question in the literature, Is iron a requisite component of the pMMO active site? It does appear that iron is the essential feature in generating the NO-induced g~4.0 region EPR spectra that have been reported here and elsewhere. The spectra were only detectable when iron

concentrations were sufficient, and demonstrated a large effect upon isotopic enrichment with ^{57}Fe. However, it does not appear that iron was an essential element in the active site: low-iron concentrations did not hamper cell growth, nor pMMO activity, and oxidizing the metal centers of pMMO through reaction with acetylene provided very little to affect generation of the iron-nitrosyl adduct. Lastly, the proteolysis experiments demonstrate that sub-stoichiometric levels of iron cannot be removed by specific (or non-specific) cleavage reagents, which indicates that iron is likely bound in a highly non-specific fashion -- neither entirely within the membrane-domains, nor outside of it. All of these pieces of evidence point toward iron being bound by pMMO, but not for the sake of catalysis. It is unclear what role, if any, iron has in the pMMO system.

References Cited

1)Ruggiero, C. E.; Carrier, S. M.; Antholine, W. E.; Whittaker, J. W.; Cramer, C. J.; Tolman, W. B. *J. Am. Chem. Soc.* **1993**, *115*, 11285-11298.

2)Stevens, T. H.; Brudvig, G. W.; Bocian, D. F.; Chan, S. I. *Proc. Natl. Acad. Sci. USA* **1979**, *76*, 3320-3324.

3)Martin, C. T.; Morse, R. H.; Kanne, R. M.; Gray, H. B.; Malmstrom, B. G.; Chan, S. I. *Biochemistry* **1981**, *20*, 5147-5155.

4)Brudvig, G. W.; Stevens, T. H.; Chan, S. I. *Biochemistry* **1980**, *19*, 5275-5285.

5)Coufal, D. E.; Tavares, P.; Pereira, A. S.; Hyunh, B. H.; Lippard, S. J. *Biochemistry* **1999**, *38*, 4504-4513.

6)Haskin, C. J.; Ravi, N.; Lynch, J. B.; Munck, E.; Que, L. *Biochemistry* **1995**, *34*, 11090-11098.

7)Arciero, D. M.; Lipscomb, J. D. *Journal of Biological Chemistry* **1986**, *261*, 2170-2178.

8)Arciero, D. M.; Lipscomb, J. D.; Huynh, B. H.; Kent, T. A.; Munck, E. *Journal of Biological Chemistry* **1983**, *258*, 4981-4991.

9)Arciero, D. M.; Orville, A. M.; Lipscomb, J. D. *Journal of Biological Chemistry* **1985**, *260*, 4035-4044.

10)Chen, V. J.; Orville, A. M.; Harper, M. R.; Frolik, C. A.; Surerus, K. K.; Munck, E.; Lipscomb, J. D. *J. Biol. Chem.* **1989**, *264*, 21677-21681.

11)Nelson, M. J. *J. Biol. Chem.* **1987**, *262*, 12137-12142.

12)Farrar, J. A.; Grinter, R.; Pountney, D. L.; Thomson, A. J. *Journal of the Chemical Society-Dalton Transactions* **1993**, 2703-2709.

13)Zahn, J. A.; DiSpirito, A. A. *Journal of Bacteriology* **1996**, *178*, 1018-1029.

14)Zahn, J. A.; Arciero, D. M.; Hooper, A. B.; DiSpirito, A. A. *Febs Letters* **1996**, *397*, 35-38.

15)Takeguchi, M.; Ohashi, M.; Okura, I. *BIOMETALS* **1999**, *12*, 123-129.

16)leBrun, N. E.; Andrews, S. C.; Moore, G. R.; Thomson, A. J. *Biochemical Journal* **1997**, *326*, 173-179.

Chapter 7: The Regio- and Stereoselectivity of Particulate Methane Monooxygenase Alkane Activation

Abstract

The regiospecificity and stereoselectivity of alkane hydroxylation and alkene epoxidation by the particulate methane monooxygenase from *Methylococcus capsulatus* (Bath) was evaluated over a range of substrates. Oxidation products were identified by conventional GC analysis, and the stereoselectivity of oxidation was determined by a combination of chiral- GC and HPLC methods, as well as ^{1}H NMR analysis of the corresponding (*R*)-2-acetoxy-2-phenylethanoate ester derivative in the case of alkanol products. Alkane hydroxylation was found to proceed favoring attack at the C-2 position in all cases, and the stereoselectivity for *n*-butane and *n*-pentane was characterized by an ee of 46% and 80% respectively, with preference for the (*R*) alcohol noted for both substrates. Epoxides were formed with smaller stereoselectivities. Together, the regio- and stereoselectivity results suggest that an equilibrium of competing binding modes of substrate exist. A simple substrate binding model that incorporates preferential C-2 oxidation with the observed stereoselectivity of alkane hydroxylation is proposed, and hypotheses for the general mechanism are suggested and discussed.

Introduction

The particulate methane monooxygenase (pMMO) from *Methylococcus capsulatus* (Bath) catalyzes the dioxygen-dependent, two electron oxidation of methane to methanol[1-3]. The enzyme is a copper-containing membrane protein comprised of 3 subunits of 47, 23, and 20 kDa molecular weight[1,3]. Similar to its soluble counterpart (sMMO), pMMO has garnered increased attention of late due to its ability to activate dioxygen and hydrocarbon C-H bonds. In cell cultures, the copper (II) content has been correlated to pMMO hydroxylation activity[4], as well as the active repression of sMMO transcription[5]. The addition of copper(II) has been shown to stimulate pMMO activity in a cell-free membrane system, while other divalent transition metals such as nickel (II) and zinc (II) do not[6]. Further, in cell-free assays, the inhibition of pMMO activity by the suicide substrate acetylene has been correlated to the total concentration of copper (II) ions in the assay[6]. The active site of pMMO is surmised to contain a trimeric copper

cluster[1], whereas the sMMO active site contains a diiron, hydroxyl bridged cluster[7]. The hydroxylase component of sMMO exists as a $\alpha_2\beta_2\gamma_2$ dimer which has been crystallized recently, and its three-dimensional structure determined by x-ray crystallography[8,9]. pMMO is expressed under copper-containing growth conditions in all known methanotrophs, while sMMO has been found only in a subset of methanotrophic organisms, and it is expressed in copper-free, iron-rich growth conditions only. Further, while sMMO has demonstrated a wide range of substrate specificity, including straight-chain, branched, and aromatic C-H bonds[10-13], pMMO mediates hydroxylation and epoxidation for a small set of straight-chain alkane and alkene substrates solely[3,14].

Determining the mechanism of C-H bond activation in biological systems is of great interest currently[15,16]. To this end, the mechanism of sMMO-mediated hydroxylation has been studied with radical spin-traps[17] as well as radical clock substrate probes[18]. Several mechanisms which have been suggested to account for the observations, invoke alkyl free radical and/or carbocation structures as potential intermediate species[13,18-20], or a concerted process involving direct oxygen insertion into a substrate carbon-iron bond[21,22]. Unfortunately, while pMMO warrants similar consideration due to its pervasive presence in methanotrophs, analogous studies using pMMO have been hindered by difficulty in maintaining the activity of the purified pMMO, as well as the limited substrate range of the enzyme[1]. However, the hydroxylation mechanisms of sMMO from *Methylosinus trichosporium* (OB3b) and pMMO from *M. capsulatus* (Bath) have recently been investigated by the use of cryptically chiral ethanes[19,23,24]. The determination of the stereoselectivity in ethanol production using either (*R*)- or (*S*)-[1-$^3H_1$,$^2H_1$] ethane demonstrated essentially 100% stereoselection for pMMO, and retention accompanied by substantial inversion of configuration for sMMO. In this light, a concerted reaction mechanism was proposed for pMMO-mediated hydroxylation of methane and ethane, with the further suggestion of a pentacoordinate carbon species serving as an intermediate[23]. Alternatively, sMMO-

mediated hydroxylation was determined to proceed *via* a short-lived alkyl radical in the case of the *M. trichosporium* (OB3b) enzyme[19], and that a concerted, yet nonsynchronous mechanism that contains an extremely short-lived alkyl radical structure in the transition state is a more appropriate description for sMMO from *M. capsulatus* (Bath)[24,25]. The mechanistic hypotheses associated with each of these systems are of great interest currently, and have yet to be resolved unequivocally.

In light of our previous observation of the stereospecific oxidation of chiral ethanes by pMMO, we have proceeded to investigate the potential of pMMO for mediating regio- and stereoselective oxidations of hydrocarbon substrates. In part, such a study focuses on the issue of the presentation of substrate molecules in the active site (regio-chemistry); however, the results may well also shed additional insights into the nature of the previously suggested concerted mechanism (stereoselectivity). Previously, investigators have studied the product distribution and regiospecificity of alkane and alkene oxidations mediated by MMOs from *M. capsulatus* (Bath) and *M. trichosporium* (OB3b), finding that both purified sMMO as well as sMMO-containing cell-free extracts oxidize a wide range of aliphatic and aromatic hydrocarbons, with little rigorous regiospecificity[10-13]. On the other hand, using the purified multi-component sMMO system from *M. trichosporium* (OB3b), it has been shown that alteration of the ratio of regulatory and reductase components greatly alters the regiospecificity of hydroxylation for a given substrate[26].

Here we present a study of the regiospecificity of pMMO-catalyzed alkane and alkene oxidation by utilizing a broader range of substrates than attempted heretofore. We also present additional nuances on the *stereo*specificity of these oxidation reactions.

Experimental Procedures

Enzyme-mediated oxidations. Cultures of *M. capsulatus* (Bath) were grown on a 10 liter scale on nitrate mineral salts medium, and pMMO-containing membrane fractions from *M. capsulatus* (Bath) were isolated as described previously[1]. These membrane fractions were highly enriched in pMMO and provided an ideal source of enzyme, and were used to prepare oxidation products from the substrates listed in Table 1. The products were generated by the incubation of 2.5 ml of a pMMO-containing membrane suspension (with a total protein concentration of 12-16 mg/ml and a specific activity of 10-15 nmol/min•mg) with 35 μmol of NADH (Sigma) in 25 ml of 50 mM PIPES buffer (pH 7.3) at 45°C, as described previously[23]. The reactions were initiated by the injection of 10 ml of gaseous substrate, so that all reactions were carried out in the presence of excess substrate such that the reaction velocity was assumed to be at V_{max}. For the assays carried out to determine product distribution and relative rates of product formation, products were generated on a 1ml scale, using 0.1 ml of membrane suspension, while the determination of the stereospecificity of oxidations was carried out on a 25ml scale, using 2.5ml of membranes, as described above.

Product identification and quantification. The identification of products, as well as the quantitation of products for the purpose of determining relative rates of formation, was achieved by the comparison of GC retention times using a Hewlett-Packard HP5840A gas chromatograph fitted with a 1% AT-1000/Carbograph 60/80-mesh column and a flame ionization detector. Primary and secondary alcohol standards, as well as epoxidation standards, obtained from Aldrich were used to identify and quantify the distribution of products. Aliquots of reaction products were taken aside at 2-4-minute intervals for the first 20 minutes of the reaction and immediately placed at 0°C, quenching the reaction. Subsequent aliquots were taken aside at 7 minute intervals thereafter, monitoring the remaining time-course of the reaction (usually <1 hour). The

aliquots were centrifuged briefly, pelleting the membranes, and 1 μl of the supernatant was applied directly to the GC. The integrated peaks from GC-traces corresponding to products were then used to determine the respective rates of formation for each of the products under study. Each product was quantified by comparing the peak size to a calibration curve for each of the possible oxidation products. Only membrane preparations demonstrating a k_{obs} for ethane oxidation of 12-17 nmol of ethanol/min•mg protein and a k_{obs} for propylene oxidation of 10-15 nmol propylene oxide/min•mg protein were used in these experiments. Relative rates of formation of products are reported due to slight variation (~10%) between the baseline activities of ethane/propylene oxidation between membrane preparations.

Stereochemical assignments. For those experiments designed to determine stereoselectivity of product formation, the reaction products were extracted into ether from the reaction mixture, and the ethereal layer was dried over $MgSO_4$ and concentrated under a nitrogen stream while immersed in an ice-salt bath. The stereochemical identity of the hydroxylation products of the oxidation of butane and pentane was assigned by comparison of the 300 MHz ^1H NMR spectra of the (*R*)-2-acetoxy-2-phenylethanoate ester derivatives with authentic standards, prepared from (*R*)- and (*S*)-butan-2-ol (Aldrich)[27]. These data were confirmed by HPLC analysis of the derivatized products and standards using a D-DNB-Leucine chiral column. Similarly, the absolute configuration of the epoxidation products was determined directly using either Chiraldex-ATA or Chiraldex-GTA GC-LC methodologies on an Hewlett-Packard 5890 Series II instrument, by comparing the products to the authentic standards (*R*)- and (*S*)-propylene oxide (Fluka), (*R*)- and (*S*)- epichlorohydrin (Fluka) and the trichloroacetic acid ester of (*R*)- and (*S*)-glycidol (Aldrich). Due to the commercial unavailability of enantiomerically pure standards for 1-epoxybutane and 1,3-butadienemonoxide, we used the epicholorohydrin and glycidol-based standards as product analogs, which yielded consistent enantiomeric resolution, and assumed analogous elution behavior of the (*R*)-

and (*S*)- isomers. A Chiraldex-ATA column (20m x 0.25 mm) was used for analysis of propylene oxide formed from the oxidation of propylene, while a Chiraldex-GTA column (20m x 0.25 mm) was used to evaluate the stereochemical configuration of the 1-epoxybutane and 1,3-butadienemonoxide produced from 1-butene and 1,3-butadiene, respectively. The ee values are defined as |(R-S)| / (R+S), where R and S are the total amounts of each stereoisomer as determined by GC-peak integration.

Results and Discussion

Regioselectivity of hydrocarbon oxidation - In our hands, pMMO-mediated oxidations of alkanes and alkenes are limited to straight-chain hydrocarbons containing 5 carbon atoms or less (Table 1). No oxidation products were detected for any substrate containing more than 5 carbon atoms. Further, branched hydrocarbons are not oxidized by pMMO, with a sole exception being 2-methylbutane, which yielded 3-methyl-butan-1-ol in trace quantities. Substrates containing conformation-limiting double-bonds, such as *cis-* or *trans*-2-butene, were oxidized exclusively to the corresponding epoxide, indicating that a loss in the conformational flexibility of a substrate does not terminate catalysis. Remarkably, oxidation was overwhelmingly favored in the C-2 position, *e.g.,* propane was oxidized to propan-2-ol solely, strongly contrasting to the wide-ranging regiospecificity of sMMO[10-13] and unlike a previous account of pMMO-mediated propan-1-ol and propan-2-ol formation[14]. Further, we found that oxidation of *cis* - and *trans*- 2-butene yielded an epoxidation product only, and not the hydroxylation product crotyl alcohol or the further oxidation product, crotonaldehyde, as has been reported elsewhere[14].

Stereoselectivity of hydrocarbon oxidation - Earlier studies of the stereoselectivity of pMMO using cryptically chiral ethanes revealed ~100% retention of

configuration in the hydroxylation products formed,[23] suggesting that a single stereoisomer should result with the other alkane substrates used in this study. However, while the stereoselectivity of the hydroxylation chemistry reported in Table 1 strongly favors the formation of (*R*)-alcohols, the chemistry is not 100% stereoselective. The observed ee values for the oxidation of *n* -butane and *n* -pentane vary significantly (46%

Substrate	Products *(% total)*	k^{rel} *(a)*	Dominant stereoisomer	ee *(%)*
Ethane	Ethanol	1.00	*n.a.*	--
Propane	Propan-2-ol (~100)	0.90	*n.a.*	--
	Propan-1-ol (*trace*)	*n.d.*	*n.a.*	--
n -Butane	Butan-2-ol (95)	0.4	*R* [c]	46±4.5
	Butan-1-ol (5)	0.02	*n.a.*	--
n -Pentane	Pentan-2-ol (95)	0.17	*R* [c]	80±2
	Pentan-1-ol (5)	>0.01	*n.a.*	--
2-Methylpropane	*None*	*n.a.*	*n.a.*	--
2-Methylbutane	3-Methylbutan-1-ol *(trace)*	*n.d.*	*n.a.*	--
Propylene	Propylene oxide	1.0	*S* [d]	18.5±2
1-Butene	1-Epoxybutane (58)	.62	*S* [e]	37±2
	3-Buten-2-ol (42)	.70[b]	*R* [c]	50±4
1,3-Butadiene	1,3-Butadienemonoxide	.96	*R* [e]	15±2
cis-But-2-ene	2,3-*cis*- Epoxybutane	.29	*n.a.*	--
trans-But-2-ene	2,3-*trans*- Epoxybutane	.26	*n.d.*	--

Notes: n.a.: not applicable; n.d., not determined). [a]*For alkane substrates (above the line) rates are relative to ethane hydroxylation; for alkene substrates, rates are relative to propylene epoxidation.* [b]*Relative to ethane hydroxylation.* [c]*Assigned by comparison to the (R)-2-acetoxy-2-phenylethanoate ester derivative of (R)-butan-2-ol by* ^1H *NMR.* [d] *The absolute configuration was assigned by GC analysis using a Chiraldex A-TA column (20m x 0.25mm) by comparison with authentic standards of (R)- and (S)-propylene oxide (Fluka).* [e]*The absolute configuration was assigned using a Chiraldex G-TA column, with comparison to (R)- and (S)-epichlorohydrin (Aldrich) and the trichloroacetic acid derivative of (R)- and (S)- glycidol (Aldrich) , assuming identical elution behavior of (R)- and (S)-isomers.*

Table 1. Regio- and stereochemical oxidation of hydrocarbons by pMMO

and 80%, respectively), indicating that subtle steric constraints must be very important in determining the stereoselectivity (vide infra).

The uncertainties in the reported ee values were determined by carrying out several replicates using a series of preparations of pMMO-containing membrane extracts. For example, the determination of the stereoselectivity of *n* -butane hydroxylation was repeated seven times with a total of three different pMMO preparations, and the ee value reported in Table 1 is an average of all the data accumulated. The standard deviation of data acquired from multiple experiments performed with samples from a given preparation was found to be small (typically this was found to be < 2). As noted in Table 1, deviations between ee values acquired from different pMMO preparations were also acceptable. Other pMMO-mediated oxidations were carried out (at least) in duplicate, using different preparations, and again the variation between experiments was found to be small in comparison to the differences observed in the ee value for the different substrates. It should be noted that all experiments were carried out using membrane preparations of comparable activity, and the use of membrane extracts of lower activity uniformly resulted in insufficient formation of products, which prohibited further stereochemical analysis.

The alkene substrates studied did not yield ee values greater than 40%, and frequently yielded marginal stereoselectivity only. In part, the spectrum of ee values may be attributed to variable binding of the substrate. In the case of propylene, variable binding modes may cause the near racemization observed if attack is conserved to a single side. If propylene binds either "methyl-first" or "vinyl-first" with nearly the same affinity, then the combination of binding modes would lead to both the (*R*)- and (*S*)-products. However, a preferred binding mode must exist, as completely racemic products are not attained. Further, the observed dominance of (*S*)-epoxide and (*R*)-alcohols suggests equivalent attack on the same face of butane and 1-butene, as shown in Figure 1. In the case of 1-butene, the binding mode (vinyl- or methyl-first) determines which

product is formed as well as guides the stereospecificity. However, the binding of substrate is not rigorous. As demonstrated by the substrate 1,3-butadiene, the product 1,3-butadienemonoxide is produced with a small majority of the (*R*)-isomer. Such variable stereoselectivity has been observed previously in the epoxidation of a series of vinyl and allyl-halide substrates oxidized by *M. trichosporium* (OB3b) in a whole-cell assay.[28,29]

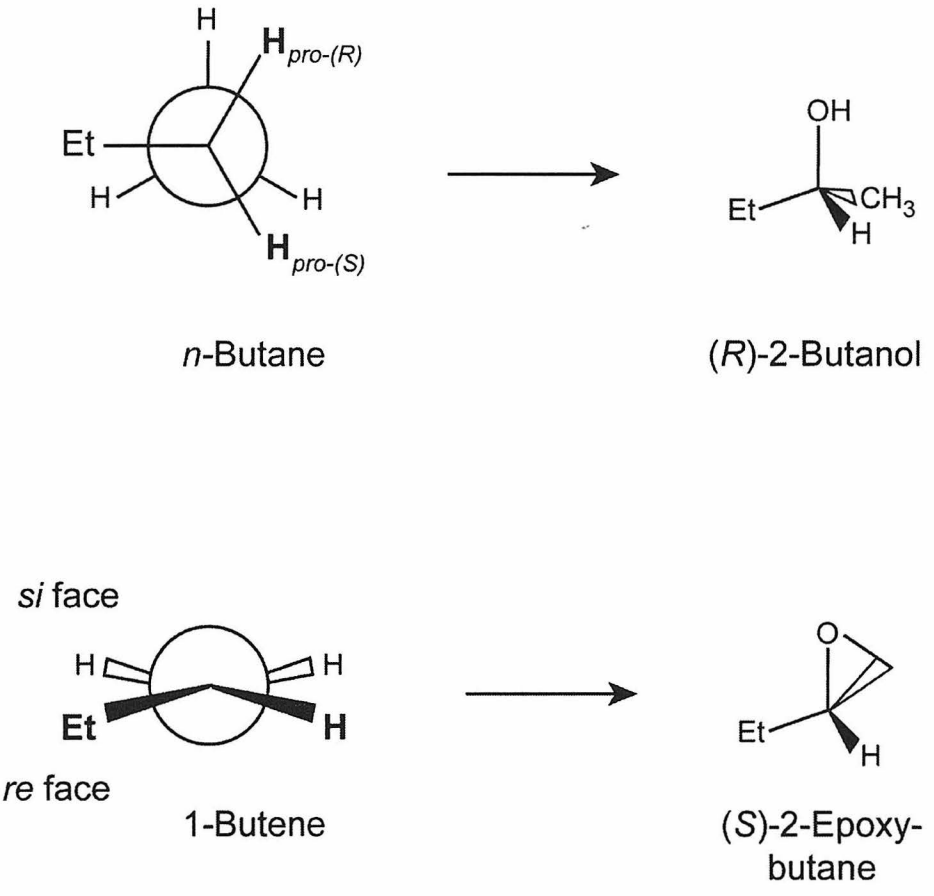

Figure 1

A model for dioxygen activation and alkane hydroxylation by pMMO - As noted above, interpreting the observed regio- and stereoselectivities for a given substrate requires invoking substrate recognition and binding (or, how a substrate in presented

within the active site) in addition to the intrinsic substrate reactivity (*i.e.,* mechanism). In the case of ethane, the stereochemical results offer a measure of the intrinsic reactivity because of the symmetry of the substrate. Thus, it appears that a concerted mechanism is at work for the oxygen atom insertion step as previously proposed[23]. For other substrates, an understanding of the observed regioselectivity and stereoselectivity must include such considerations as the size and symmetry of the substrate molecule as well as the steric constraints imposed by the shape and symmetry of the active site pocket.

We will first consider the steric requirements of the active site. As pMMO carries out regio- and stereoselective hydroxylation chemistry, it is evident that the active site must induce asymmetry upon a highly symmetric hydrocarbon substrate molecule. In addition to the simple steric considerations which may be insufficient to limit rotational freedom of the pseudo-cylindrically symmetric hydrocarbon, the asymmetric catalysis may be facilitated by a copper-oxygen adduct which is of lower intrinsic symmetry. As mentioned above, pMMO is surmised to contain a trimeric copper cluster in the active site, and recent work has demonstrated the ability of dimeric[30-32] and trimeric copper clusters[33] to generate complexes that bind dioxygen and cleave the O-O bond by using electron equivalents from multiple copper atoms. In such model systems the resulting adducts contain either a bis(μ_2-oxo)-binuclear copper(III)-core[30,32,34] or a bis(μ_3-oxo)-trinuclear copper(II,II,III) core[33]. The displayed propensity of low-nuclearity copper clusters to form such bridged copper(III)-oxo adducts is helpful in considering the nature of pMMO-mediated oxygen activation and hydroxylation, particularly as copper is unlikely to form a terminal copper(III)-oxo species[35]. Further, within the regime of the $[Cu(III)_2(\mu\text{-}O)_2]^{2+}$ core, Tolman and co-workers have noted the proclivity of the thermally unstable complexes to activate an internal C-H bond upon warming[32,36,37] as have Stack and co-workers[34]. This process appears to have significant contributions from electrophilic oxo-centered acceptor orbitals[31,37]. Also, a single electron reduction of this oxo-bridged moiety apparently further destabilizes the core, leading to unresolved

decomposition of the dimeric complex prior to warming[34]. This new insight from model chemistry is useful toward considering pMMO-mediated dioxygen activation and hydroxylation, although the model systems have a higher degree of symmetry than would account for the asymmetric catalysis described above, prompting consideration of an asymmetric dioxygen-adduct for pMMO-mediated oxidations.

Thus, in the presentation of a substrate molecule in the active site, we first consider a simple model for asymmetric hydroxylation that emphasizes attack on a single face of a hydrocarbon substrate (as in Figure 1) and attempt to rationalize the observed

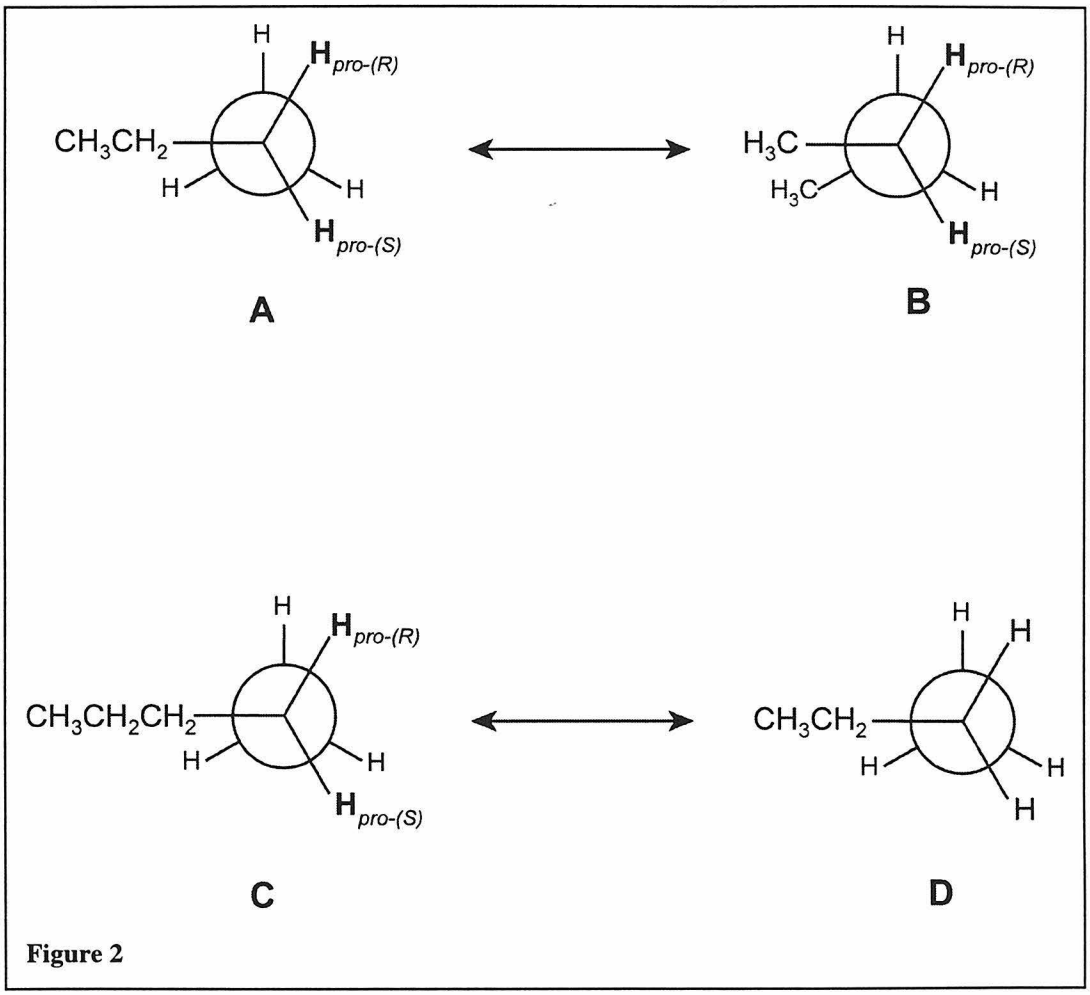

Figure 2

variation in ee value due to variability in the substrate binding. In the case of propylene, either the *re* or the *si* faces may be presented in essentially the same orientations and this should lead to a racemic mixture of the *(R)*- and *(S)*- epoxides, as observed. Similarly,

the formation of 3-Butan-2-ol and 1-Epoxybutane in essentially equal proportions can be understood in terms of such a binding scheme and equilibrium. If the asymmetric hydroxylation or epoxidation involves attack on the same face of the hydrocarbon substrate as in Figure 1, the stereochemical configuration of the alcohol and the epoxide should be *(R)* and *(S)* respectively, as observed, if the attack proceeds with retention of configuration.

A possible scheme to account for the stereoselectivity of butane hydroxylation is shown in Figure 2. As shown therein, butane can be thought of having two binding modes, **A** and **B**, which differ *translationally* as the butane molecule slides forward and backward in the binding site, such that either a *pro-(R)* (**A**) or a *pro-(S)* hydrogen (**B**) is presented in a similar orientation within the active site. Presuming catalysis proceeds with retention of configuration as was demonstrated for ethane[23], **A** leads entirely to *(R)*-butan-2-ol and **B** leads to *(S)*- butan-2-ol. Thus, the observed stereoselectivity may be rationalized if a butane molecule shifts within the equilibrium by a small translational motion. However, such a binding scheme fails to account for the hydroxylation of pentane, which would similarly bind in forms **C** and **D**, yielding *(R)* -pentan-2-ol and pentan-3-ol. This model predicts the formation of pentan-3-ol in analogous fashion to the formation of *(S)*- butan-2-ol. Based on the observed ee value for butane hydroxylation, pentan-3-ol should comprise 27% of the hydroxylation products. Yet no pentan-3-ol is observed. Similarly, propane should reorient in the binding site and the equilibrium would yield ~27% of the total products as propan-1-ol; yet propan-1-ol has been detected at trace levels only. Thus, this "translational binding model" cannot account for the regiospecificity observed so long as the substrates are assumed to freely reorganize within the active site.

While it seems unlikely that pentane would be able to reorganize due to steric reasons (as compared to butane), propane should be allowed to move quite freely.

However, the stringent oxidation of propane at the C-2 position can be explained by invoking some feature of the protein environment such as a small hydrophobic pocket that can accommodate a methyl group of propane, but not any group larger. In such a scenario, this small pocket would hold a propane molecule in a position that exposes the C-2 position for alkane substrates, and preferentially deters reorganization of the substrate. Thus, attack at the C-2 position is enforced. However, when the substrate is not fully extended into this pocket, some reactivity can occur at the C-1 position, as is observed in Table 1. With these types of boundary conditions, it seems that most substrates are bound in a single translational conformer preferentially, with some potential for translation reorganization that results in the observed regiospecificity. The regioselectivity observed would then reflect the free energy difference between the various modes of presenting the hydrocarbon substrate to the hydroxylation site, as imposed by the steric constraints.

Further consideration of the substrate range displayed by pMMO can aid in revising the model proposed in Figure 2. Linear straight-chain hydrocarbons no more than five carbons in length appear to be favored substrates. As the data seem to preclude the notion of significant translational motion of the substrate within the binding site, it may be concluded that the active site pocket in pMMO has a limited depth and is closed at one end in the small pocket mentioned above, such that longer hydrocarbon chains (*i.e.,* hexane, heptane, etc.) are not appropriate substrates because their size interferes with a conformational change of the binding pocket that is required for catalysis. This suggestion is supported by the propensity for small 1-alkynes, such as acetylene[38] and 1-butyne to act as suicide substrates, while the larger putative suicide substrate 1-hexyne does not interfere with normal catalysis[39]. These observations further confirm that pMMO contains a small active site that binds substrate very tightly, allowing only minimal translational reorganization of substrate molecules.

With these considerations in mind, Figure 3 presents a further refinement of a binding scenario in which either (*R*)- or (*S*)- alcohol product results *via* a non-specific oxidation of substrate molecules bound with the same translational orientation. Within this model subtle differences in binding mode influence the stereoselectivity of the reaction and, potentially, the mechanism itself. Figure 3 implicitly assumes that the translational freedom allowed in Figure 2 is minimized, but as before, substrates interact with a single face of a dicopper core. Further, we propose that steric interactions, and the conformation constraints of the protein environment, allow for two binding modes (**I** and **II**) to position either the *pro- (R)* or *pro-(S)* hydrogen such that attack by the dicopper core proceeds, but the overall preference in substrate binding (**I**) yields the observed preferential oxidation at the *pro-(R)* hydrogen. The two binding modes also correspond to two active site conformations that differ slightly, yielding the overall preference in exposing the *pro- (R)* or *pro-(S)* hydrogen while maintaining the hydrophobic contacts that result in preferential attack at the C-2 position. The two modes clearly will be close in energy, to be consistent with the ee ratios reported in Table 1. Even in the case of the greatest stereoselectivity, an ee of 80% for n-pentane hydroxylation, the 1:9 distribution of (*S*)- to (*R*)- alcohol can be accounted for by a small free energy differences between the substrate conformers: a mere 5.75 kJ/mol, which is less than 2*k*T per molecule at 315 K. The analogy between alkane and alkene binding modes illustrated in Figure 1 still holds within this scheme, although it can be imagined that if pMMO does bind alkanes very tightly, the increased rigidity of the olefin may reduce the ability of the substrate to conform to the preferred binding modes allowed by the conformational flexibility of the active site. Thus, the stereoselectivity of alkene epoxidation would be reduced, as is observed.

The dioxygen adducts and mechanistic hypotheses - Finally, we turn to the question of the dioxygen adduct that may be involved in catalysis. The observed thermal decomposition of model complexes containing a $[Cu(III)_2(\mu\text{-}O)_2]^{2+}$ core is satisfied by

the trinuclear copper cluster implicated as the active site here. In particular, the findings of Stack and co-workers regarding bolstered reactivity of $[Cu(III)_2(\mu\text{-}O)_2]^{2+}$ upon a one-electron reduction suggest that injection of an additional electron into the reaction site, potentially by another copper ion, may enhance (or indeed, be required for) reactivity. Such a process would imply that the redox states of the two copper ions within the core need not be identical in conventional formalisms, *i.e.*, in Figure 3 $m \neq n$. In addition, proximity and orientation of the substrate can guide the decomposition pathway as the binding of substrate, and its potential for slight reorganization, can affect both the character of the resulting dicopper core, and which oxygen atom of the dicopper core is incorporated into product, thereby leading to *(R)-* and *(S)-* isomers. The correlation between oxidation state, substrate orientation and reactivity is specifically depicted in Scheme 1.

This catalytic hypothesis is attractive in that it directly links binding of a small substrate to reactivity: substrate binding can be thought of triggering the redox linkage necessary for the further reduction of the $[Cu(III)_2(\mu\text{-}O)_2]^{2+}$ core, thereby increasing the energy of the ground state electronic structure of the intermediate, lowering the kinetic barrier for catalysis.

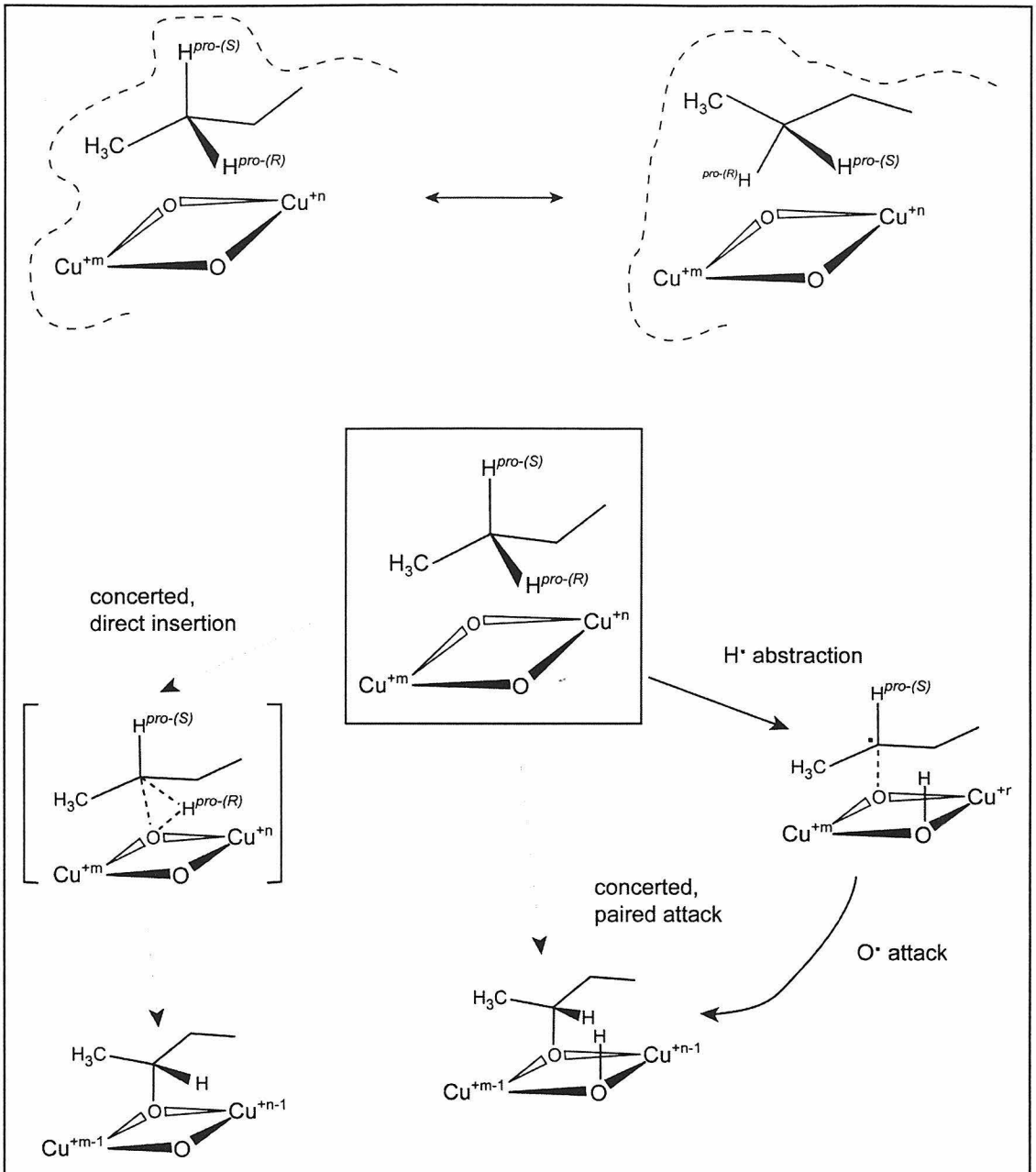

Figure 3. An alternative substrate binding scheme that does not allow for translational motion between conformers. Forms I and II are related by differential insertion into the active site, which alternatively places either the *pro-(R)-* or the *pro-(S)-* hydrogen of the C-2 position in close proximity to an oxygen atom of a proposed dicopper-oxo core, as found in model complexes previously. (Bottom) Mechanistic hypotheses based on above binding model. This model readily allows for concerted mechanisms, such as a direct insertion of an activated oxygen atom into the *pro-(R)-* C-H bond (left pathway) or a concerted pair-wise process (middle pathway). A non-synchronous mechanism such as hydrogen atom abstraction followed by attack of an oxygen-based radical (right pathway) is equally feasible.

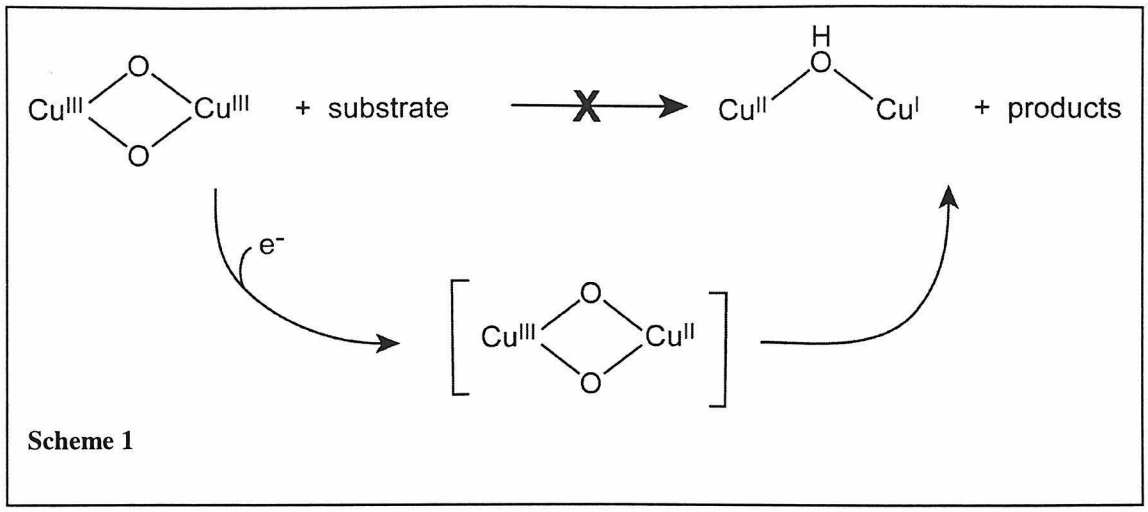

Scheme 1

Generally speaking, this binding model can serve as suitable grounds for subsequent mechanistic hypotheses. For example, conformer **I** may be better suited for a concerted reaction process, as it agrees with the steric constraints of the preferred transition state structure proposed previously[40] for the insertion of an electrophilic oxygen atom into a methylene C-H bond of *n* -butane by a solvated oxenoid species. Interestingly, this type of insertion process has already been proposed for sMMO by Shestakov and Shilov[41]. While Tolman and co-workers have postulated that the bridging oxygen atoms have significant electrophilic character[31,37] we cannot rigorously discount other possibilities, such as the invocation of the direct formation of a high-valent organo-copper intermediate, as suggested by Barton and co-workers[42,43]. The direct involvement of one or both of the proposed oxo-bridges is also circumspect, as a concerted process may be accommodated by either possibility: one satisfying mechanism couples nucleophilic attack of the substrate *pro-(R)* proton by one bridging oxygen atom to the concomitant electrophilic attack of the methylene carbon by the other bridging oxygen, thus requiring in a cyclic transition state (central pathway). However, direct oxygen insertion may involve only a single oxygen atom (left pathway). A radical rebound mechanism may account for the findings as well, so long as the active site poses severe steric constraints on the structure of resulting radical intermediates, and/or the rebound

rate for methane and ethane hydroxylation is too large to allow the extended existence of a discreet population of R• species (right pathway). However, the previous study of chiral ethane oxidation, described earlier[23], clearly demonstrates that the lifetime of such a alkyl radical would have to be shorter than $<1x10^{-14}$ s, implying that the contribution of such a process is most unlikely in the oxidation of ethane.

Thus, the above discussion describes how the competition between substrate binding modes may affect the observed stereoselectivity, and how a number of possibilities might be consistent with a hydroxylation mechanism that proceeds through retention of configuration as has been ascribed to the hydroxylation of ethane[23]. However, as just discussed, the regio- and stereochemical characterization of reaction products cannot rigorously exclude one mechanism or another, although a model describing an appropriate binding mode can be developed. It can be noted that if a substrate is unable to adopt the preferred conformer for a given mechanism, it is quite possible that the hydroxylation chemistry proceeds through one of the alternative processes. Indeed, the existence of parallel pathways cannot be ruled out at this time, and it seems most probable that the electronic structure of the activated oxygen species will be controlled by the arrangement of the inner-sphere ligands around the copper atoms. This means that the steric effects for a given substrate molecule may perturb the electronic structure of the site, and thereby, perturb the reactivity of the site as well.

Conclusions

The observed regio- and stereospecificity of alkane hydroxylation and alkene epoxidation mediated by pMMO are reported here. This study has delineated the issues of substrate binding in the activation of alkanes by pMMO, generating a model for substrate binding that can be related to known copper-dioxygen chemistry and previously

proposed mechanism for alkane activation. It is apparent that multiple pathways for alkane hydroxylation and alkene epoxidation contribute to the observed regio- and stereoselectivity and that these results may vary between substrates in a manner that is determined by the substrate binding mode. Specifically, while pMMO demonstrates stringent substrate specificity, we can rationalize a preferential binding model that presents a substrate such that nonspecific, concerted, catalysis yields stereoselectivities that vary with substrate size and shape. Moreover, in the case of alkane hydroxylation, the binding mode of the substrate at the active site can expose either the *pro* -(*R*) or *pro*-(*S*) C-H bond at the C-2 position in a substrate-specific manner. Although ethane oxidation appears to proceed through a concerted mechanism, whether this is rigorously the case for other alkanes remains to be seen. Further studies using diagnostic kinetic isotope techniques will hopefully elucidate the mechanistic aspects of this problem, expanding on the model presented herein.

References Cited

1) Nguyen, H.-H. T.; Shiemke, A. K.; Jacobs, S. J.; Hales, B. J.; Lidstrom, M. E.; Chan, S. I. *J. Biol. Chem.* **1994**, *269*, 14995.

2) Bédard, C.; Knowles, R. *Microbiol. Rev.* **1989**, *53*, 68.

3) Nguyen, H.-H. N. T.; Zhu, M.; Elliott, S. J.; Nakagawa, K. H.; Hedman, B.; Costello, A. M.; Peeples, T. L.; Wilkinson, B.; Morimoto, H.; Williams, P. G.; Floss, H. G.; Lidstrom, M. E.; Hodgson, K. O.; Chan, S. I. In *Microbial Growth on C_1 Compounds*; Lidstrom, M. E.; Tabita, F. R., Eds.; Kluwer Academic Publishers: 1996; p 150.

4) Semrau, J. D.; Zolandz, D.; Lidstrom, M. E.; Chan, S. I. *J. Inorg. Bioch.* **1995**, *58*, 235.

5) Nielsen, A. K.; Gerdes, K.; Degn, H.; Murrell, J. C. *Microbiology - UK* **1996**, *142*, 1289.

6) Cook, S. A.; Shiemke, A. K. *J. Inorg. Biochem.* **1996**, *63*, 273.

7) Lipscomb, J. D. *Annu. Rev. Microbiol.* **1994**, *48*, 371.

8) Rosenzweig, A. C.; Frederick, C. A.; Lippard, S. J.; Nordlund, P. *Nature* **1993**, *366*, 537.

9) Rosenzweig, A. C.; Nordlund, P.; Takahara, P. M.; Frederick, C. A.; Lippard, S. J. *Chem. Biol.* **1995**, *2*, 409.

10) Colby, J.; Stirling, D. I.; Dalton, H. *Biochem. J.* **1977**, *165*, 395.

11) Stirling, D. I.; Dalton, H. *European Journal of Biochemistry* **1979**, *96*, 205.

12) Higgins, I. J. ;. B., D.J.; Hammond, R.C. *Nature* **1980**, *286*, 561.

13) Green, J.; Dalton, H. *J. Biol. Chem.* **1989**, *264*, 176980.

14) Smith, D. D. S.; Dalton, H. *Eur. J. Biochem.* **1989**, *182*, 667.

15) Feig, A. L.; Lippard, S. J. *Chem. Rev.* **1994**, *94*, 759.

16) Shteinman, A. A. *FEBS Lett.* **1995**, *362*, 5.

17) Dalton, H.; Wilkins, P. C.; Jiang, Y. In *Microbial Growth on* C_1; Murrell, J. C.; Kelly, D. P., Eds.; Intercept: United Kingdom, 1993; p 65.

18) Liu, K. E.; Johnson, C. C.; Newcomb, M.; Lippard, S. J. *J. Am. Chem. Soc.* **1993**, *115*, 939.

19) Priestly, N. D.; Floss, H. G.; Froland, W. A.; Lipscomb, J. D.; Williams, P. G.; Morimoto, H. *J. Am. Chem. Soc.* **1992**, *114*, 7561.

20) Ruzicka, F.; Huang, D.-S.; Donnelly, M. I.; Frey, P. A. *Biochemistry* **1990**, *29*, 1696.

21) Barton, D. H. R.; Csuhai, E.; Doller, D.; Ozbalick, N.; Balavoine, G. *Proc. Natl. Acad. Sci. USA* **1990**, *87*, 3401.

22) Barton, D. H. R.; Beviere, S. D.; Chavasiri, W.; Csuhia, E.; Doller, D.; Liu, W.-G. *J. Am. Chem. Soc.* **1992**, *114*, 2147.

23) Wilkinson, B.; Zhu, M.; Priestley, N. D.; Nguyen, H.-H. T.; Morimoto, H.; Williams, P. G.; Chan, S. I.; Floss, H. G. *J. Am. Chem. Soc.* **1996**, *118*, 921.

24) Valentine, A. M.; Wilkinson, B.; Liu, K. E.; Komar-Panicucci, S.; Priestly, N. D.; Williams, P. G.; Morimoto, H.; Floss, H. G.; Lippard, S. J. *J. Am. Chem. Soc.* **1997**, *119*, 1818.

25) Choi, S.-Y.; Eaton, P. E.; Hollenber, P. F.; Liu, K. E.; Lippard, S. J.; Newcomb, M.; Putt, D. A.; Upadhyaya, S. P.; Xiong, Y. *J. Am. Chem. Soc* **1996**, *118*, 6547.

26) Froland, W. A.; Andersson, K. K.; Lee, S.-K.; Liu, Y.; Lipscomb, J. D. *J. Biol. Chem.* **1992**, *267*, 17588.

27) Parker, D. *J. Chem. Soc., Perkin Trans. 2* **1983**, 83.

28) Ono, M.; Okura, I. *J. Mol. Catal.* **1990**, *61*, 113.

29) Seki, Y.; Shimoda, M.; Sugimori, D.; Okura, I. *J. Mol. Catal.* **1994**, *87*, L17.

30) Halfen, J. A.; Mahapatra, S.; Wilkinson, E. C.; Kaderli, S.; Young, V. G.; Que, L.; Zuberbühler, A. D.; Tolman, W. B. *Science* **1996**, *271*, 1397.

31) Mahapatra, S.; Halfen, J. A.; Wilkinson, E. C.; Pan, G.; Wang, X.; Young, V. G.; Cramer, C. J.; Que, L.; Tolman, W. B. *J. Am. Chem. Soc.* **1996**, *118*, 11555.

32) Mahapatra, S.; Young, V. G.; Kaderli, S.; Zuberbühler, A. D.; Tolman, W. B. *Angew. Chem. Int. Ed. Engl.* **1997**, *36*, 130.

33) Cole, A. P.; Root, D. E.; Mukherjee, P.; Solomon, E. I.; Stack, T. D. P. *Science* **1996**, *273*, 1848.

34) Stack, T. D. P. Personal communication.

35) Mayer, J. M. *Comments Inorg. Chem.* **1989**, *8*, 125.

36) Mahapatra, S.; Halfen, J. A.; Wilkinson, E. C.; Que, L.W.; Tolman, W. B. *J. Am. Chem. Soc.* **1994**, *116*, 9785.

37) Mahapatra, S.; Halfen, J. A.; Tolman, W. B. *J. Am. Chem. Soc.* **1996**, *118*, 11575.

38) Prior, S. D.; Dalton, H. *FEMS Microbiol. Lett.* **1985**, *29*, 105.

39) Data not shown.

40) Bach, R. D.; Andrés, J. L.; Su, M.-D.; McDouall, J. J. W. *J. Am. Chem. Soc.* **1993**, *115*, 5768.

41) Shestakov, A. F.; Shilov, A. E. *J. Mol. Catal. A* **1996**, *105*, 1.

41) Barton, D. H. R.; Bévière, S. D.; Chavasiri, W.; Csuhai, É.; Doller, D. *Tetrahedron* **1992**, *48*, 2895.

43) Barton, D. H. R.; Csuhai, E.; Doller, D. *Tetrahedron Lett.* **1992**, *33*, 4389.